Mitochondria and effector functions of human $CD8^+$ T cells

Inauguraldissertation

zur

Erlangung der Würde eines Doktors der Philosophie

vorgelegt der
Philosophisch-Naturwissenschaftlichen Fakultät
der Universität Basel

von
Marco Guido Fischer
aus Stetten, Aargau

Basel, 2015

Genehmigt von der Philosophisch-Naturwissenschaftlichen Fakultät

auf Antrag von

Prof. Christoph Hess and Prof. Christoph Handschin

Basel, den 08.12.2015

Prof. Dr. Jörg Schibler

Table of contents

Summary 4

Abbreviations 6

1. Introduction 8
1.1. $CD8^+$ T cells 8
1.2. Mitochondria 11
1.3. T cell metabolism and immune function 16
1.4. Metabolic differences in $CD8^+$ T cell subsets 18
1.5. Mitochondrial biogenesis in T cells 20

2. Hypothesis 21

3. Mitochondrial biogenesis in human naïve $CD8^+$ T cells supports early cytokine secretion via mitochondrial ROS (Manuscript 1) 22
3.1. Introduction 22
3.2. Materials and Methods 23
3.3. Results 27
3.4. Discussion 38
3.5. Supplemental Material 40

4. Glucose oxidation in the mitochondria is important for $CD8^+$ memory recall response (Manuscript 2) 43
4.1. Introduction 43
4.2. Materials and Methods 44
4.3. Results 49
4.4. Discussion 58

5. Dual antibody bead coupling: a semi quantitative approach (Manuscript 3, Technical note) 61
5.1. Introduction 61
5.2. Materials and Methods 61
5.3. Results 64
5.4. Discussion 67
5.5. Supplemental Material 68

6. Future perspective 69
6.1. Modulation of cellular metabolism to increase immune responses 69
6.2. Modulation of cellular metabolism to limit T cell responses 71

7. References 72

8. Acknowledgments 81

9. Curriculum vitae 82

Summary

Naïve $CD8^+$ T cells become activated if they recognize their specific antigen in the presence of co-stimulatory signals and inflammatory cytokines. This activation is followed by a rapid clonal expansion and differentiation into effector cells. These energetically demanding processes require significant changes in cellular metabolism. T cell activation induces metabolic reprogramming from oxidative phosphorylation to aerobic glycolysis, proving both energy and metabolic intermediates. When the pathogen is cleared, the majority of antigen-specific $CD8^+$ T cells undergo apoptosis. Only a small subset switch back to oxidative phosphorylation and survives this contraction phase to form a long-lived memory T cell pool with the ability to respond faster and stronger after reinfection.

Although both naïve and memory $CD8^+$ T cells use oxidative phosphorylation to generate ATP for their housekeeping functions, there are fundamental metabolic differences between these two subsets. Our group recently demonstrated that memory $CD8^+$ T cells are able to rapidly induce glycolysis upon reactivation. This immediate-early glycolytic switch is required for memory recall response and it is regulated by the mTORC2-Akt axis. Interestingly, memory $CD8^+$ T cells have higher mitochondrial mass and functionality than their naïve counterparts. Whether the rapid increase in glucose metabolism in memory T cells also involves oxidation in the mitochondria via TCA cycle remains to be elucidated.

How and when mitochondrial biogenesis occurs in the naïve to effector transition is still unknown. The kinetics, regulation and functional implications of mitochondrial biogenesis in naïve $CD8^+$ T cells are the main focus of manuscript 1. Naïve $CD8^+$ T cells were activated *in vitro* and mitochondrial mass and functions were assessed. We found that mitochondrial mass was increased in naïve $CD8^+$ T cells early after activation and before the first division. In parallel to glycolysis, both mitochondrial respiration and mROS generation were increased in early-activated naïve $CD8^+$ T cells. Inhibition of mitochondrial biogenesis diminished activation-induced mROS generation and IL-2, TNF and IFN-γ secretion. Notably, direct inhibition of mROS had a similar effect on early-effector cytokine secretion. The study presented here assigned additional roles for mitochondrial biogenesis early after activation, and that this event is mROS dependent, which results in increased IL-2 secretion and the modulation of TNF and IFN-γ production.

How mitochondrial differences contribute to early effector response in memory $CD8^+$ T cells is still elusive. In manuscript 2, we studied the impact of glucose oxidation in mitochondria on early effector functions in both naïve and memory $CD8^+$ T cells. Metabolomic and glucose tracing experiments assessing metabolic intermediates in both subsets revealed that glycolysis and TCA cycle intermediates

were elevated in activated memory $CD8^+$ T cells upon activation. Moreover, we demonstrated that mitochondrial respiration was increased early after activation in memory $CD8^+$ T cells. Blocking mitochondrial respiration diminished early-recall response in memory $CD8^+$ T cells. This suggests that both glycolysis and glucose flux into the TCA are important for rapid IFN-γ secretion. Additionally, we also demonstrated that key components of the mTORC2-Akt axis are present in the mitochondria associated membrane of the endoplasmic reticulum in $CD8^+$ T cells, suggesting a close association between mTORC2-Akt signaling and mitochondrial function. These results further established metabolic differences between naïve and memory $CD8^+$ T cells. Thus, the resulting metabolic plasticity in memory $CD8^+$ T cells could be a requirement to support effector functions in competitive microenvironments.

Lastly, to mimic a $CD8^+$ T cell - APC interaction in *vitro* we established a protocol using dual antibody coupling on polystyrene beads and assessed distinct antibody ratios loaded on the beads. This is the topic of manuscript 3 (technical notes). We found that input ratios of antibody were not always directly reflected by the final ratio loaded on the beads. Moreover, differently loaded beads showed differences in $CD8^+$ activation, *in vitro.*

All together, the studies presented here contribute to a better understanding on how T cell metabolism supports immune function and could have implications for future strategies aiming to therapeutically manipulate $CD8^+$ effector and memory functions.

Abbreviations

Abbreviaton	Full name
2-DG	2-Deoxy-D-glucose
3PG	3-phophoglyerate
ABCB1	ATP-binding cassette transporter B1
ADP	Adenosine di-phosphate
AMP	Adenosine mono-phosphate
AMPK	AMP-activated protein kinase
ANT	Adenine nucleotide translocase
APC	Antigen-presenting cell, Allophycocyanin
ATP	Adenosine tri-phosphate
Ca^{2+}	Calcium
CD	Cluster of differentiation
CFSE	Carboxyfluorescein succinimidyl ester
CM	Central memory $CD8^+$ T cells
CoA	Coenzyme A
CRAC	Ca^{2+} release-activated Ca^{2+} channel
CTL	Cytotoxic effector T cells
EAE	Experimental autoimmune encephalomyelitits
ECAR	Extracellular acidification rate
ELISA	Enzyme-linked immunosorbent assay
EM	Effector-memory $CD8^+$ T cells
ER	Endoplasmic reticulum
ERRα	Estrogen-related receptor α
ERRβ	Estrogen-related receptor β
ERRγ	Estrogen-related receptor γ
ETC	Electron transport chain
F1,6 BP	Fructose-1,6-bisphosphate
$FADH_2$	Flavin adenine dinucleotide
FAO	Fatty acid oxidation
FBS	Fetal bovine serum
FCCP	Carbonyl cyanide 4-(trifluoromethoxy)phenylhydrazone
FITC	Fluorescein isothiocyanate
FSC	Forward scatter
GABP	GA-binding protein (NRF-2)
GAPDH	Glyeraldehyde-3-phophate dehydrogenase
HK	Hexokinase
IFN-γ	Interferon γ
IL-2	Interleukin 2
IP3R	Inositol 1,4,5-trisphosphate receptor
IS	Immunological synapse
KD	Dissociation constants
LDHA	Lactate dehydrogenase A
mAb	Monoclonal antibody
MAM	Mitochondrial associated membrane
MCU	Mitochondrial calcium uniporter
MESF	Molecules of equivalent soluble fluorochrome
MFI	Mean fluorescence intensity
MHC	Major histocompatibility complex
MPEC	Memory precursor effector cell
mROS	mitochondrial reactive oxygen species
mtDNA	mitochondrial DNA
MTG	Mitotracker green
MTR	Mitotracker red
mTORC	Mammalian target of rapamycin complex
NADH	Dihydronicotinamide adenine dinucleotide
NRF-1	Nuclear respiratory factor 1
OXPHOS	Oxidative phosphorylation
OCR	Oxygen consumption rate
PB	Pacific blue

PBMC	Peripheral blood mononuclear cells
PBS	Phosphate buffered saline
PDH	Pyruvate dehydrogenase
PE	Phycoerythrin
PEP	Phosphoenol pyruvate
PGC-1α	Peroxisome proliferator-activated receptor γ coactivator-1 α
PGC-1β	Peroxisome proliferator-activated receptor γ coactivator-1 β
PI3K	Phosphatidylinositol 4,5-bisphosphate 3-kinase
PPARα	Peroxisome proliferator-activated receptor α
PPARγ	Peroxisome proliferator-activated receptor γ
PPARδ	Peroxisome proliferator-activated receptor δ
PRC	PGC-1-related coactivator
qPCR	quantitative polymerase chain reaction
rep. Ab	reporter antibody
RIP140	Receptor-interacting protein 140
RM	Tissue-resident memory
SCM	Stem cell memory $CD8^+$ T cells
SD	Standard deviation
SLE	Systemic lupus erythematosus
SLEC	Short-lived effector cell
SRC	Spare respiratory capacity
SSC	Side scatter
TBP	TATA-box binding protein
TCR	T cell receptor
TCA	Tricarboxylic acid cycle
TEM	Transmission electron microscopy
TFAM	Transcription factor a, mitochondrial
TFB1M	Transcription factor B1, mitochondrial
TFB2M	Transcription factor B2, mitocondrial
TIL	Tumor infiltrating lymphocyte
TNF	Tumor necrosis factor
VDAC	Voltage-dependent anion selective channel

1. Introduction

1.1. $CD8^+$ T cells

1.1.1. Naïve to effector to memory transition in $CD8^+$ T cells

$CD8^+$ T cells are central players in the adaptive immune response, controlling intracellular infections and eradicating tumor cells. Each T cell has a unique T cell receptor (TCR) to recognize one specific antigen. After positive and negative selection in the thymus, naïve $CD8^+$ T cells are released into the circulation. They migrate between the blood circulation and through secondary lymphoid tissues to survey all areas of the body for their cognate antigen (1-3). Within the lymph-nodes, naïve $CD8^+$ T cells scan antigen-presenting cells (APC) such as dendritic cells for their specific antigen (4). APCs are able to present antigens as major histocompatibility complex class I (MHC I) - peptide complexes. Naïve $CD8^+$ T cells become primed if they recognize their specific antigen by their TCR in the presence of co-stimulatory signals and inflammatory cytokines (5-7). This activation is followed by a rapid clonal expansion (8,9), differentiation into cytotoxic effector $CD8^+$ T cells (6,10), and migration towards the inflamed tissues (3,11).

Effector $CD8^+$ T cells recognize and directly eliminate infected, transformed and allogeneic graft cells expressing their specific antigen (12). They kill target cells by inducing apoptosis in a calcium (Ca^{2+})-dependent (Perforin, Granzyme B) and a Ca^{2+}-independent (FasL-Fas interaction) manner (13). In addition to this cell-mediated cytotoxicity, effector $CD8^+$ T cells produce cytokines such as interferon (IFN)-γ and tumor necrosis factor (TNF), which alter viral gene expression in infected cells to facilitate viral clearance (14). However, effector $CD8^+$ T cells don't form a uniform population, there are distinct effector subpopulations at the peak of the immune response. Short-lived effector cells (SLEC) (**Fig. 1** blue population) and memory precursor effector cells (MPEC) (**Fig. 1** red population) can be discriminated due to their differences in effector function, migration, proliferation capacity and potential to become memory $CD8^+$ T cells (15,16). SLEC are the most abundant effector subpopulation at the peak of the expansion phase, however in contrast to the MPEC the majority of this antigen specific $CD8^+$ T cell population undergoes apoptosis when the pathogen is cleared (8,15,17). Only a small subset of antigen specific $CD8^+$ cells survives this contraction phase and forms a long-lived T cell pool, which can respond faster and stronger after reinfection (10,18,19) **(Fig. 1).**

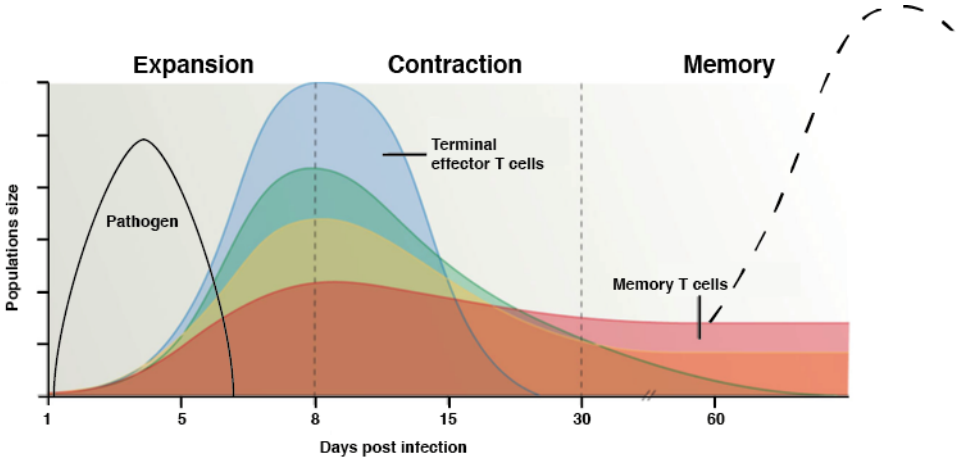

Figure 1) Memory CD8+ T cell generation
Adapted by permission from Macmillan Publishers Ltd: Nature Reviews Immunology. Kaech et al. 2012 (16)

1.1.2. Different CD8$^+$ memory subsets

Similar to the differences within the effector population, the human CD8$^+$ memory population is heterogeneous and contains distinct memory subsets. They can be separated on the basis of specific surface markers and show differences in effector functions, proliferation capacity, multipotency and migration (**Fig. 2**) (20,21).

Central-memory (CM) and **effector-memory** (EM) are the two most abundant CD8$^+$ memory subsets in the circulation (22,23). They both express the memory marker CD45RO (**Fig. 2**), but not the alternative splicing variant CD45RA (21). These two subsets are distinct in their functional and migratory capacity (22) and can be discriminated due to the different expression of both CCR7 and CD62L (both lymph-node homing molecules). CM CD8$^+$ T cells co-express both CCR7 and CD62L and are predominantly located in the lymphoid tissue. Compared to EM, they produce more interleukin (IL)-2, have a higher proliferative capacity, but lack the immediate effector function of their EM counterparts (22,24,25).

EM lack the expression of CCR7 and CD62L and are located mainly in non-lymphoid peripheral tissue. They are able to migrate to inflamed tissue and display immediate effector functions such as IFN-γ and TNF secretion (25,26). Due to their peripheral location it was initially thought that EM are permanently resident in the periphery. However, recent studies showed that the **tissue resident memory T cells (RM)** are a separate subpopulation within the CD8$^+$ memory population.

RM form and maintain a long-lived population for effective host defense in the periphery (23). RM can be found in various tissues after infection (skin, lung, brain, sensory ganglia, salivary glands and the female reproductive tract) (27). Tissue-resident memory can be distinguished from circulating memory subsets due to their expression of high level of CD103 and CD69 (28,29).

T stem cell memory cells (SCM) were also recently found in humans and contribute towards 2-3% of the total circulating $CD8^+$ T cells. As their name indicates they have stem-cell like qualities such as high proliferative, self-renewing and multipotent capacity to give rise to CM, EM and effector T cells (26).

These differences within the $CD8^+$ memory populations in localization, proliferative and effector capacity contribute to optimal protective immunity in the context of a recall response. Both EM and RM are able to mount immediate effector functions at the point of pathogen entry, whereas SCM and CM can generate large numbers of secondary effector cells (16).

Proliferation, differentiation and acquiring effector functions are energetically demanding processes (30). This suggest that naïve $CD8^+$ T cells have to undergo substantial adaptation in their cellular metabolism to provide both energy and metabolic intermediates following activation.

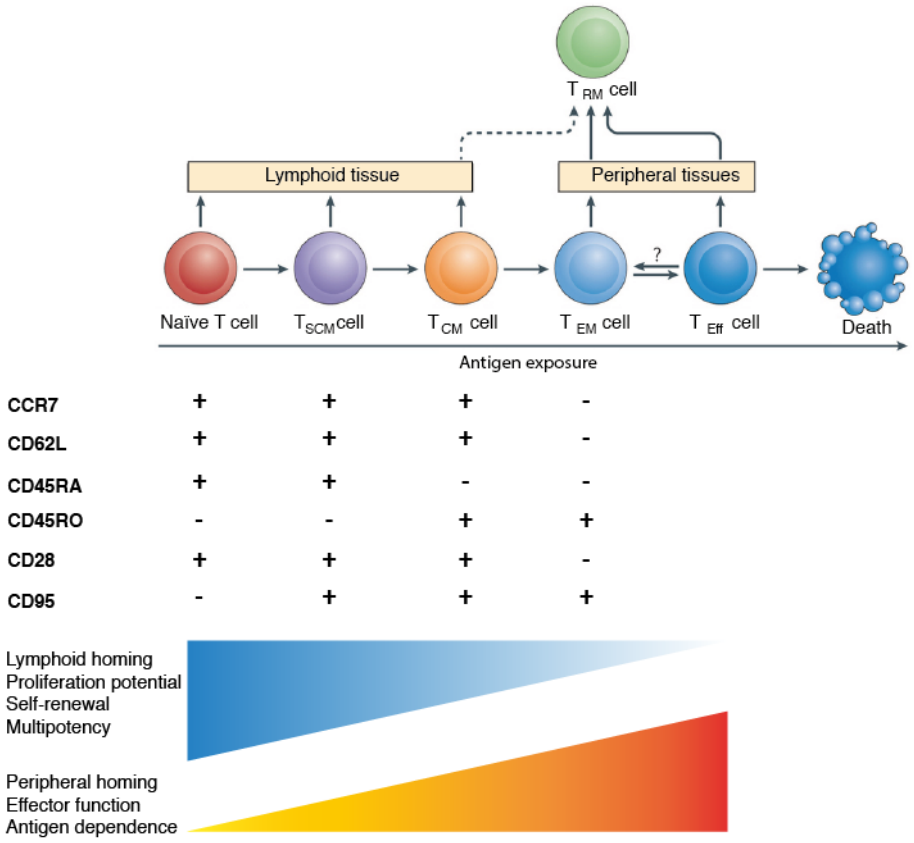

Figure 2) Memory CD8+ heterogeneity
Adapted by permission from Macmillan Publishers Ltd:
Nature Reviews Immunology. Farber et al. 2014 (21) and Mahnke et al. 2013 (20)

1.2. Mitochondria

Mitochondria are organelles which operate as a central hub for both energy production (catabolic) and provision of metabolic intermediates (anabolic) required for macromolecule biosynthesis (31,32). However, they are essential for a broad range of cellular processes summarized in **Fig. 3** (33)**.**

The mitochondrion contains two membranes, which create four different sub-compartments. The outer and the inner membrane shape the inter-membrane space(34). The inner membrane forms cristae to increase the surface area towards the mitochondrial matrix (**Fig. 3)** (35,36). However, more recent evidence indicate a more complex reticular-network like structure (37), which is highly dynamic and a balance between mitochondrial mobility, fusion and fission in response to changing circumstances contributing to optimal mitochondrial function (36,38,39).

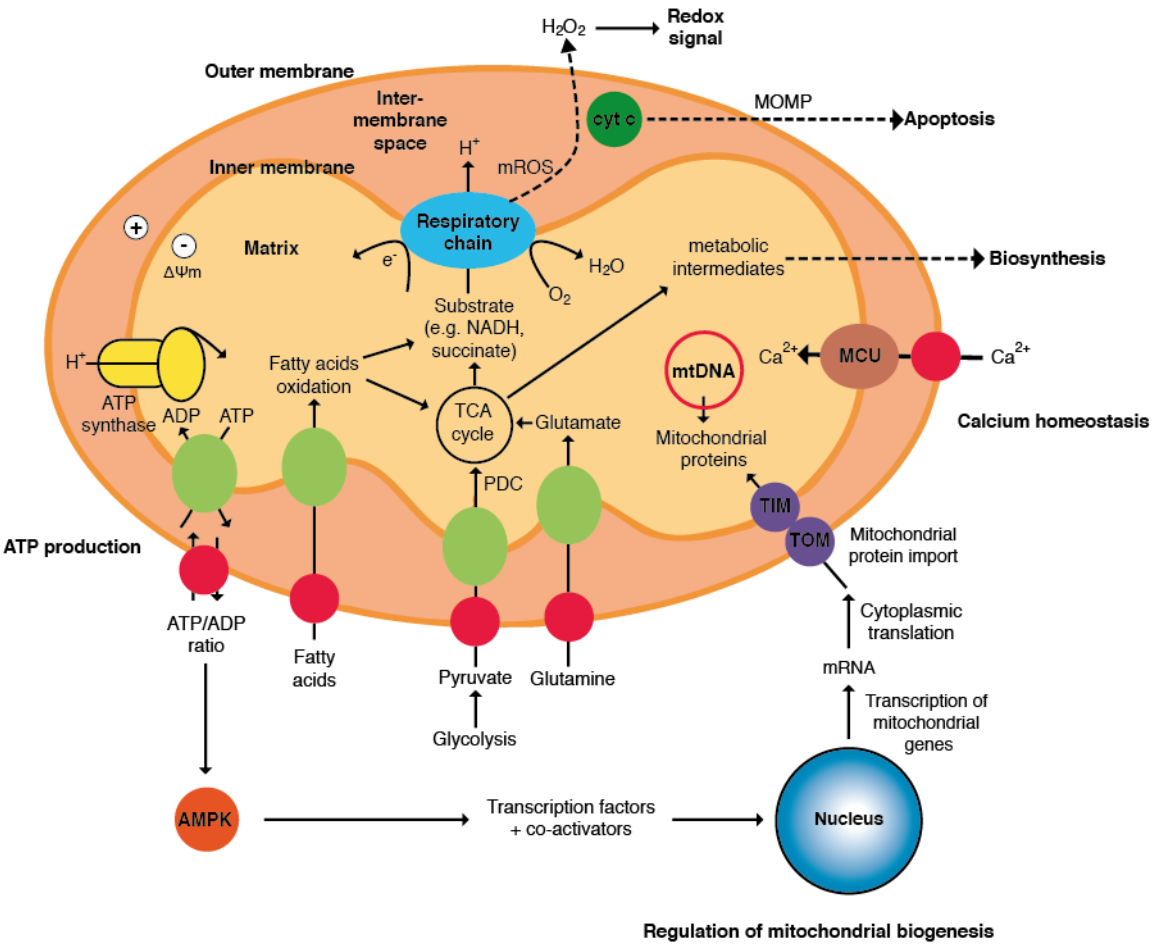

Figure 3) Mitochondrial function Adapted from Trends in Pharmacological Sciences. Smith et al. 2012 (33)

1.2.1. Mitochondria as central hub for energy and metabolic intermediates production

Glucose gets converted to pyruvate through glycolysis in the cytoplasm. Pyruvate, glutamine and fatty acids can enter the mitochondrial matrix through specific mitochondrial transporters. Subsequently, pyruvate is converted by pyruvate dehydrogenase (PDH), and fatty acids through β-oxidation into acetyl coenzyme A (CoA), which enters the tricarboxylic acid (TCA) cycle. Alternatively glutamine can enter the TCA cycle via conversion to glutamate and α-ketoglutarate. The TCA cycle completely oxidizes the substrates to CO_2 and electron donors. Alternatively, TCA cycle intermediates can be used through different biosynthetic pathways to generate glucose, amino acids, lipids, heme and nucleotides (33,36,40-42)(**Fig. 3**).

Electrons obtained by glycolysis, the TCA cycle and β-oxidation accumulate on the reduced electron carrier NADH or $FADH_2$ (33). Through oxidative phosphorylation (OXPHOS) these electron carriers fueling electrons into the electron transport chain (ETC) to build up an electrochemical gradient, which is required to generate adenosine tri-phosphate (ATP) (43)(**Fig. 4**). The ETC consists of five multi-subunit complexes, which are located within the inner mitochondrial membrane. Complex I of the respiratory chain oxidizes NADH to NAD^+ (33). Electrons from the TCA cycle can also feed -via succinate and $FADH_2$- to complex II (33). Both Complex I and II pass electrons via Coenzyme Q (CoQ) to Complex III and subsequently via Cytochrome c to Complex IV. Complex IV finally transfers the electrons to molecular oxygen as final electron acceptor to reduce oxygen to water. The redox energy generated through the electron transfer can be used by Complexes I,III and IV to pump protons across the inner membrane into the inter-membrane space. This builds up an electrochemical proton gradient ($\Delta\Psi_m$) across the mitochondrial inner membrane, known as membrane potential (44). This membrane potential can be used by Complex V (ATP-Synthase) to generate ATP from adenosine di-phosphate (ADP) and phosphate. ATP is exported to the cytoplasm in exchange with ADP through adenine nucleotide translocase (ANT) (**Fig. 3**) (32,33).

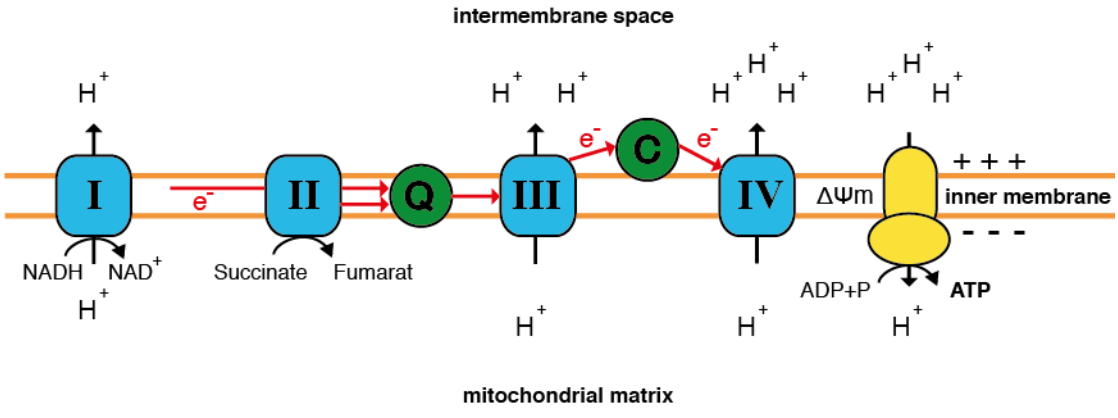

Figure 4) Electron transfer chain and mitochondrial ATP generation

A recently discovered additional function of mitochondrial respiration is to provide electron acceptors by oxidation of cellular NADH to regenerate NAD^+. This is required for aspartate biosynthesis in the mitochondrial matrix important to enable cell proliferation (44,45).

In addition to both catabolic (energy) or anabolic processes (metabolic intermediates), mitochondria can act as signaling organelles.

1.2.2. Mitochondria as signaling organelle

Mitochondria have a central role in cellular metabolism and retrograde signals from the mitochondria to the rest of the cells are important to confirm their functional status. Intermediates or products of mitochondrial functions such as ATP, mitochondrial reactive oxygen species (mROS), TCA cycle intermediates or mitochondrial Calcium (Ca^{2+}) can act as signals (46). These metabolic checkpoints are important prior to cell-fate decisions such as differentiation or proliferation (32,46,47).

Since ATP production is one of the key mitochondrial functions, inhibition of the respiratory chain or mitochondrial ATP synthesis can result in a decrease in cellular energy status and can be detected by the energy sensor AMP-activated protein kinase (AMPK) (48). AMPK is an important metabolic checkpoint, activated by an increase in AMP:ATP or ADP:ATP ratios (49). It can restore energy homeostasis by activation of catabolic reactions to generate more ATP, inducing mitochondrial biogenesis and by inhibition of ATP-consuming (anabolic) processes (49,50).

Beside ATP, mROS are additional products of the respiratory chain. Complex I, II and III can provide electrons directly to oxygen in the form of mROS (46,51). Originally mROS were thought to be byproducts of the respiratory chain, however more recent evidence indicated the importance of low level mROS as signals for the cell (46,52).

In contrast to ATP and mROS, mitochondrial Ca^{2+} uptake can act both as an anterograde (cell-mitochondria) and retrograde (mitochondria-cell) signal (42). Ca^{2+} released by the endoplasmic reticulum (ER) can be taken up through the mitochondrial calcium uniporter (MCU) into the mitochondrial matrix (47). This increase in mitochondrial Ca^{2+} concentration can increase the functionality of PDH and different TCA cycle enzymes and thereby stimulate OXPHOS (32,41,53). However, as a consequence of mitochondrial Ca^{2+} uptake, the cytosolic Ca^{2+} concentration alters and influences Ca^{2+}-dependent signaling events (47).

TCA cycle intermediates such as citrate, released into the cytosol can be cleaved to acetyl-CoA and modulate protein activity through protein acetylation (32,47,54).

In addition to intermediates or end products of mitochondrial functions, the outer mitochondrial membrane associated to the endoplasmic reticulum (mitochondrial associated membrane or MAM) can serve as a scaffold for signaling complexes and facilitate calcium flux from the ER to the mitochondrion (41,46,55). An increased MAM formation is associated with increased mitochondrial Ca^{2+} accumulation and mROS generation (56).

1.2.3. Mitochondrial adaptation and biogenesis

Given the broad range of mitochondrial function and cellular requirements, a constant adaptation of mitochondrial protein composition is important to respond accurately to different physiological and environmental conditions (57).

The vast majority of mitochondrial proteins (around 1500) are nuclear encoded, are being synthesized within the cytosol and translocated into the mitochondrion (58). However, the OXPHOS system contains genetically chimeric multi-subunit complexes, which are assembled from both nuclear and mitochondrial DNA (mtDNA) encoded proteins (59,60). The mtDNA encodes 13 essential subunits of the ETC and ATP synthase, 2 ribosomal RNAs and 22 transfer RNAs (61) and its replication, transcription, translation and repair are controlled through nuclear encoded proteins(36).

1.2.4. Regulation of mitochondrial adaptation and biogenesis

Given their dual origin and tissue- and signal-specificity, mitochondrial protein expression is highly regulated and coordinated. This regulation is controlled through transcription co-activators and transcription factors in a hierarchical structure (33,58,62) (**Fig. 5**).

The transcription co-activator of the peroxisome proliferator activated receptor gamma coactivator-1 (PGC-1) family is composed of PGC-1α, PGC-1β and PGC-related co-activator (PRC) (57). The activation of these transcription co-activator is regulated in response to a variety of signals through expression and post-translational modifications (63). PGC-1 family members have a tissue-specific expression pattern (64,65) and regulate overlapping gene expression programs (63). They do not bind to DNA directly but coordinate nuclear-encoded mitochondrial gene expression through interaction with several transcription factor families (60). These transcription factors stimulate the expression of nuclear encoded mitochondrial genes for distinct mitochondrial functions (**Fig. 5**)(66).

Mitochondrial transcription factor A (TFAM) is a nuclear encoded protein, which synchronizes nuclear and mitochondrial gene expression by regulating mtDNA replication, protein expression and maintenance (39,60,67).

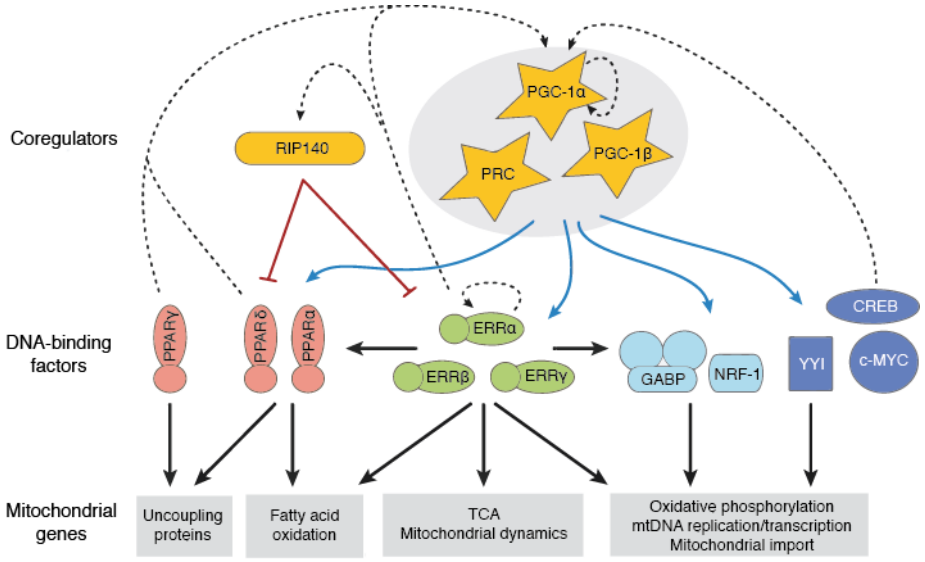

Figure 5) Regulation of mitochondrial biogenesis from Annual Reviews of Physiology. Hock et al. 2009 (62)

Mitochondrial research has been performed predominantly in mitochondrial rich tissues such as skeletal muscle, liver, heart, kidney and neural tissue. However, the regulation and composition of mitochondrial protein is highly tissue specific (68).

Given the central role of mitochondria in cellular metabolism, anabolic processes and signaling, mitochondrial functions are likely to be important in the context of the $CD8^{+}$ mediated immune response.

1.3. T cell metabolism and immune function

1.3.1. Metabolic reprogramming in T cells upon activation

Quiescent naïve and memory T cells display unique metabolic signatures compared to that of activated effector cells (69). The former rely predominantly on fatty acid, pyruvate and glutamine oxidation through the TCA cycle (2,70). The resulting reducing intermediates can be used through OXPHOS to generate ATP for housekeeping functions in quiescent T cells (2).

T cell activation through the specific antigen and additional co-stimulatory signals induce metabolic reprogramming from OXPHOS to aerobic glycolysis (Warburg effect). Glucose uptake is increased and is converted into pyruvate and subsequently into lactate despite the presence of sufficient oxygen (71,72) (**Fig. 6**). Although aerobic glycolysis is less efficient to generate ATP per molecule of glucose, it allows the activated T cell to generate rapidly ATP and biochemical intermediates and maintaining redox balance (30). These intermediates of the glycolytic pathway can be used as precursors fueling cellular biosynthesis pathways such as nucleotide and amino acid synthesis (**Fig. 6**) (73). Inhibition of glycolysis results in decreased $CD8^+$ proliferation and effector function (IFN-γ, TNF and cytolytic activity) (74). In addition to glucose, glutamine uptake is increased upon activation in T cells; both being driven by simultaneous CD3 and CD28 stimulation (75,76). T cells upregulate enzymes converting glutamine to α-ketoglutarate to replenish TCA cycle intermediates used for biosynthesis (**Fig. 6**) (76,77). In this process called glutaminolysis, glutamine acts as a nitrogen and carbon source for both biosynthesis and mitochondrial respiration and is required for cell growth, proliferation and full induction of IL-2 (76-78).

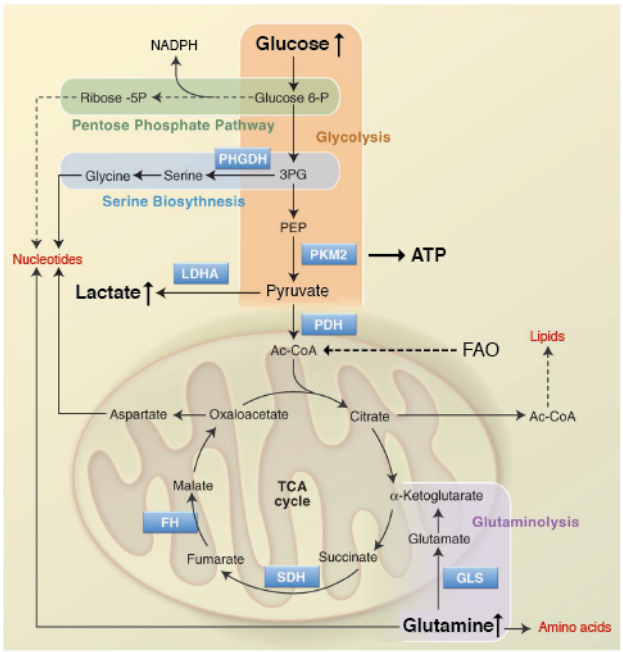

Figure 6) Metabolic pathways and biosynthesis in activated T cells
from Science. Pearce et al. 2013 (73). Reprinted with permission from AAAS.

Taken together, metabolic reprogramming towards aerobic glycolysis and glutaminolysis is important to provide biochemical intermediates and ATP required for T cell expansion and effector functions (77-79).

1.3.2. Mitochondrial respiration and T cell proliferation and effector function

Although aerobic glycolysis and glutaminolysis increase during T cell activation, mitochondrial OXPHOS still plays an important role. Moreover, mitochondrial respiration and glycolysis have been shown to be intricately connected, which is critical for early metabolic reprogramming in T cells (80). Mitochondrial associated hexokinase (HK) utilizes mitochondrial ATP to phosphorylate glucose to glucose 6-phospate (81). Inhibition of mitochondrial ATP generation or dissociation of HK from the mitochondria impairs the glycolytic switch and subsequently proliferation in memory $CD8^+$ T cells (79-81). Therefore, mitochondrial respiration has a significant role in T cell activation and is required for glycolytic reprogramming and consequently for proliferation (78). Interestingly, T cells which are already proliferating do not require mitochondrial ATP for further proliferation, suggesting the important role for mitochondrial ATP in glycolytic reprogramming is restricted to the early phase of activation (81).

Additionally, naïve $CD8^+$ T cells also increase both mitochondrial membrane potential and production of mROS upon activation (82) (**Fig. 7**). Blocking electron flux in both $CD8^+$ and $CD4^+$ T cells diminishes activation-induced mROS generation and significantly impacts cytokine secretion and proliferation (78,83). IL-2 secretion is particularly linked to mROS generation in T cells, since both mitochondrial-targeted antioxidant and inhibition of mitochondrial membrane potential diminished activation-induced IL-2 expression (78). Moreover, IL-2 is important to sustain glycolysis in effector $CD8^+$ T cells, underlining the interconnection of both mitochondrial respiration and glycolysis in activated T cells (71).

In conclusion, activated T cells increase mitochondrial respiration for both ATP generation and mROS production. Mitochondrial ATP is required early after activation for glycolytic reprogramming and consequently supporting proliferation. Whereas mROS act as important signals supporting T cell activation and effector function (42).

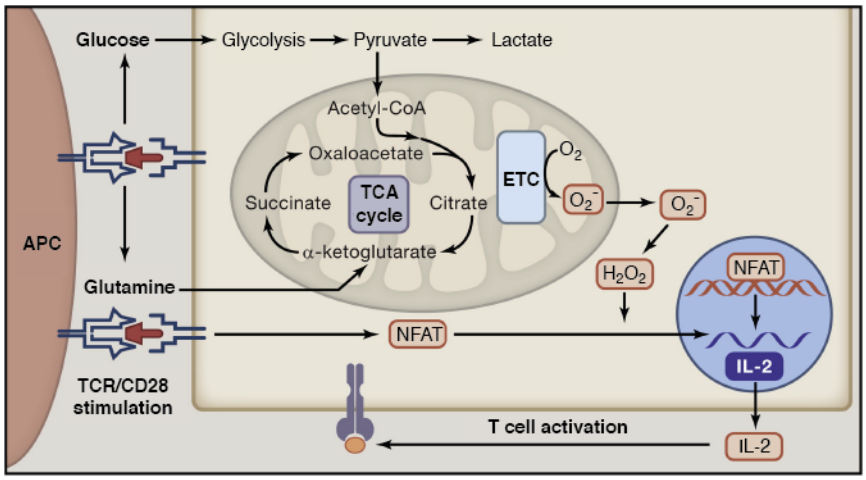

Figure 7) Metabolic reprogramming in activated T cells
Reprinted from Immunity. Weinberg et al. 2015 (42), with permission from Elsevier.

1.4. Metabolic differences in CD8$^+$ T cell subsets

Memory CD8$^+$ T cells are able to proliferate faster and produce more cytokines (IFN-γ and IL-2) upon secondary infection (18,19,81). Although, both naïve and memory CD8$^+$ T cells use OXPHOS to generate ATP, there are fundamental differences in cellular metabolism, supporting this memory recall response.

1.4.1. Glycolytic differences in CD8$^+$ T cell subsets

As mentioned above, effector CD8$^+$ T cells use glycolysis to a higher extent than both naïve and memory CD8$^+$ T cells (84). However, both naïve and memory CD8$^+$ T cells increase glycolysis immediately upon activation, but only memory CD8$^+$ T cells are able to sustain this increase in glycolysis (81,85). This glycolytic switch is dependent on both CD3 and CD28 stimulation (75,85). We could show that memory CD8$^+$ T cells are metabolically primed, having more abundant cytosolic glyeraldehyde-3-phosphate dehydrogenase (GAPDH), and furthermore that this “immediate-early” glycolytic switch is required for their early effector function (IFN-γ production) (85).

This finding adds to the Warburg effect a new role beyond supporting proliferation; it regulates the immediate-early effector response of memory CD8$^+$ T cells(85).

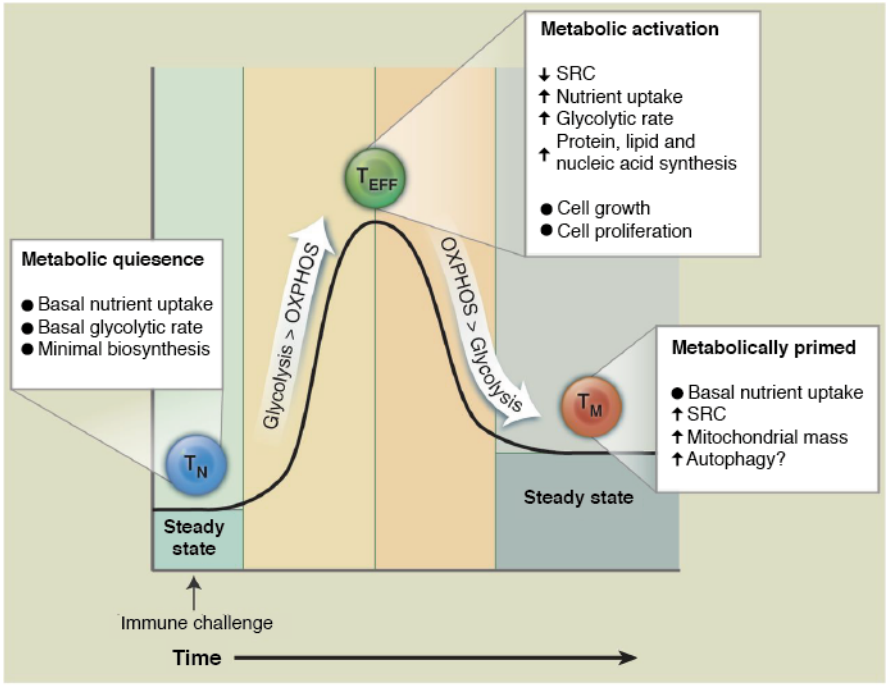

Figure 8) Metabolic differences in CD8+ T cell subsets from Science. Pearce et al. 2013 (73)
Reprinted with permission from AAAS.

1.4.2. Mitochondrial differences in CD8$^+$ T cell subsets

Although activated T cells switch towards aerobic glycolysis, mitochondrial respiration is not replaced by glycolysis. As described above, bulk T cells and especially memory CD8$^+$ T cells increase mitochondrial respiration early after activation (78,80,81). Moreover, the formation of an immunological synapse (IS) induce Ca^{2+} release-activated Ca^{2+} (CRAC) channel accumulation and mitochondrial translocation towards the IS in T cells (86). Mitochondrial calcium uptake in close proximity to the IS is important to buffer high local Ca^{2+} concentration to sustain Ca^{2+} flux into the cell and contribute to Ca^{2+} dependent T cell activation (86,87).

This suggests mitochondrial function is important early after activation in T cells. Moreover, there are fundamental differences in mitochondrial mass and functionality between naïve and memory CD8$^+$ T cells.

1.4.2.1. Differences in mitochondrial mass

Memory CD8$^+$ T cells have more mitochondrial mass and mtDNA than both naïve and effector CD8$^+$ T cells (**Fig. 8**) (84). Moreover, upon reactivation memory CD8$^+$ T cells are able to increase mitochondrial respiration and glycolysis more than activated naïve CD8$^+$ T cells and they generate more ATP (81). In addition to the difference in mitochondrial content of memory CD8$^+$ T cells, the intracellular mitochondrial location is distinct. Interestingly, in memory CD8$^+$ T cells mitochondria appear to be networked and closely associated to the ER, suggesting potential functional implications for Ca^{2+} homeostasis and signaling (30,88).

1.4.2.2. Differences in mitochondrial substrate utilization

We and others could demonstrate that memory CD8$^+$ T cells have a higher mitochondrial spare respiratory capacity (SRC) than naïve CD8$^+$ T cells (**Fig. 8**) (84,85). This parameter is the difference between the basal and the maximal respiration and indicate the mitochondrial reserve to react to increased workload or stress (84). It appears that fatty acid oxidation (FAO) significantly contributes to this reserve capacity, since inhibition of FAO impairs both SRC and proliferation in memory CD8$^+$ T cells (81). Interestingly, in contrast to effector cells, memory CD8$^+$ T cells are independent of external fatty acids. Rather, they use glucose to generate lipids and then use lipolysis to provide fatty acids for FAO and mitochondrial respiration. Blocking fatty acid synthesis decrease both survival and proliferation in memory CD8$^+$ T cells (88).

In conclusion memory $CD8^+$ T cells are metabolically primed, having an increased mitochondrial mass, SRC and the capacity to generate substrates for FAO. Together, this supports a greater increase in mitochondrial OXPHOS upon re-encounter with antigen (73,81) and suggests an important role of mitochondrial function in memory $CD8^+$ T cells recall response.

1.5. Mitochondrial biogenesis in T cells

How mitochondrial biogenesis is regulated in $CD8^+$ T cells, such that memory cells have increased mitochondrial mass, is largely unknown. Mitochondrial mass, membrane potential and mtDNA copy numbers increase early after activation in T cells when studied *in vitro* (89). Conversely, as previously mentioned, *bona fide*, *ex vivo* effector $CD8^+$ T cells have lower mitochondrial mass than their naïve counterparts (84).

Interestingly, the transcription co-activators PGC-1α and PGC-1β are both expressed in quiescent $CD4^+$ T cells. However, PGC-1β is 200 times higher expressed in comparison to PGC-1α (90). The expression of the transcription factor estrogen-related receptor-α (ERRα) is increased early after activation. Blocking ERRα expression impairs expression of genes encoding both ETC components and proteins involved in glucose metabolism, subsequently reducing glucose uptake, mitochondrial respiration and mitochondrial membrane potential. Interestingly ERRα -/- $CD4^+$ T cells produce less cytokines (IFN-γ and IL-2) and have a decreased *in vitro* $CD4^+$ differentiation. Moreover, ERRα deficient mice are not able to accumulate effector or memory $CD4^+$ and $CD8^+$ T cells (90).

A recent study indicated the central role of TFAM for the expression of mtDNA-encoded subunits of the ETC in $CD4^+$ T cells. Both TFAM expression and mtDNA levels increase early after activation. Consequently, TFAM deficient $CD4^+$ T cells have an impaired ETC functionality and reduced mitochondria ATP, mROS generation and NAD^+/NADH homeostasis. These cells have deficits in proliferation and surprisingly develop a stronger inflammatory response both *in vitro* and *in vivo* (39).

In conclusion, there is little evidence in $CD8^+$ T cells for when mitochondrial biogenesis occurs and how it is regulated. However, evidence from $CD4^+$ T cells suggests mitochondrial biogenesis is important for T cell effector maturation and proliferation.

2. Hypothesis

Studies both in humans and in murine models indicate important mitochondrial differences between naïve and memory $CD8^+$ T cells (84,85). However, there is little and conflicting evidences at which stage of naïve to memory transition mitochondrial biogenesis occurs (84,89).

Moreover, we demonstrated the importance of the metabolic switch towards glycolysis for early effector functions in memory $CD8^+$ T cells (85). Interestingly memory $CD8^+$ T cells increase mitochondrial respiration early after activation to a higher extent than naïve $CD8^+$ T cells (81). However, how mitochondrial differences contribute to early effector response in memory $CD8^+$ T cells is still elusive.

To address these questions, we assessed the impact of mitochondrial biogenesis in naïve $CD8^+$ T cells early after activation (Manuscript 1) and studied the impact of glucose oxidation in mitochondria on early effector functions in both naïve and memory $CD8^+$ T cells (Manuscript 2). Additionally, since polarized activation is important for mitochondrial translocation towards the immune synapse, we established an *in vitro* bead-based T cell activation protocol (Manuscript 3, Technical note)(**Fig. 9**).

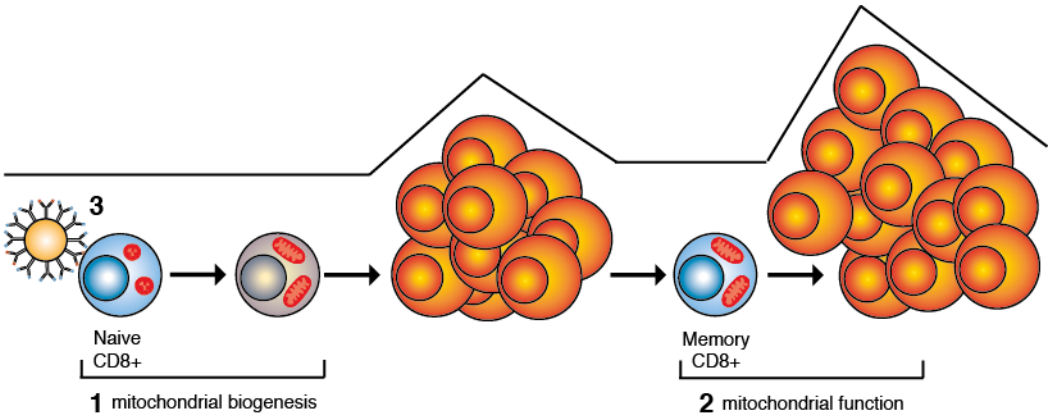

Figure 9) Graphical overview of different manuscripts

3. Mitochondrial biogenesis in human naïve CD8$^+$ T cells supports early cytokine secretion via mitochondrial ROS (Manuscript 1)

3.1. Introduction

T cell activation by cognate MHC–peptide complexes and additional co-stimulatory signals induce a metabolic switch from mitochondrial respiration to aerobic glycolysis (72). Although aerobic glycolysis is less efficient in generating ATP per molecule glucose, it allows the activated T cell to rapidly accumulate biochemical intermediates required for T cell expansion and effector maturation (84,91,92).

This concept of metabolic switch is typically focused on the massive upregulation of glycolysis in activated T cells, and many studies have focused on dissecting the functional implications of increased glycolysis on T cell effector functions (79,85,93). An often ignored aspect in the metabolic reprogramming of activated T cells is the parallel increase in mitochondrial respiration (78,80). Mitochondrial ATP is important for the initial phase of activation and required for proliferation (79,80). T cells increase their mitochondrial mass following activation (89). Intriguingly, *bona fide* effector cells have lower mitochondrial mass and mtDNA copy number than both quiescent naïve and memory CD8$^+$ T cells (84). Together, these data suggest that the dynamic regulation of mitochondrial biogenesis is an important aspect of T cell responses to cognate antigens. However, how mitochondrial biogenesis supports and impacts early CD8$^+$ T cell activation, differentiation and effector maturation has not been elucidated.

In this report, we demonstrated that human naïve CD8$^+$ T cells increase mitochondrial mass and key mitochondrial functions early after activation, prior to the first round of cell division. This increase in mitochondrial functionality was coupled to the increased accumulation of activation-induced mROS and consequently early cytokine secretion. Surprisingly in addition to IL-2, both TNF and IFN-γ secretion were sensitive to mitochondrial biogenesis and mROS inhibition. These findings revealed a connection of mitochondrial biogenesis and early effector function in naïve CD8$^+$ T cells.

3.2. Materials and Methods

3.2.1. $CD8^+$ Isolation

Blood samples were obtained from healthy blood donors as buffy coats after written informed consent (Blood donor centre, Basel). Peripheral blood mononuclear cells (PBMC) were isolated by standard density-gradient centrifugation protocols (Lymphoprep Fresenius Kabi, Norway)(85). $CD8^+$ T cells were positively selected using magnetic $CD8^+$ beads (MiltenyiBiotec, Germany) following manufacturer's instructions. Cells were rested overnight for flow sorting accessibility in RPMI-1640 medium (Gibco, USA) containing 10% fetal bovine serum (FBS, Gibco, USA), 50U/ml penicillin and 50µg/ml streptomycin (Gibco, USA) (R10FBS).

3.2.2. Cell Sorting

For isolation of naïve $CD8^+$ T cells, positively selected $CD8^+$ were incubated with allophycocyanin (APC)-conjugated anti-CD62L (ImmunoTools, Germany) and pacific blue (PB)-conjugated anti-CD45RA (Beckman Coulter, USA). $CD62L^+$ $CD45RA^+$ $CD8^+$ T cells were sorted with a BD influx cell sorter (BD Bioscience, USA) (**Fig. S1**). Cells were then rested for 4 hours in R10FBS at 37°C prior to further experiments.

3.2.3. Activation beads

Activation beads were coated and assessed as described in the technical note (Manuscript 3). Briefly, to load antibodies on beads, 100µl of a 2.5% suspension of Polybead Microspheres 4.5µm (Polyscience Eppenheim) and 900µl borate buffer containing 0.1M boric acid pH8.5 (Sigma-Aldrich) were prepared according to manufacturer's instructions. 100µg anti-human CD28 IgG1 antibody (CD28.2 Biolegend, USA) diluted in 100µl borate buffer was added to beads and incubated for 30min at room temperature. Thereafter, 1µg anti-human CD3 IgG2a antibody (HIT3a, Biolegend, USA) was diluted in 300µl borate buffer and gently mixed with the beads for 30min. Blocking and storage of antibody-loaded beads was performed according to manufacturer's instruction.

Antibody coupling was tested using 2^{nd} antibodies against IgG1 or IgG2a (SouthernBiotech, USA) respectively. To determine the amount of antibody molecules per bead Quantum MESF APC and PE (Bangslab, USA) were used. Data were acquired using a BD AccuriC6 flow cytometer (Becton Dickinson, USA) and analyzed with FlowJo 10.0.8 (Tree Star, USA).

3.2.4. T cell activation

Unless otherwise stated, sorted naïve $CD8^+$ T cells were plated into flat-bottom 96 well plates ($3x10^5$ cells per well) and stimulated using activation beads or control beads ($6x10^5$ beads per well) in R10FBS.

3.2.5. Proliferation and cell growth

Cells were loaded prior to activation with 5µM of the cell-proliferation dye carboxyfluorescein succinimidyl ester (CFSE, Molecular probes, USA) according to manufacturer's instructions. Proliferation and forward scatter were measured every 12h after activation using a BD AccuriC6 flow cytometer and analyzed with Flowjo 10.0.8 (Tree Star, USA).

3.2.6. Mitotracker green and red

Cells were harvested every 12h and incubated for 20min at 37°C/5% CO_2 with 100nM Mitotracker green (MTG, Invitrogen, USA) or 100nM Mitotracker red (MTR, Invitrogen, USA) respectively. Cells were washed twice using staining buffer (PBS plus 1% bovine serum albumin) at 1800 RPM for 3min each. Cells were then measured and analyzed as described above(94).

3.2.7. Electron microscopy

Transmission electron microscopy (TEM) was performed at the Biocenter (University of Basel, CH) as previously described(95). Briefly, cells were washed twice using cold PBS and sequentially fixed in Karnofski 3% paraformaldehyde and 0.5% glutaraldehyde for 1h. Cells were reduced using 1% osmium tetraoxide, embedded for 24-48h at 60°C and cut into 60nm sections using microtom Ultracut E (Leica). Micrographs were obtained with a Morgagni 268 transmission electron microsocope (FEI, Hillsboro OR, USA) at 80kV. To quantify mitochondrial, nuclear and cytoplasmic area Image J software (NIH, USA) was used.

3.2.8. mtDNA

Cell pellets were washed twice using cold PBS. Total cellular DNA was isolated as previously described (89). Real time PCR was performed using the Taqman techniques and the 7500 Fast Real time PCR system (Applied Biosystems, USA). Commercially designed primers from LifeTechnology were used to probe for both DNA copies (Hs03929097_g1, GAPDH) and mtDNA copies

(Hs02596864_g1, MT-CO1). Absolute copy numbers per cell were determined using plasmid standards inserted with the PCR product for MT-CO1 (forward, 5'-TTCGGCGCATGAGCTGGAGTC-3', and reverse, 5'- TTGCTTCCGTGGAGTGTGGCG) or for GAPDH (forward, 5'-AGTACGCTGCAGGGCCTCACT-3', and reverse 5'- AGACGTCTGAGCGGGAAGCA) respectively. The accuracy of the assay was validated using previously published clinical samples (96).

3.2.9. Citrate Synthase activity

Cell lysates were harvested and citrate synthase activity was measured using Citrate Synthase activity assay kit (abcam, UK) according to manufacturer's instruction. Lysates from $1x10^6$ cells were used to determine Citrate synthase activity.

3.2.10. OCR and ECAR measurement

Cells were activated in 48-well plates coated with anti-CD3 mAb (1µg/ml in phosphate buffer saline, PBS) and anti-CD28 mAb (10µg/ml in PBS) in R10FBS for 36h. Oxygen consumption rate (OCR, pmol/min) and extracellular acidification rates (ECAR, in mpH/min) were measured using the Seahorse XF-96e Extracellular Flux Analyzer (Seahorse Bioscience, USA). Mitochondrial perturbation was performed by sequentially injection of oligomycin (1µM), carbonyl cyanide 4-(trifluoromethoxy)phenylhydrazone (FCCP, 2µM) and rotenone (1µM) (all from Sigma Aldrich). Mitochondrial parameters were calculated as previously described (85).

3.2.11. MitoSOX red

Mitochondrial reactive oxygen species (mROS) were measured using 5µM MitoSox red superoxid indicator (Molecular probe, USA). Cells were washed twice with HBSS/Ca/Mg (life technology) and incubated for 10min at 37°C/5% CO_2 with 5µM MitoSox Red in HBSS/Ca/Mg. Cells were washed twice, measured and analyzed as described above.

3.2.12. Cytometric bead array

Supernatant was harvested every 12h (for cytokine timecourse) or 36h after activation and stored at -80°C. Concentration of IL-2, TNF and IFN-γ were measured using Legendplex, human Th1 Panel kit (Biolegend, USA) according to manufacterer's instructions and on a BD Accuri C6 flow cytometer. Analysis was performed with Flowjo 10.0.8 (Tree Star, USA).

3.2.13. Flow cytometry (Effector phenotype)

Cells were incubated with one of the following antibodies for 30min in the dark at 4°C: αCCR7 mAb-phycoerythrin (PE) (clone #150503, R&D systems, United Kingdom), αCD62L mAb-fluorescein isothiocyanate (FITC) (clone LT-TD180, Immunotools, Germany), αCCR5 mAb-FITC (clone 2D7, BD Pharmingen, USA), αCD28 mAb-PE (clone CD28.2, Biolegend, USA), αCD25 mAb-FITC (clone BC96, Biolegend, USA), αCD45RO mAb-PE (clone UCHL1, Biolegend, USA), αCD44 mAb-PE (clone G44-26, BD Pharmingen, USA), αCD38 mAb-FITC (clone HIT2, Biolegend, USA). Cells were measured and analyzed as described above.

3.2.14. Real-time PCR analysis

Cell pellets were washed twice with cold PBS and resuspended with 1ml Trizol reagent (life technology). RNA was extracted using RNeasy Mini Kit (Qiagen) and cDNA was generated using GoScript Reverse Transcription System (Promega) according to manufacturer's instructions. Quantitative PCR was performed in triplicates using Go Taq qPCR Master Mix (Promega) on a ViiA7 Real-Time PCR System (life technology). The primer pairs are listed in **Table S1**. Gene expression was normalized to TATA-box binding protein (TBP) expression and calculated relative to the non-activated control.

3.2.15. Chemicals

Inhibitor studies were performed using the mROS inhibitor mitotempo (100µM), the antibiotics azthromycin (50µM), tigecycline (5µM) or the ATP synthase inhibitor oligomycin (1µM) respectively (Sigmal-Aldrich). CD25 Inhibition was performed using Basiliximab (10µg/ml, Novartis, Basel).

3.2.16. Statistical analysis

Statistic significance was analyzed using Prism 6.0h (GraphPad Software, USA). Normally distributed data were assessed either by Student's t-test or in case of normalized data by Mann-Whitney test. Not normally distributed data were tested using the Wilcoxon test. P values of less than 0.05 were considered statistically significant.

3.3. Results

3.3.1. Mitochondrial biogenesis preceded proliferation in recently activated naïve CD8$^+$ T cells

Mitochondrial biogenesis and division is intricately linked to cell proliferation (97). Whether early alterations in mitochondrial mass and function in newly activated naïve T cells shapes effector maturation and lineage differentiation has not been explored. To dissociate the role of mitochondria during early effector maturation from proliferation, we assessed the kinetics of cell division in relation to mitochondrial biogenesis. Naïve CD8$^+$ T cell (CD62L$^+$ CD45RA$^+$) proliferation were loaded with the carboxyfluorescein succinimidyl ester (CFSE), activated with anti-CD3/anti-CD28 coated beads and CFSE dilution was assessed every 12 hours following activation. Cell division was not observed at 36 hours post-activation (**Fig. 1A**). Consistent with previous findings, the first round of cell division occurred between 36 and 48 hours after activation (80). We also monitored the forward scatter profile of activated cells, every 12 hours, to evaluate the kinetics of cell growth. At 36 hours post activation, the forward scatter of activated cells was increased (**Fig. 1B**), indicating that T cells undergo considerable changes in cell mass prior to proliferation.

Next, we tracked changes in mitochondrial mass using the non-voltage dependent mitochondrial dye, mitotracker green (MTG) (89). We detected increased mitochondrial mass at 36h post-activation (**Fig. 1C**). Following a peak in MTG intensity at 48h post-activation, a decrease in intensity was observed. However, T cells can efflux MTG through the ATP-binding cassette transporter B1 (ABCB1), and a CD8$^+$ T cell subset-specific expression of ABCB1 could impact MTG uptake (94). To confirm the increase in mitochondrial mass in activated T cells, we used transmission electron microscopy (TEM) (**Fig. 1D/S2**). Mitochondria number (**Fig. 1E/S2**), size (**Fig. 1F/S2**) and total mitochondrial area per cell (**Fig. 1G/S2**) were increased in activated naïve CD8$^+$ T cells prior to the first division. To further confirm mitochondrial biogenesis in naïve CD8$^+$ T cells following activation, we also examined mitochondrial DNA (mtDNA) copy number (**Fig. 1H**) and citrate synthase activity (**Fig. 1I**). Significant increases in both parameters were also observed in activated CD8$^+$ T cells prior to proliferation. Taken together, these results indicated that mitochondrial mass is increased in naïve CD8$^+$ T cells early after activation and prior to the first division.

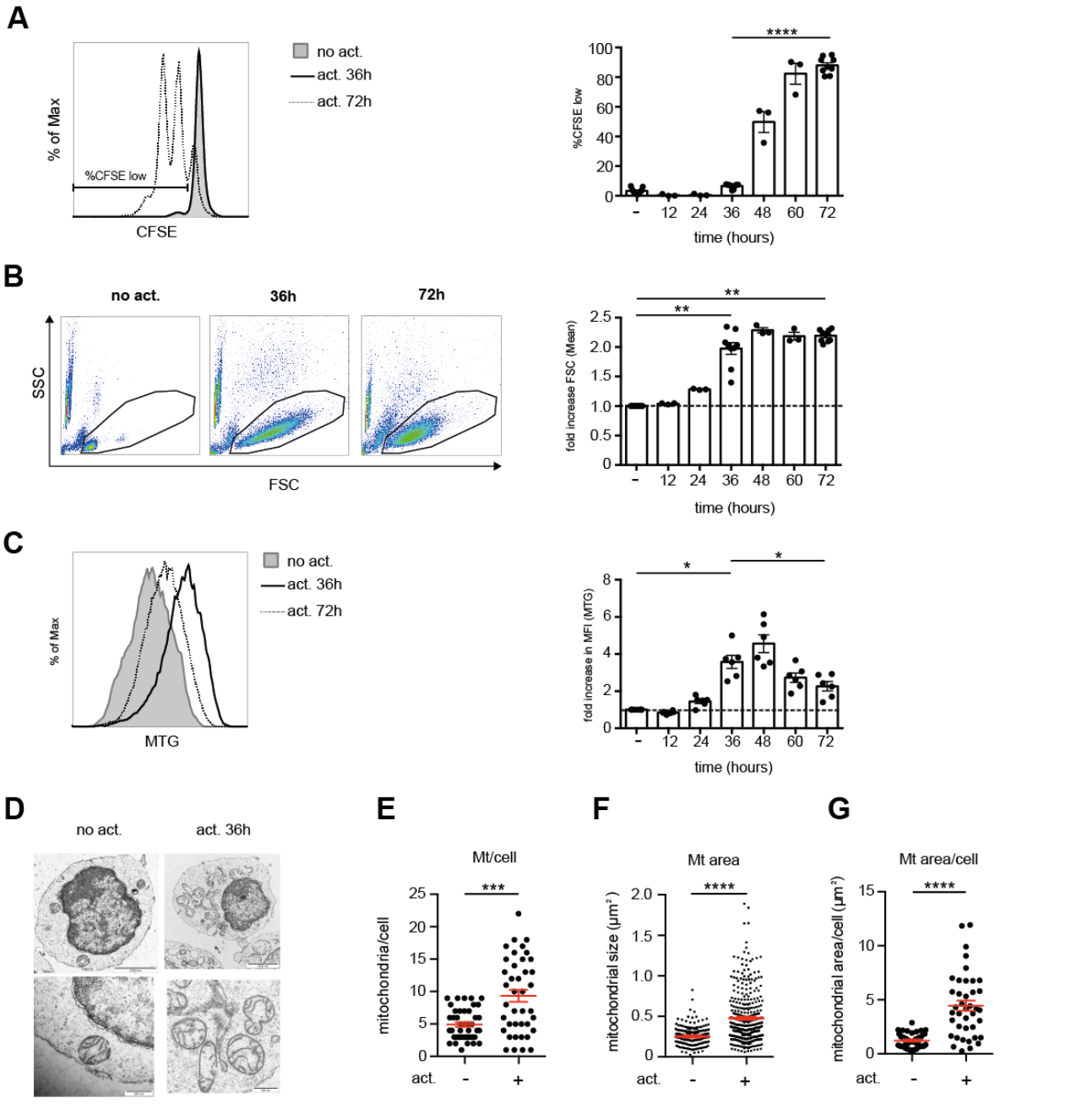

Figure 1. Mitochondrial mass is increased early after activation in naïve CD8+ T cells.
(A) Representative CFSE profile (left) of non-activated (grey) and 36h (continuous line) or 72h (dashed line) activated naïve CD8+ T cells. The bar graph (right) indicates the frequency of CFSE low activated naïve CD8+ T cells assessed every 12h post-activation. (n=3-9).
(B) Representative forward (FSC) and side scatter (SSC) profiles (left) of non-activated (grey) and 36h (continuous line) or 72h (dashed line) activated naïve CD8+ T cells. Summary bar graph (right) of fold increase in mean FSC (activated relative to non-activated controls) assessed every 12h post-activation. (n=3-9).
(C) Representative MTG profiles (left) of non-activated (grey) and 36h (continuous line) or 72h (dashed line) activated naïve CD8+ T cells. Summary bar graph (right) of fold increase in MTG MFI (activated relative to non-activated controls) assessed every 12h post-activation. (n=3-9)
(D) Transmission electron micrographs (magnification = x27'000) of non-activated and 36h activated naïve CD8+ T cells. Scale bars = 2000 nm (top), 500 nm (bottom).
(E-G) Summary graphs of mitochondria counts per cell **(E)**, mitochondrial area per mitochondrion **(F)** and total mitochondrial area per cell **(G)**. Data shown are from 1 of 3 independent donors. Additional donors in **Fig. S2**. One dot represent one cell **(E,G)** or one mitochondrion **(F)**.
(H) Mitochondrial DNA (mtDNA) copy number of non-activated and 36h activated naïve CD8+ T cells. Absolute copy numbers were determined by using qPCR and known plasmid standards. (n=6).
(I) Citrate Synthase activity (per 1x10^6 cells) of non-activated or 36h activated naïve CD8+ T cells. (n=5).
(A-I) Data shown are mean±SEM. Statistical significance assessed by paired t-test **(A, H, I)**, Wilcoxon test **(B, C)** or Mann-Whitney test **(E, F, G)** respectively. *p < 0.05, **p < 0.01, ***p < 0.001, ****p < 0.0001

3.3.2. Mitochondrial function was increased early after activation

Mitochondrial biogenesis involves the upregulation of proteins involved in the tricarboxylic acid (TCA) cycle and in the electron transport chain. In order to determine whether increased mitochondrial mass translates to increased respiration, we used a metabolic flux analyzer. Mitochondrial respiration between non-activated and 36h activated naïve $CD8^+$ T cells was compared under basal conditions and mitochondrial stress (98). In agreement with previous reports, $CD8^+$ T cells increased both mitochondrial respiration and glycolysis upon activation, but there was a more striking increase in glycolysis (79) (**Fig. 2A**). Consequently, the OCR/ECAR ratio was decreased in activated $CD8^+$ T cells (data not shown). Consistent with increased mitochondrial mass, we also detected an increase in both basal and maximal respiration in activated naïve $CD8^+$ T cells (**Fig. 2B-D**); however, the spare respiratory capacity was similar (**Fig. 2E**). Next, we assessed changes in mitochondrial membrane potential by using the voltage dependent mitochondrial dye, mitotracker red. In agreement with the above findings, we detected an increase in mitochondrial membrane potential early after activation (**Fig. 2F**).

It was previously shown that elevated mitochondrial respiration is linked to increased mitochondrial ROS (mROS) production, which acts as an important activation signal in T cells (78). We thus measured activation-induced mROS in cells by using mitoSOX red. Mitosox red MFI was greater in $CD8^+$ T cells following activation, indicating increased generation of mROS (**Fig. 2G**).

In summary, these results suggested that mitochondrial biogenesis occurred early after activation and prior to the first cellular division. Moreover, this increased mitochondrial mass was associated with an increased mitochondrial membrane potential and activation-induced mROS.

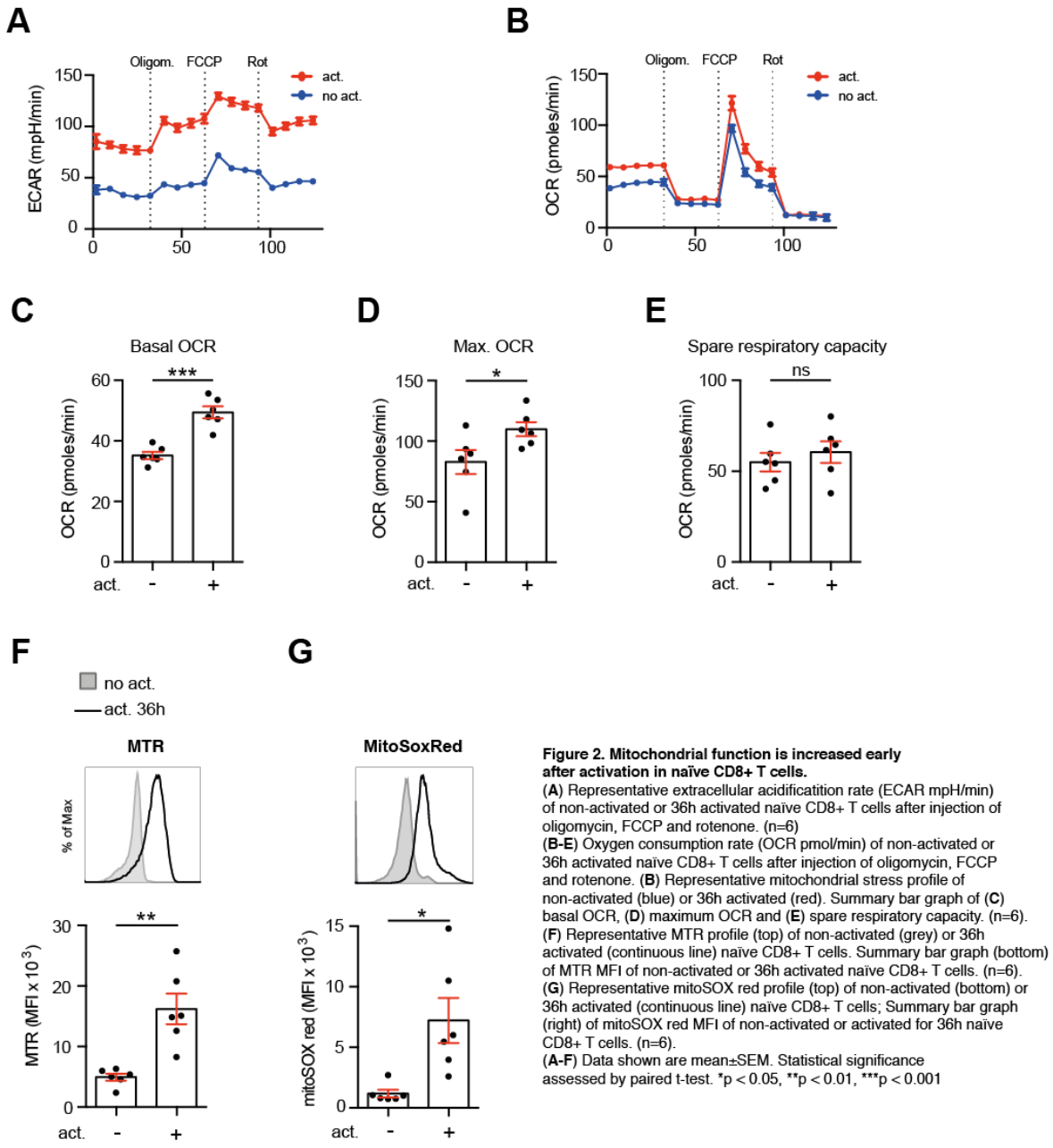

Figure 2. Mitochondrial function is increased early after activation in naïve CD8+ T cells.
(**A**) Representative extracellular acidificatition rate (ECAR mpH/min) of non-activated or 36h activated naïve CD8+ T cells after injection of oligomycin, FCCP and rotenone. (n=6)
(**B-E**) Oxygen consumption rate (OCR pmol/min) of non-activated or 36h activated naïve CD8+ T cells after injection of oligomycin, FCCP and rotenone. (**B**) Representative mitochondrial stress profile of non-activated (blue) or 36h activated (red). Summary bar graph of (**C**) basal OCR, (**D**) maximum OCR and (**E**) spare respiratory capacity. (n=6).
(**F**) Representative MTR profile (top) of non-activated (grey) or 36h activated (continuous line) naïve CD8+ T cells. Summary bar graph (bottom) of MTR MFI of non-activated or 36h activated naïve CD8+ T cells. (n=6).
(**G**) Representative mitoSOX red profile (top) of non-activated (bottom) or 36h activated (continuous line) naïve CD8+ T cells; Summary bar graph (right) of mitoSOX red MFI of non-activated or activated for 36h naïve CD8+ T cells. (n=6).
(**A-F**) Data shown are mean±SEM. Statistical significance assessed by paired t-test. *$p < 0.05$, **$p < 0.01$, ***$p < 0.001$

3.3.3. Transcriptional regulation of mitochondrial biogenesis in T cells

The regulation of mitochondrial biogenesis is highly tissue specific (68). The transcription co-activator peroxisome proliferator-activated receptor γ coactivator-1 (PGC-1) family is composed of PGC-1α, PGC-1β and PGC-related co-activator (PRC) (57). Transcriptional co-activators do not bind directly to DNA but regulate nuclear-encoded mitochondrial gene expression indirectly by enhancing the activity of several transcription factors such as GABP and ERRα (**Fig. 3A**) (60). PGC-1α is the master regulator of mitochondrial biogenesis in muscle cells. However, its regulation in T cells is largely unknown. To assess the transcriptional regulation of mitochondrial biogenesis in naïve T cells, we used qPCR to probe for the expression levels of known key regulators (62). PGC-1α was not detectable in non-activated and activated $CD8^+$ T cells (data not shown). This result is consistent with a recent publication indicating a 200 fold higher expression of PGC-1β than PGC-1α (39). Although, both PGC-1β (**Fig. 3B**) and PRC (**Fig. S3A**) were detectable, only PGC-1β showed a significant increase in early-activated $CD8^+$ T cells. Both GABP (NRF-2) and ERRα, transcription factors that regulate the expression of nuclear encoded mitochondrial proteins (60), were increased upon activation (**Fig. 3C and D**). Interestingly, Michalek *et al.* reported an increased ERRα protein expression in $CD4^+$ T cells early after activation and linked ERRα to ETC gene expression, suggesting an important role in mitochondrial biogenesis (90). There was no detectable change in transcript levels for RIP140, PPARγ, PPARδ, PPARα, ERRβ, and NRF-1 (**Fig. S3**). GABP and ERRα targets include the mitochondrial transcription factor A (TFAM), mitochondrial transcription factor b1 (TFB1M) and b2 (TFB2M) involved in mtDNA encoded mRNA transcription and protein translation (60). TFAM, TFB1M, and TFB2M transcripts were increased in activated $CD8^+$ T cells (**Fig. 3E-G**).

All together, these data indicated that, in contrast to other cell types, mitochondrial biogenesis in $CD8^+$ T cells is not regulated through PGC-1α, but potentially through PGC-1β, GABP and ERRα.

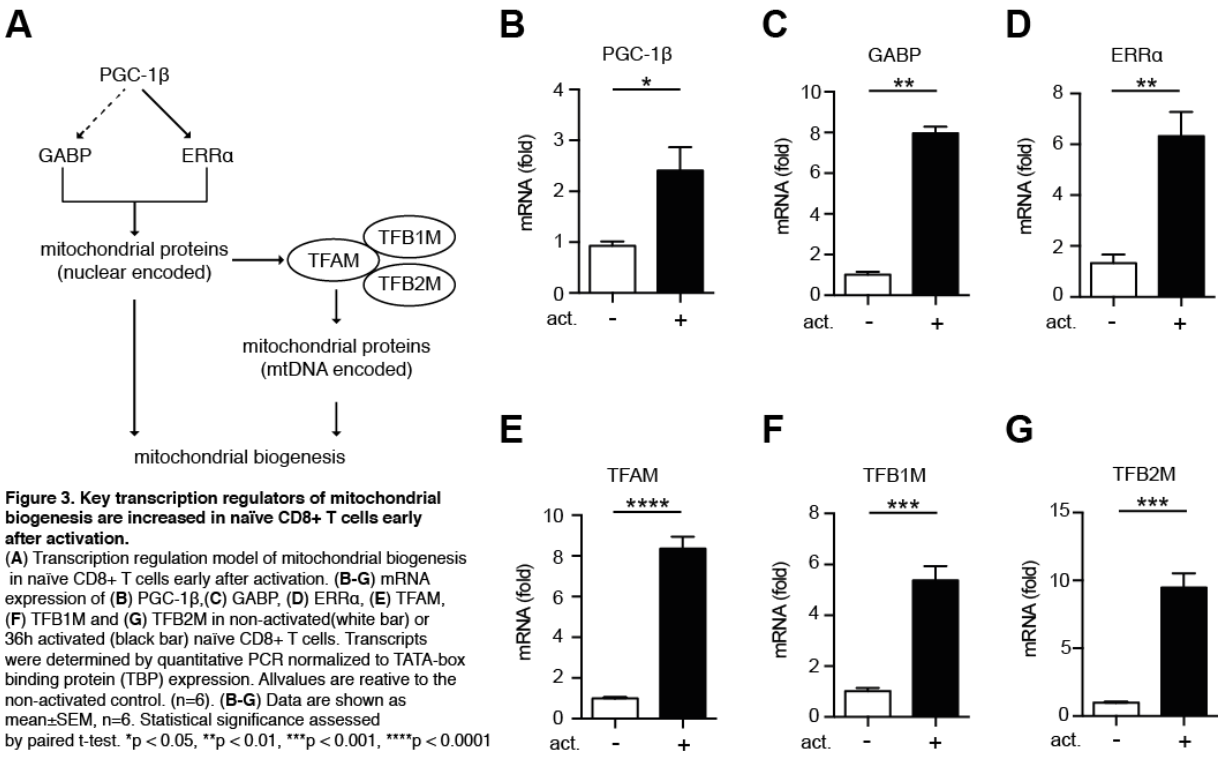

Figure 3. Key transcription regulators of mitochondrial biogenesis are increased in naïve CD8+ T cells early after activation.
(**A**) Transcription regulation model of mitochondrial biogenesis in naïve CD8+ T cells early after activation. (**B-G**) mRNA expression of (**B**) PGC-1β,(**C**) GABP, (**D**) ERRα, (**E**) TFAM, (**F**) TFB1M and (**G**) TFB2M in non-activated(white bar) or 36h activated (black bar) naïve CD8+ T cells. Transcripts were determined by quantitative PCR normalized to TATA-box binding protein (TBP) expression. Allvalues are reative to the non-activated control. (n=6). (**B-G**) Data are shown as mean±SEM, n=6. Statistical significance assessed by paired t-test. *p < 0.05, **p < 0.01, ***p < 0.001, ****p < 0.0001

3.3.4. IL-2 and TNF were rapidly expressed in naïve CD8$^+$ T cells following activation

We compared the expression levels of various T cell activation markers in newly activated cells. We found an effector phenotype in early-activated naïve CD8$^+$ T cells (**Fig. 4A**), with elevated surface expression of CCR5, CD25, CD45RO, CD44 and CD38. Moreover, the lymph node homing molecules CCR7, CD62L and the co-stimulatory receptor CD28 showed reduced expression levels in contrast to non-activated counterparts. Consistent with an early-effector phenotype the marker KLRG-1 was not expressed and CD127 surface expression was decreased (data not shown) (99).

Given the potential link between mitochondrial function and IL-2 secretion (78), we assessed IL-2, TNF and IFN-γ secretion by naïve CD8$^+$ T cells every 12 hours following activation. Surprisingly, both IL-2 and TNF secretion (**Fig. 4B and C**) shared similar kinetics as the increase in mitochondrial mass (**Fig. 1C**), with a marked increase around 36h and peaking at around 48h, with subsequent decreased cytokine levels. This suggested a potential link between mitochondrial biogenesis and early activation-induced IL-2 and TNF secretion. In contrast, IFN-γ (**Fig. 4D**), whose expression was previously linked to glycolysis (85), displayed a slow and steady increase over time. The rapid increase in IL-2 and TNF indicated that both cytokines could play a role in early CD8$^+$ T cell differentiation.

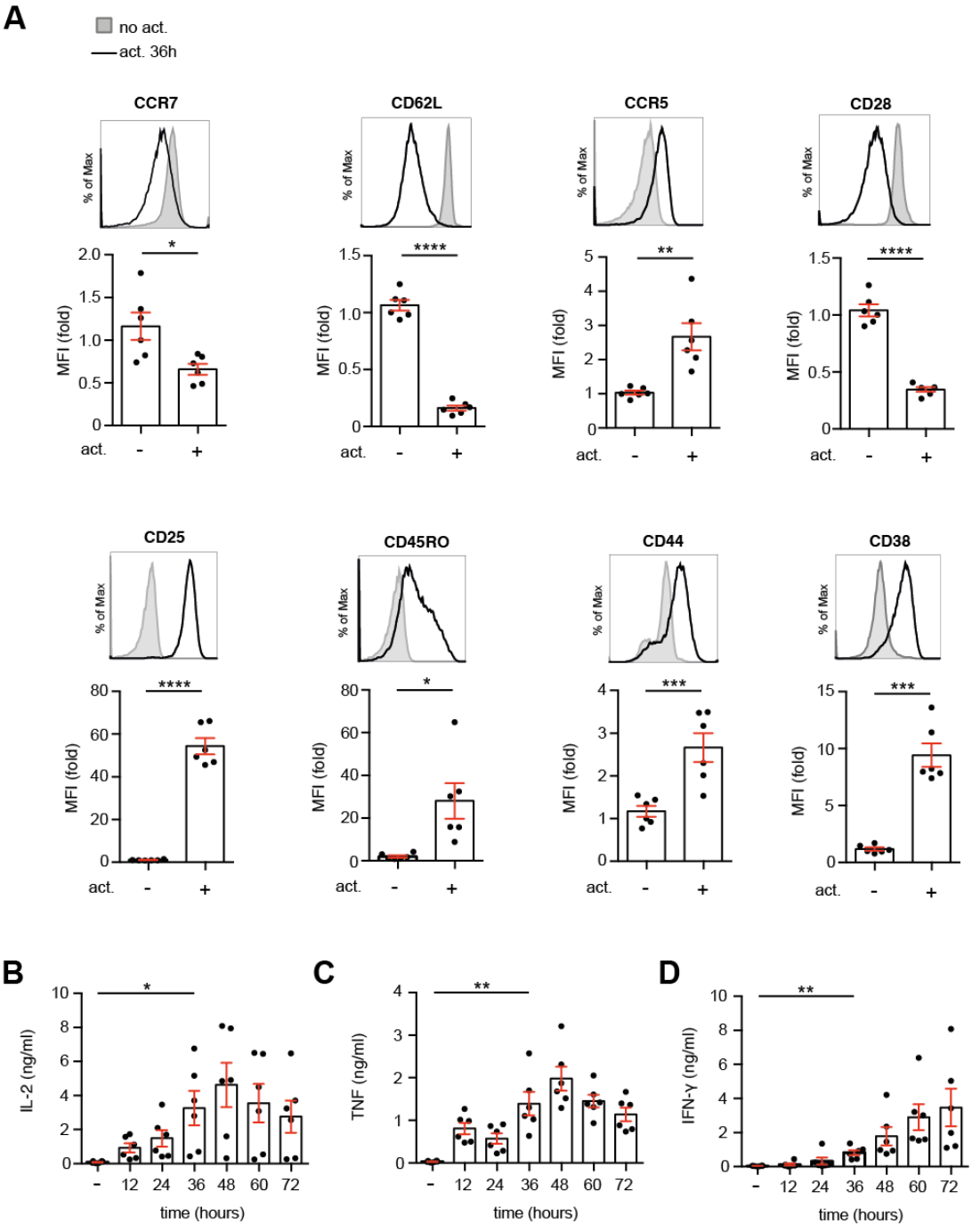

Figure 4. Naïve CD8+ T cells displayed effector phenotype early after activation. IL-2 and TNF but not IFNγ showed similar kinetics to mitochondrial mass.
(**A**) Effector maturation of naïve CD8+ T cells at 36h after activation was assessed by flow cytometry. Representative histograms (top panel) of activation and differentiation markers expressed on non-activated (grey) or 36h activated (continous line) naïve CD8+ T cells. Summary bar graph (bottom panel) of fold difference in MFI of 36h activated cells relative to non-activated controls. (n=6).
(**B-D**) Cell culture supernatants were harvested every 12h and (**B**) IL-2, (**C**) TNF and (**D**) IFNγ secretion were measured using a bead-based immunoassay. (n=6).
(**A-D**) Data shown are mean±SEM. Statistical significance assessed by paired t-test. *p < 0.05, **p < 0.01, ***p < 0.001, ****p < 0.0001

3.3.5. Inhibition of mitochondrial protein synthesis inhibited cytokine production in T cells

The observed similarity between IL-2 and TNF expression and the kinetics of mitochondrial biogenesis suggested that these biological processes might be linked. To further address this, we used clinically approved antibiotics that also target mitochondrial protein synthesis (100,101). Antibiotics such as azithromycin and tigecycline target bacterial ribosome function. Due to similarities in bacterial and mitochondrion protein translation machinery, these antibiotics can also affect the translation of mtDNA encoded genes (101). Activated $CD8^+$ T cells treated with either antibiotic showed a moderate but significant decrease in mitochondrial membrane potential (**Fig. 5A**). Moreover, $CD8^+$ T cells treated with each drug showed a significant reduction in IL-2 (**Fig. 5B**), TNF (**Fig. 5C**) and IFN-γ (**Fig. 5D**) secretion. We also examined the impact of both antibiotics on T cell proliferation. There was no detectable decrease in proliferation following exposure of activated $CD8^+$ T cells to either antibiotic (**Fig. 5E**). However, there was a marked reduction in proliferation following treatment using oligomycin (mitochondrial ATP synthase inhibitor) (**Fig. 5E**), or rapamycin, an mTORC1 inhibitor (data not shown). This suggested that the observed effect of both antibiotics was not due to overall deficits in protein expression or mitochondrial ATP production. Since mROS and IL-2 secretion is linked in T cells, we assessed mROS in naïve $CD8^+$ T cells treated with both inhibitors. Consistent with the reduced membrane potential, we could find a significant reduction in azithromycin and a trend in tigecyline treated naïve $CD8^+$ T cells for activation-induced mROS generation (**Fig. 5F**).

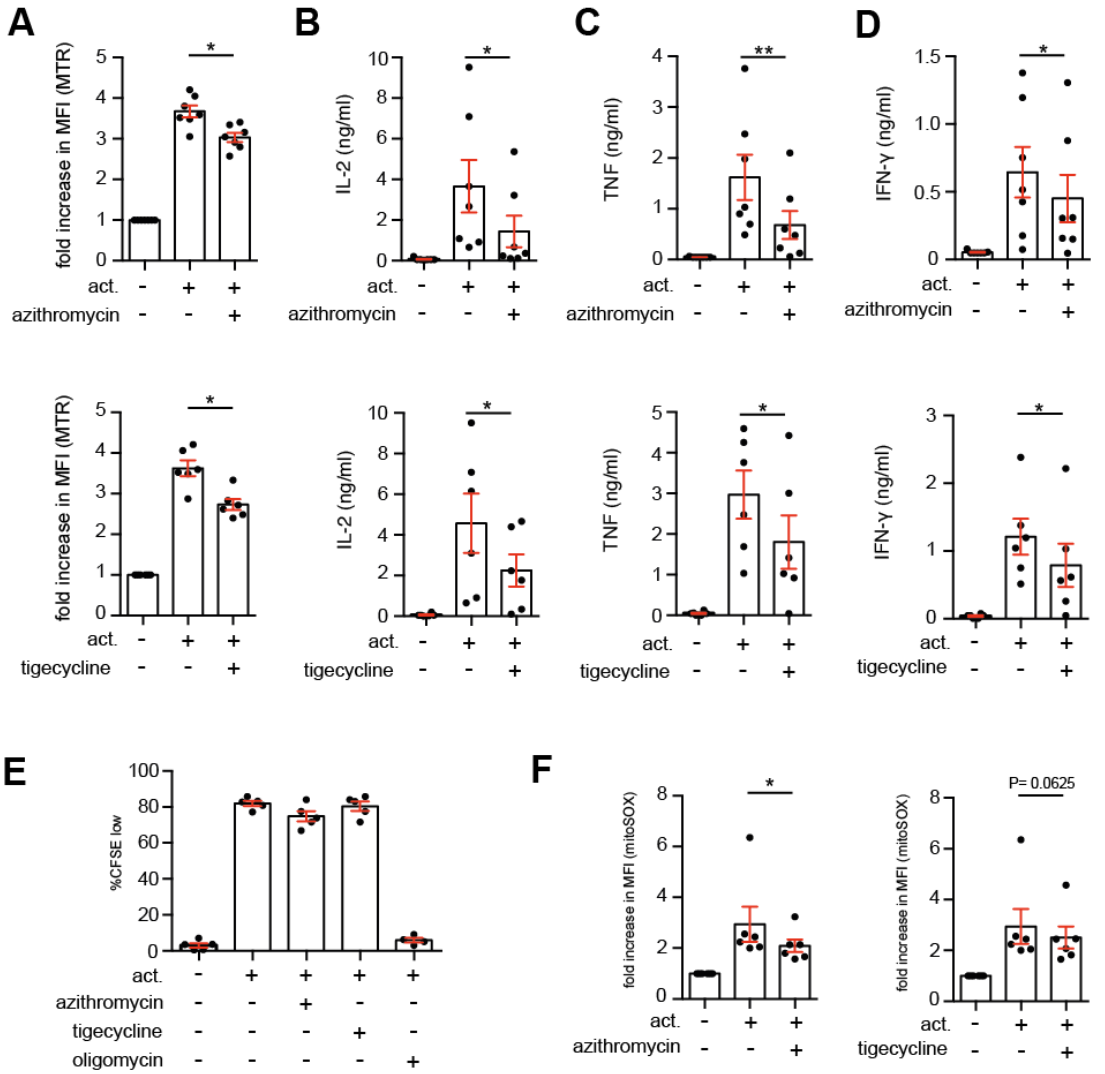

Figure 5. Inhibition of mitochondrial protein synthesis impaired cytokine secretion and mROS production.
(**A**) Bar graph of fold increase in MTR MFI (activated cells relative to non-activation controls) in the presence or absence of azithromycin (top panel) or tigecycline (bottom panel). (n=6-7).
(**B-D**) Cell culture supernatants were harvested from non-activated or activated naïve CD8+ T cells after 36h in culture in the presence of azithromycin (top panel) or tigecycline (bottom panel) and (**B**) IL-2, (**C**) TNF and (**D**) IFNγ secretion were measured using a bead-based immunoassay. (n=7).
(**E**) Bar graph indicates the frequency of CFSE low naïve CD8+ T cells following activation in the presence of azithromycin, tigecycline or oligomycin. (n=4-5).
(**F**) Summary bar graph of mitoSOX Red MFI from naïve CD8+ T cells cultured under non-activating or activating conditions for 36h, in the presence of azithromycin (left panel) or tigecycline (right panel). (n=6).
Data shown are mean±SEM. Statistical significance assessed by Wilcoxon test (**A, F**) or paired t-test (**B-D**), respectively. *p < 0.05, **p < 0.01

3.3.6. mROS were important contributors to the early effector maturation of naïve CD8$^+$ T cells

Given the increased activation-induced mROS generation and the similar kinetics of mitochondrial biogenesis and IL-2 and TNF production, we hypothesized that increased mROS could link mitochondrial biogenesis to cytokine secretion. To modulate mROS in activated cells, the well-established mROS scavenger, mitotempo, was used (33). Mitotempo decreased activation-induces mROS in naïve CD8$^+$ T cells early after activation (**Fig. 6A**). Consistent with previously published data on CD4$^+$ T cells (78), IL-2 secretion was decreased in naïve CD8$^+$ T cells treated with mitotempo (**Fig. 6B**). Surprisingly, we also detected a significant decrease in TNF (**Fig. 6C**) and IFN-γ (**Fig. 6D**) secretion in activated T cells treated with mitotempo. Additionally, exposure of T cells to mitochondrial ROS scavengers decreased mitochondrial mass and membrane potential (**Fig. 6E+F**).

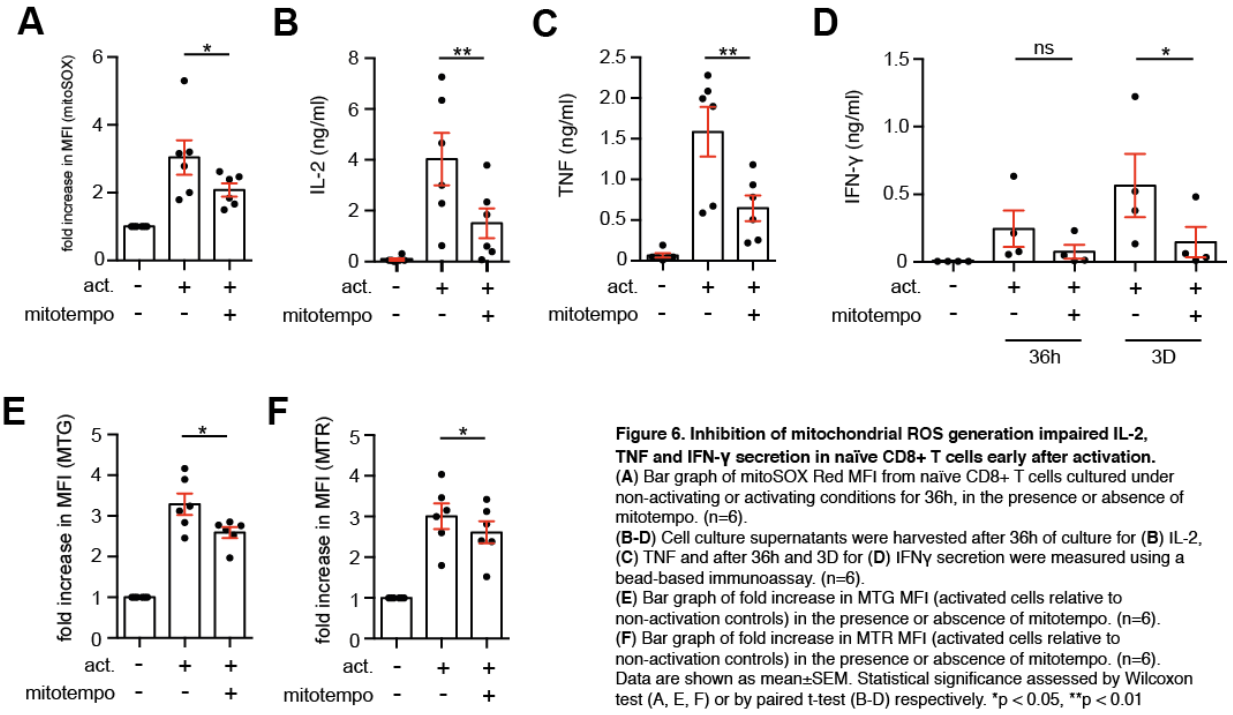

Figure 6. Inhibition of mitochondrial ROS generation impaired IL-2, TNF and IFN-γ secretion in naïve CD8+ T cells early after activation.
(**A**) Bar graph of mitoSOX Red MFI from naïve CD8+ T cells cultured under non-activating or activating conditions for 36h, in the presence or absence of mitotempo. (n=6).
(**B-D**) Cell culture supernatants were harvested after 36h of culture for (**B**) IL-2, (**C**) TNF and after 36h and 3D for (**D**) IFNγ secretion were measured using a bead-based immunoassay. (n=6).
(**E**) Bar graph of fold increase in MTG MFI (activated cells relative to non-activation controls) in the presence or abscence of mitotempo. (n=6).
(**F**) Bar graph of fold increase in MTR MFI (activated cells relative to non-activation controls) in the presence or abscence of mitotempo. (n=6).
Data are shown as mean±SEM. Statistical significance assessed by Wilcoxon test (A, E, F) or by paired t-test (B-D) respectively. *p < 0.05, **p < 0.01

3.3.7. CD25 blockade inhibited activation-induced TNF and IFN-γ secretion

Autocrine IL-2 signaling of activated naïve $CD8^+$ T cells directs effective memory T cell differentiation and recall function (102). To address the role of autocrine IL-2 signalling on mitochondrial biogenesis and early effector maturation of naïve $CD8^+$ T cells, we used the clinically approved CD25 blocking antibody – basiliximab (103). Both, mitochondrial mass (**Fig. 7A**) and membrane potential (**Fig. 7B**) were slightly but significantly reduced in basiliximab treated cells compared to control cells. Interestingly, the decrease was similar to cells treated with mROS scavengers (**Fig. 6E and F**). This suggested that mitochondrial biogenesis is partially regulated by a positive feedback loop mediated through autocrine IL-2 signalling. CD25 blockade did not have an effect on IL-2 secretion (**Fig. 7C**). However, there was a decrease in secretion of both TNF (**Fig. 7D**) and IFN-γ (**Fig. 7E**).

In all, this suggested that mROS regulated IL-2 production, and that via autocrine signaling IL-2 mediated TNF and IFN-γ secretion.

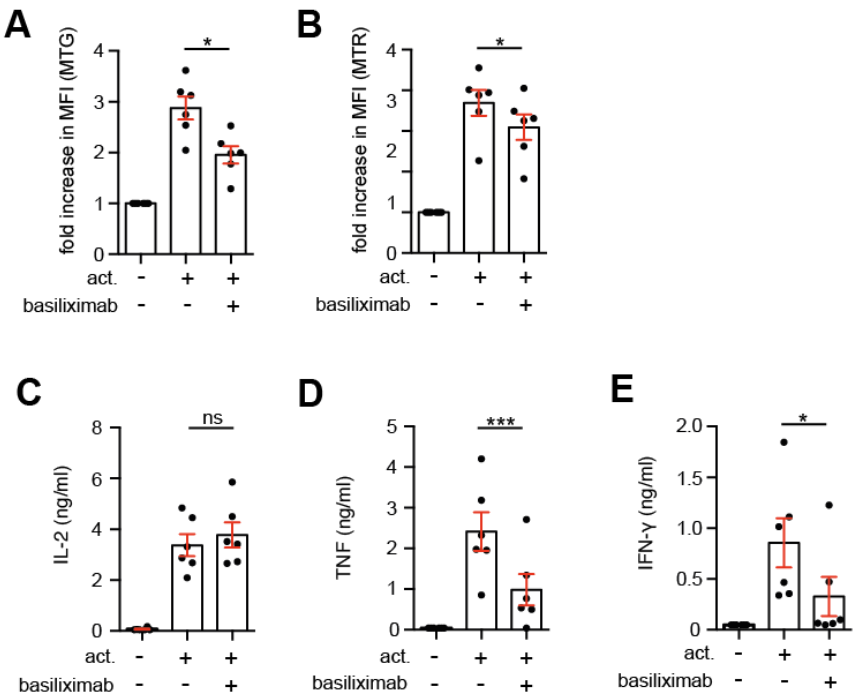

Figure 7. CD25 blockade inhibited IL-2 mediated mitochondrial biogenesis and impaired TNF and IFN-γ secretion in naïve CD8+ T cells early after activation.
(**A**) Bar graph of fold increase in MTG MFI (activated cells relative to non-activation controls) in the presence or absence of basiliximab. (n=6).
(**B**) Bar graph of fold increase in MTR MFI (activated cells relative to non-activation controls) in the presence or absence of basiliximab. (n=6).
(**C-E**) Cell culture supernatant of non-activated or activated for 36h naïve CD8+ T cells in the presence or absence of basiliximab and (**C**) IL-2, (**D**) TNFα and (**E**) IFNγ secretion were measured using a bead-based immunoassay. (n=6).
Data shown are mean±SEM. Statistical significance assessed by Wilcoxon test (**A, B**) or paired t-test (**C-E**) respectively.
*$p < 0.05$, **$p < 0.01$, ***$p < 0.001$

3.4. Discussion

Mitochondrial biogenesis occurs early after activation in T cells (89). However, the functional implication of this increase in mitochondrial mass is not well defined. Here, we provided evidence that mitochondrial biogenesis impacts early effector function in naïve $CD8^+$ T cells.

Mitochondrial mass and mitochondrial function were both increased early after activation and prior to the first division. Interestingly, mitochondrial mass alterations began within the first 48h of activation but decreased subsequently. In support of this finding, Baixauli *et al.* recently reported similar kinetics for mitochondrial transcription factor A (TFAM) expression, a key regulator of mtDNA expression, in recently activated $CD4^+$ T cells (39). Moreover, *bona fide* effector $CD8^+$ T cells have lower mitochondrial mass than their naïve counterpart (84). Together with the finding that mitochondrial ATP generation is critical for glycolytic reprogramming after $CD8^+$ T cell activation (81), this suggests that the role of mitochondrial function is restricted to the early phase of activation in naïve $CD8^+$ T cells. Interestingly, we observed an increase in PGC-1β, ERRα and GABP mRNA expression, suggesting the potential regulation of mitochondrial biogenesis through this network. Surprisingly, we could not detect PGC-1α, the master regulator of mitochondrial biogenesis in muscle cells. This observation was similar to previous findings, showing a 200 times higher expression level of PGC-1β in quiescent $CD4^+$ T cells (90). However, knock-down experiments are required to further assess the regulation of mitochondrial biogenesis in $CD8^+$ T cells after activation.

Interestingly, both IL-2 and TNF secretion shared similar kinetics as the increase in mitochondrial mass. Inhibition of mitochondrial biogenesis using antibiotics that also target mitochondrial protein synthesis, revealed a decrease in mROS generation and cytokine secretion (IL-2, TNF and IFN-γ). Notably, direct inhibition of activation-induced mROS had a similar effect on early-effector cytokine secretion. Basiliximab, a clinical approved anti-IL-2 receptor alpha (IL-2Rα, CD25) antibody, revealed that mROS dependent IL-2 secretion is required for TNF and IFN-γ production. These results not only validated the importance of mROS for IL-2 secretion in T cells (78), but further interconnected mROS with TNF and IFN-γ secretion. However, how mROS signaling modulates IL-2 secretion and early-effector maturation remains to be determined.

Azithromycin, a broad-spectrum macrolide antibiotic (104) is used in chronic inflammatory disorders such as cystic fibrosis for its immune modulatory functions and beyond its antimicrobial effects (105). Interestingly, macrolide antibiotics decrease pro-inflammatory cytokines and reduce activated T cells in brochoavelolar lavage in diffuse panbronchiolitits patients (106). We found that azithromycin decreased mitochondrial biogenesis, mROS generation and subsequently effector cytokine secretion in

naïve $CD8^+$ T cells. Whether mitochondrial biogenesis inhibition in naïve T cells contributes to the immune modulatory effect of macrolides is unclear. Studies focusing on mitochondrial biogenesis and effector function of T cells from azithromycin treated patients need to be performed.

Early mitochondrial function and ATP production is important to facilitate glycolytic reprogramming in $CD8^+$ T cells to support proliferation (80,107). However, our findings assign increased mitochondrial function in naïve $CD8^+$ T cells an added role, this is mROS-dependent IL-2 secretion and through autocrine mechanism modulating TNF and IFN-γ generation.

Further experiments addressing mitochondrial biogenesis, mROS and $CD8^+$ T cell effector maturation could have implications for future strategies aiming to therapeutically manipulate $CD8^+$ effector and memory functions.

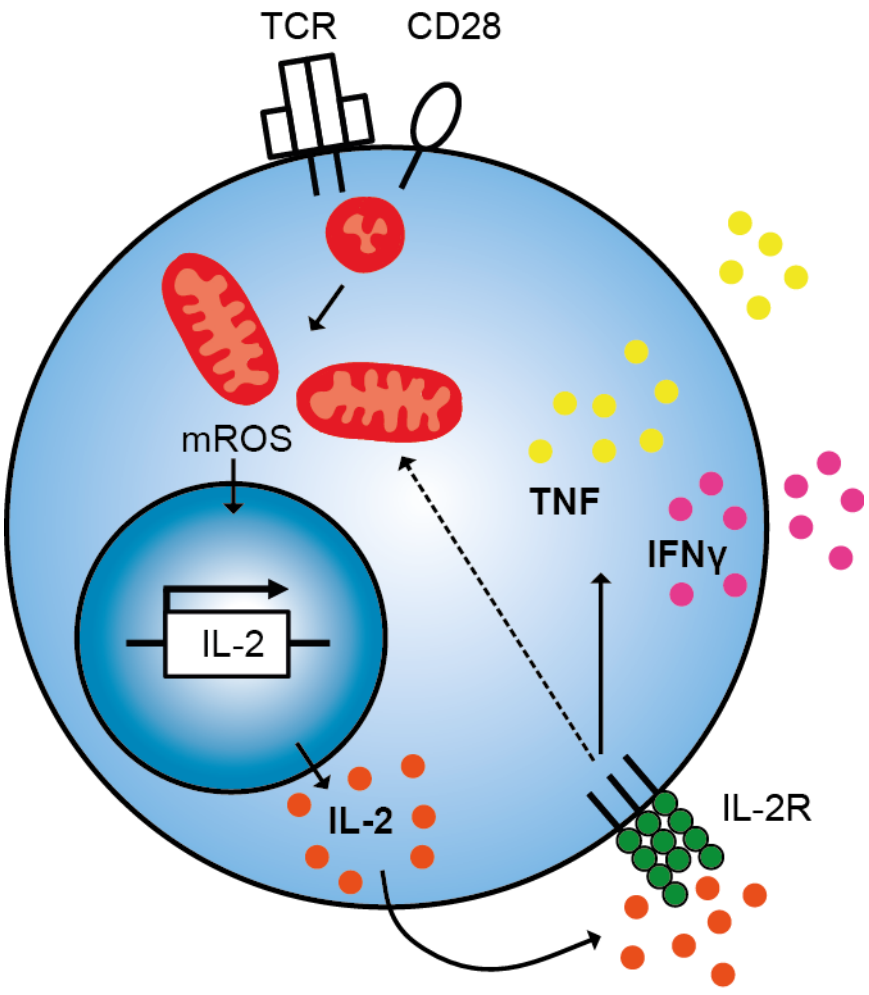

Graphical overview

3.5. Supplemental Material

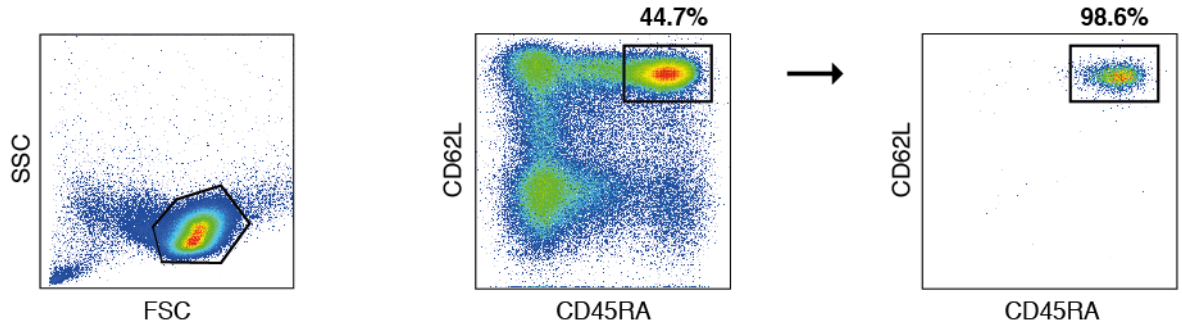

Figure S1) Sorting strategy
Naïve CD8+ T cells were sorted using the surface markers CD62L and CD45RA. Representative forward (FSC) and side scatter (SSC) profile (left) of bulk CD8+ T cells. Representative dot plot and gating strategy (middle) of naïve CD8+ T cells (CD62L+, CD45RA+). Purity of naïve CD8+ T cells after FACS sorting (right panel).

Gene	Foward primer	Reverse primer
PGC-1α	TCTGAGTCTGTATGGAGTGACAT	CCAAGTCGTTCACATCTAGTTCA
PGC-1β	AGGTGGCCGAGTCAAAGTC	CAACTATCTCGCTGACACGC (108)
PRC	GAGCAGGTTATCTCTGGAGGA	GTGAGCAGCGACACTTCATT
NRIP1	ATGCAGCAAAGCGGAAGAG	CCTTTAGGCACACTGTCAACC
PPARG	ACCAAAGTGCAATCAAAGTGGA	AGGCTTATTGTAGAGCTGAGTCT
PPARD	GTGATCCACGACATCGAGACA	TGCACGCTGATCTCCTTGTAG
PPARA	AGAGATTTCGAAATCCATCGG	ACTGGTATTCCGTAAAGCCAAAG
ERRα	CGCTTGGTGATCTCACACTC	GCTACCACTATGGTGTGGCA (108)
ERRβ	TGGAGGCCGTCAGAAATACAA	CAATGGCTTTTTAGCAGGTGGA
ERRγ	CCAGTGGGAGCTACAGTTCAA	AGTCAAGTCCGTTCTGATGGC
GABPB1	GCTATGCAGAACCAAATCAACAC	CCCCTCCAGGTCCAATGATAAA
NRF-1	TGGCTACTTACACCGAGCATA	AGAAGGCGAGTCTTCATCAGC
TFAM	GAACAACTACCCATATTTAAAGCTCA	GAATCAGGAAGTTCCCTCCA (109)
TFB1M	CCTCCGTTGCCCACGATTC	GCCCACTTCGTAAACATAAGCAT (110)
TFB2M	CGCCAAGGAAGGCGTCTAAG	CTTTCGAGCGCAACCACTTTG (110)
TBP	TGCCTCCAGAATATGCCTCT	CAATGGTTTTCAAGCTTTCCA (111)

Table S1. RT-PCR primer

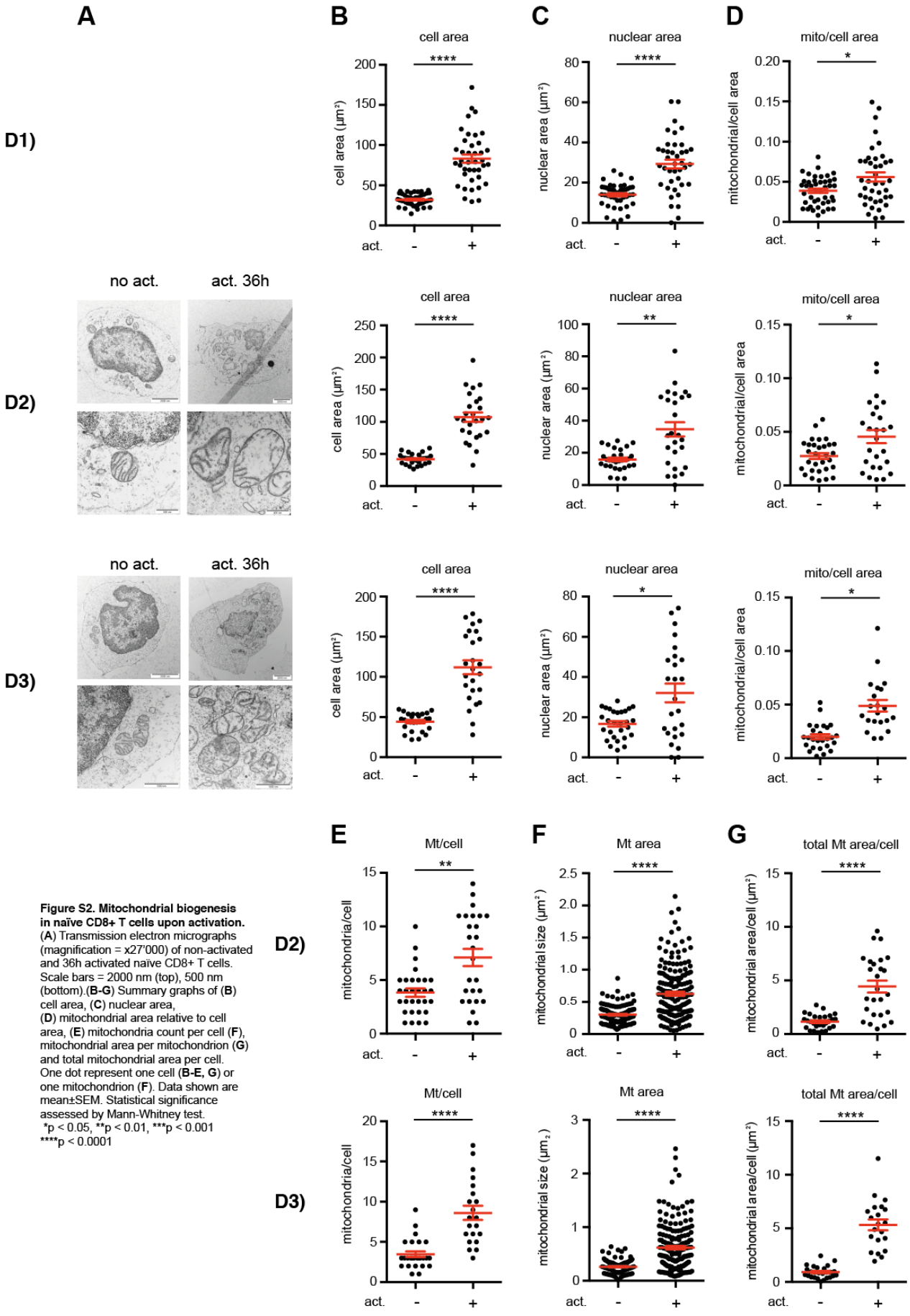

Figure S2. Mitochondrial biogenesis in naïve CD8+ T cells upon activation. (**A**) Transmission electron micrographs (magnification = x27'000) of non-activated and 36h activated naïve CD8+ T cells. Scale bars = 2000 nm (top), 500 nm (bottom).(**B-G**) Summary graphs of (**B**) cell area, (**C**) nuclear area, (**D**) mitochondrial area relative to cell area, (**E**) mitochondria count per cell (**F**), mitochondrial area per mitochondrion (**G**) and total mitochondrial area per cell. One dot represent one cell (**B-E, G**) or one mitochondrion (**F**). Data shown are mean±SEM. Statistical significance assessed by Mann-Whitney test.
*p < 0.05, **p < 0.01, ***p < 0.001
****p < 0.0001

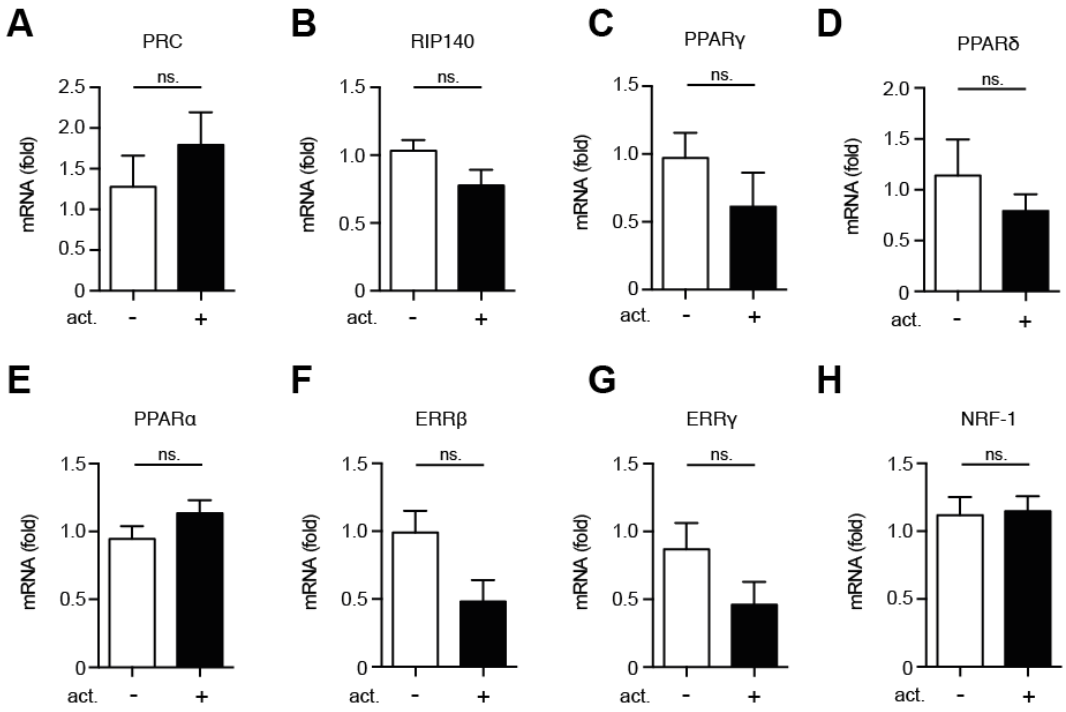

Figure S3. Additional regulators of mitochondrial biogenesis are not increased in naïve CD8+ T cells early after activation.
(**A-H**) mRNA expression of (**A**) PRC, (**B**) RIP140, (**C**) PPARγ, (**D**) PPARδ (**E**) PPARα, (**F**) ERRβ, (**G**) ERRγ or (**H**) NRF-1 in non-activated (white bar) or 36h activated (black bar) naïve CD8+ T cells. Transcripts were determined by quantitative PCR relative to TATA-box binding protein (TBP) expression and normalized to the non-activated control. (n=6). Data are shown as mean±SEM. Statistical significance assessed by paired t-test. n.s = not significant.

4. Glucose oxidation in the mitochondria is important for CD8$^+$ memory recall response (Manuscript 2)

4.1. Introduction

CD8$^+$ T cells are the foot soldiers of the cell mediated adaptive immune response. These cells play an important role in the elimination of pathogen infected cells (112). Following encounter with antigen presenting cells bearing cognate MHC:microbial peptide complexes, CD8$^+$ T cells differentiate into cytotoxic effector T cells (CTLs) that express several cytokines and cytolytic molecules, which eliminate pathogen infected cells. Successful control of the infection leads to the diminution of inflammation and differentiation of effector CTLs to memory cells (113). Re-infection by the same microbe leads to the rapid response of memory CD8$^+$ T cells. Although memory T cell precursor frequencies are higher than their naïve counterparts giving memory cells a quantitative advantage during re-infection (114), qualitative differences also exist between both CD8$^+$ T cell subpopulations that contribute to the faster and stronger response of memory T cells (81).

Our laboratory and others recently demonstrated that naïve (NV) and memory T cells also exhibit differences in their metabolic repertoire (40,73,85,115). Memory CD8$^+$ T cells have greater glycolytic reserve and spare respiratory capacity than naïve cells (84,85). Both parameters give memory cells greater metabolic plasticity in low-nutrient or low-oxygen tension microenvironments. We also established that effector-memory (EM) CD8$^+$ T cells rapidly upregulate glycolysis following TCR/co-stimulatory receptor engagement, an immunologic phenomenon we coined – immediate-early glycolytic switch (85). The ability to rapidly increase glycolysis is important for the function of EM CD8$^+$ T cells. Specifically, IFN-γ production was dependent on glycolytic engagement by EM cells. This activation-induced glycolytic increase is regulated by mTORC2–Akt signaling. Inhibition of either kinase led to the reduction in IFN-γ production (85).

Several studies have further elaborated on the impact of glycolysis on the effector maturation of CD8$^+$ T cells (79,81,116,117). However, the impact of glucose oxidation in the mitochondria on the rapid recall response of EM CD8$^+$ T cells remains unclear. Here, we show that glucose is also oxidized in the mitochondria in an Akt dependent manner. Glucose flux in the TCA cycle is important for rapid IFN-γ production by EM CD8$^+$ T cells. We also established that components of the mTORC2–Akt axis are present in the mitochondria associated membrane (MAM) of the endoplasmic reticulum. Moreover, phosphorylation of Gsk-3β, a well-established target of Akt, which is also present in the MAM, was increased in EM CD8$^+$ T cells following stimulation. Together these findings suggest a close association

between mTORC2–Akt signaling and mitochondria function, which is potentially important in the recall response of EM $CD8^+$ T cells.

4.2. Materials and Methods

4.2.1. $CD8^+$ Isolation

Blood samples were obtained from healthy blood donors as buffy coats after written informed consent (Blood donor centre, Basel). Peripheral blood mononuclear cells (PBMC) were isolated by standard density-gradient centrifugation protocols (Lymphoprep Fresenius Kabi, Norway)(85). $CD8^+$ T cells were positively selected using magnetic $CD8^+$ beads (MiltenyiBiotec, Germany) following manufacturer's instructions. Cells were rested overnight for flow sorting accessibility in RPMI-1640 medium (Gibco, USA) containing 10% fetal bovine serum (FBS, Gibco, USA), 50U/ml penicillin and 50µg/ml streptomycin (Gibco, USA) (R10FBS).

4.2.2. Cell sorting

For isolation of naïve and EM $CD8^+$ T cells, positively selected $CD8^+$ were incubated with allophycocyanin (APC)-conjugated anti-CD62L (ImmunoTools, Germany) and pacific blue (PB)-conjugated anti-CD45RA (Beckman Coulter, USA). $CD62L^+$ $CD45RA^+$ (naïve) and $CD62L^{neg}$ $CD45RA^{neg}$ (EM) subsets were sorted with a BD influx cell sorter (BD Bioscience, USA). Cells were then rested for 4 hours in R10FBS at 37°C prior to further experiments.

4.2.3. Activation beads

Activation beads were coated and assessed as described in the technical note (Manuscript 3). Briefly, to load antibody on beads, 100µl of a 2.5% suspension of Polybead Microspheres 4.5µm (Polyscience Eppenheim) and 900µl borate buffer containing 0.1M boric acid pH8.5 (Sigma-Aldrich) were prepared according to manufacturer's instructions. 10µg anti-human CD28 IgG1 antibody (CD28.2 Biolegend, USA) diluted in 100µl borate buffer was added to beads and incubated for 30min at room temperature. Thereafter, 1.5µg anti-human CD3 IgG2a antibody (HIT3a, Biolegend, USA) was diluted in 300µl borate buffer and gently mixed with the beads for 30min. Blocking and storage of antibody-loaded beads was performed according to manufacturer's instruction.

Antibody coupling was tested using 2nd antibodies against IgG1 or IgG2a (SouthernBiotech, USA) respectively. To determine the amount of antibody molecules per bead Quantum MESF APC and PE (Bangslab, USA) were used. Data were acquired using a BD AccuriC6 flow cytometer (Becton Dickinson, USA) and analyzed with FlowJo 10.0.8 (Tree Star, USA).

4.2.4. In-Seahorse activation

Extracellular acidification rates (ECAR, in mpH/min) were monitored in real time using the Seahorse XF-24 Extracellular Flux Analyzer (Seahorse Bioscience) as previously described (85). Briefly, sorted EM $CD8^+$ T cells were plated ($5x10^5$ cells/well) using Celltak (Corning, USA); various inhibitors and activation beads ($2.5x10^6$ beads/well) were sequentially added through the instrument's multi-injection port and ECAR values were recorded for 10h.

4.2.5. Cytokine measurement

Sorted EM $CD8^+$ were plated into flat-bottom 96 well plates ($3x10^5$ cells/well) using R10FBS preincubated with various inhibitors and stimulated using activation beads ($6x10^5$ beads/well). Supernatants were harvested 12h after activation and concentrations of IFN-γ were measured using an IFN-γ ELISA kit (eBioscience) or concentration of IL-2, TNF and IFN-γ were measured using Legendplex, human Th1 Panel kit (Biolegend) according to manufacterer's instructions.

4.2.6. Quantitative PCR

Sorted EM $CD8^+$ were plated into flat-bottom 48 well plates ($1x10^6$ cells/well) using R10FBS, preincubated with various inhibitors and stimulated for 4 hours using activation beads ($2x10^6$ beads/well). Cell pellets were washed twice with cold phosphate buffer saline (PBS) and resuspended with 1ml Trizol reagent (life technology). RNA was extracted using RNeasy Mini Kit (Qiagen) and cDNA was generated using GoScript Reverse Transcription System (Promega) according to manufacturer's instructions. Quantitative PCR for IFN-y and GAPDH mRNA was performed in triplicates using commercially designed primers (Hs00989291_m1, Hs03929097_g1; Life technology) and Go Taq Probe qPCR Master Mix (Promega) on a 7500 Fast Real-Time PCR System (Thermo Scientific, Rockford IL, USA). Gene expression was normalized to GAPDH expression and calculated relative to the non-activated control.

4.2.7. Metabolomic

Naïve and EM CD8+ T cells were cultured for 4h in a 24 well plate ($3x10^6$ cells/well) under non-activating and activating conditions ($6x10^6$ beads/well). For Akt inhibition, cells were treated with Akti1/2 (10uM, Sigma-Aldrich). Cell pellets were washed twice with cold PBS, snap freezed using EtOH containing dry ice and stored at -80°C. Metabolomic assays and analysis was done by Metabolon (Durham, USA) as previously described(93).

4.2.8. Mitochondrial perturbation

Cells were pretreated with various inhibitors and stimulated in 48-well plates coated with anti-CD3 mAb (1µg/ml in PBS) and anti-CD28 mAb (10µg/ml in PBS) in R10FBS for 12h. Oxygen consumption rate (OCR, pmol/min) and extracellular acidification rates (ECAR, in mpH/min) were measured using the Seahorse XF-96e Extracellular Flux Analyzer (Seahorse Bioscience) as previously described(85). Mitochondrial pertrubation was performed by sequentially injection of oligomycin (1µM, Sigma Aldrich), carbonyl cyanide 4-(trifluoromethoxy)phenylhydrazone (FCCP, 2µM, Sigma Aldrich) and rotenone (1µM, Sigma Aldrich). Mitochondrial parameters were calculated as previously described(85).

4.2.9. CFSE

Sorted EM $CD8^+$ T cells were loaded prior to activation with 5µM of the cell-proliferation dye carboxyfluorescein succinimidyl ester (CFSE, Molecular probes, USA) according to manufacturer's instructions and seeded into plated flat bottom 96-well plates ($3x10^5$ cells/well). Plated cells were pretreated with various inhibitors and 1000U/ml IL-2 (ImmunoTools, Germany) and stimulated using activation beads ($6x10^5$ beads/well) in R10FBS. Proliferation was measured 3d after activation using a BD AccuriC6 flow cytometer and analyzed with Flowjo 10.0.8 (Tree Star, USA).

4.2.10. CD69

$CD8^+$ T cells were plated into flat-bottom 96-well plates (5×10^5 cells/well), pretreated with various inhibitors and stimulated using activation beads for 5h at 37°C / 5%CO_2. Cells were stained using APC-conjugated CD62L (LT-TD180, ImmunoTools, Friesoythe, Germany), PE-conjugated CD45RA (F8-11-13, ImmunoTools, Friesoythe, Germany) and FITC-conjugated CD69 antibodies (FN50, ImmunoTools, Friesoythe, Germany). Data were acquired and analyzed as described above.

4.2.11. Reagents

Inhibitor studies were performed using 2-DG (10mM), Akti1/2 (10µM), Osi-027 (10µM), KU-0063794 (10µM), Rotenone (1µM), TTFA (200µM), Antimycin A (2µM), Oligomycin (0.1µM) or 4-(trifluoromethoxy)phenylhydrazone (FCCP, 2µM), Clotrimazol (25µM) respectively (all from Sigma-Aldrich). Methylpyruvate (2mM/10mM, Sigma-Aldrich) was used to substitute pyruvate.

4.2.12. Total cell lysate

Naïve and EM $CD8^+$ T cells were cultured for 1h in 24 well plates ($3x10^6$ cells/well) under non-activating and activating conditions ($6x10^6$ beads/well). Cell pellets were washed with cold PBS and lysed using RIPA bufffer (Thermo Scientific, Rockford IL, USA) containing phosphatase and protease inhibitors (PhosStop and cOmplete, Roche).

4.2.13. Mitochondrial fraction

Sorted naïve, EM $CD8^+$ T cells and Jurkat cells were cultured under non-activating and activating conditions. Cells were washed and homogenized with 20 strokes ($CD8^+$ T cells) or 50 strokes (Jurkat cells) using a teflon or glas homogenizer for crude or pure mitochondrial fraction isolation, respectively.

Crude mitochondrial fractions were isolated as previously described (118). Briefly, after homogenization, cells were centrifuged twice (600xg, 5min 4°C) and supernatants were transferred and centrifuged (10'300xg, 10min, 4°C). Supernatants were collected and pellets containing crude mitochondria were resuspended in RIPA buffer (Thermo Scientific, Rockford IL, USA). Preparation of pure mitochondrial fractions were performed as previously described (119).

4.2.14. Immunoblot

Protein concentrations were determined by BCA protein assay kit (Thermo Scientific). Total cell lysates, crude or pure mitochondrial fraction were separated using 4-15% Mini Protean TGX Gel (Bio-Rad, Hercules CA, USA) and transferred to nitrocellulose membranes using Trans-Blot Turbo Transfer (Bio-Rad, Hercules CA, USA). Membranes were probed with antibodies against ACC, Rictor, mTOR, Akt, HK I, Sin1, pAkt Thr308, pAkt Ser473, p-(S/T) Akt substrate, pGsk-3β (all from cell signaling),

GRP75, VDAC I (from abcam) , actin (Sigma-Aldrich) or Raptor (Bethyl) respectively. Blots were stained with appropriate secondary antibodies (LICOR, Lincoln NE, USA) and the odyssey imaging system (LICOR, Lincoln NE, USA) was used for detection.

4.2.15. Electron microscopy

Transmission electron microscopy (TEM) was performed at the Biocenter (University of Basel, CH) as previously described(95). Briefly, cells were washed twice using cold PBS and sequentially fixed in Karnofski 3% paraformaldehyde and 0.5% glutaraldehyde for 1h. Cells were reduced using 1% osmium tetraoxide, embedded for 24-48h at 60°C and cut into 60nm sections using microtom Ultracut E (Leica). Micrographs were obtained with a Morgagni 268 transmission electron microsocope (FEI, Hillsboro OR, USA) at 80kV. To quantify mitochondrial, nuclear and cytoplasmic area Image J software (NIH, USA) was used.

4.2.16. Statistical analysis

Statistical significance was analyzed using Prism 6.0h (GraphPad Software, USA). P values of less than 0.05 were considered statistically significant.

4.3. Results

4.3.1. Akt is critical for the early metabolic reprogramming of EM CD8+ T cells

T cell receptor synapse formation with cognate MHC-peptide complexes on antigen presenting cells drives T cell activation and differentiation into effector populations. To mimic this interaction *in vitro*, we activated naïve and effector-memory (EM) $CD8^+$ T cells with anti-CD3 and anti-CD28 loaded polystyrene beads (Manuscript 3, Technical notes). In agreement with our previous report using soluble activation antibodies, phosphorylation of Akt at Thr308 and Ser473 was detectable in EM $CD8^+$ T cells at 1h post-activation but not in naïve counterparts (**Fig. 1A**). Using an extracellular flux analyzer we also evaluated the impact of bead activation on immediate-early glycolytic switch in $CD8^+$ T cells. Upon injection of the activation beads, a marked increase in the extracellular acidification rate (ECAR) was observed in EM $CD8^+$ T cells (**Fig. 1B**). This glycolytic switch was diminished in cells pre-treated with the Akt inhibitor, Akti 1/2 (**Fig. 1B**). mTORC2 catalyzes the phosphorylation of Akt serine-473. Pre-treatment with OSI-027, an mTORC1/C2 inhibitor also blocked the rapid increase in glycolysis. Glycolytic switch was not observed in naïve counterparts (data not shown). Next, we probed for IFN-γ production in effector-memory T cells after 12h of stimulation. IFN-γ secretion was sensitive to the glycolysis inhibitor, 2-DG. mTORC1/C2 inhibitors (OSI-027 and KU) or Akt inhibitor (Akti-1/2) also diminished IFN-γ production in EM T cells (**Fig. 1C**). IFN-γ production at 12h post activation was not observe in naïve T cells (data not shown). Inhibition of Akt and mTORC1/C2 lowered *IFNG* transcripts (**Fig. 1D**) indicating that the decrease in IFN-γ production is partially due to decreased *IFNG* transcription.

The extracellular flux analyzer only probes for extracellular acidification, which is primarily due to increased lactic acid production by glycolytic cells. To further interrogate the metabolic reprogramming of NV and EM $CD8^+$ T cells during the early activation phase, we applied a mass spectrometry based metabolomics approach. At 2 hours post-activation, glycolytic and tricarboxylic acid cycle (TCA cycle) metabolites were unchanged in naïve cells following activation (**Fig. 1E**). However, glycolytic metabolites such as fructose-1,6-bisphosphate (F1,6BP), 3 phosphoglycerate (3PG), phosphoenol pyruvate (PEP) and lactate were elevated in EM cells within 2 h following activation (**Fig. 1E**). Metabolites from the tricarboxylic acid cycle (TCA cycle), citrate and malate, were also increased in activated EM cells. Metabolites from intermediary pathways that stem from glycolysis were not detected in both $CD8^+$ T cell subpopulations. We also examined the impact of Akt in EM $CD8^+$ T cell metabolic reprogramming. Pre-treatment of EM cells with Akti 1/2 prior to activation abolished the increase in glycolytic and TCA cycle metabolites.

In all, these findings suggest that the glycolytic pathway is rapidly mobilized in newly activated EM CD8$^+$ T cells. Moreover, the detection of TCA cycle metabolites indicates that mitochondrial metabolism is also enhanced in EM T cells. The diminution of IFN-γ production, and glycolytic and TCA cycle metabolites following Akt inhibition indicates that the kinase plays a central role in the rapid metabolic reprogramming of memory T cells during the recall response.

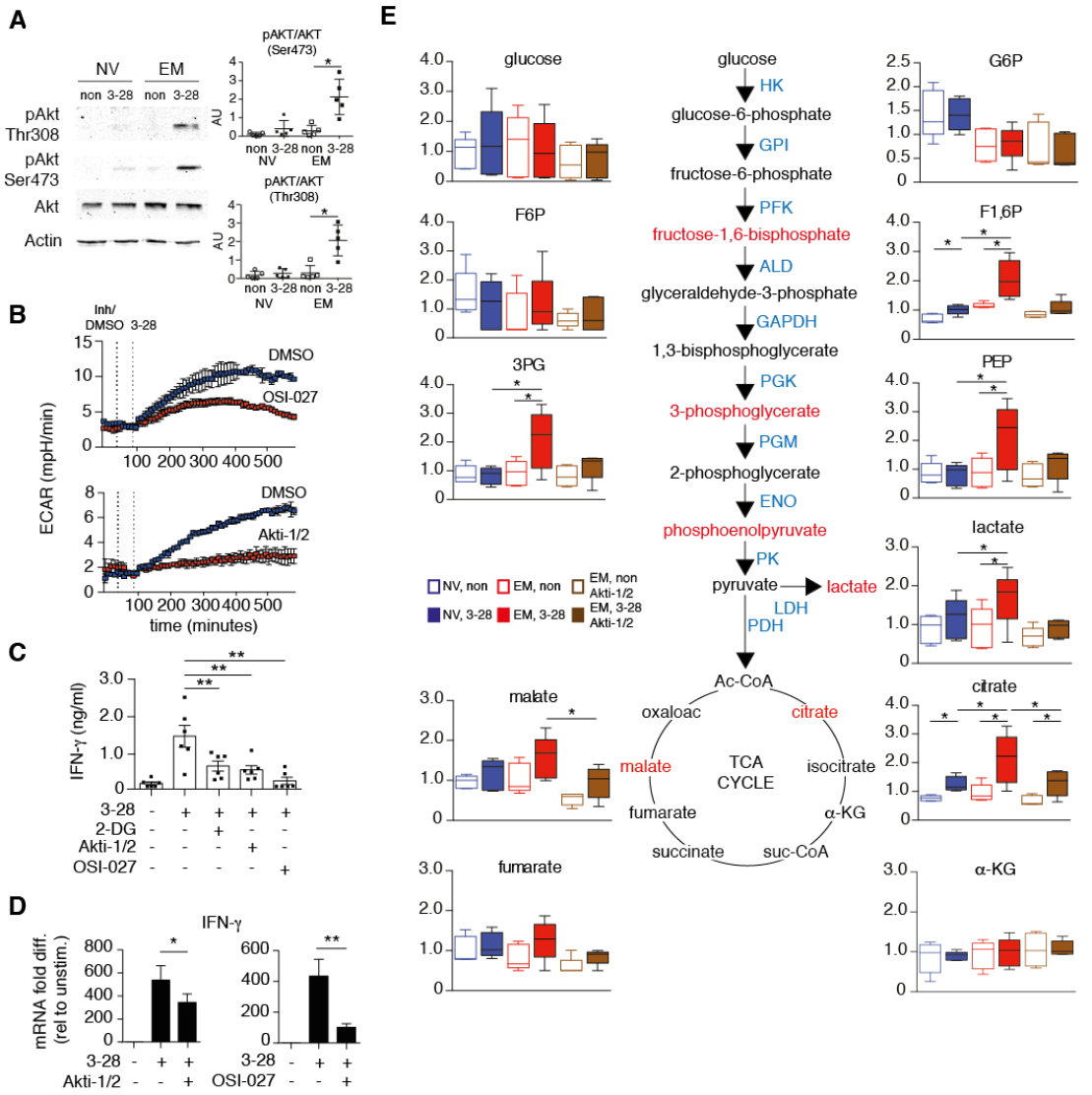

Figure 1. Metabolic remodeling in activated EM CD8+ T cells is dependent on Akt
(**A**) Immunoblot analysis of NV and EM CD8+ T cells. Cells were activated for 1h and total cell lysates were probed for expression of total Akt and phosphorylation at Thr308 and Ser473. Summary graphs of pAkt-S473 (top) and pAkt-T308 (bottom) (AU – arbitrary units, normalized to actin). (n=5)
(**B**) Representative activation induced glycolytic profile of EM CD8+ T cells before and after activation. Cells were pretreated with control medium (DMSO), OSI-027 (top panel), or Akti-1/2 (bottom panel). Data shown is a representative histogram of n=5 independent donors.
(**C**) IFN-γ ELISA on EM CD8+ T cells non-stimulated or activated for 12h in the presence of 2-DG (10 mM), Akti-1/2 (10 μM) or OSI-027 (10 μM), respectively. (n=6)
(**D**) IFNγ mRNA fold-difference between non-activated and activated EM CD8+ T cells in the absence or presence of Akti (left) or OSI-027 (right). Samples were normalized to GAPDH. (n=8-9)
(**E**) Metabolomic analysis of intracellular metabolites from NV and EM CD8+ T cells ± activation and ± Akti-1/2 (EM cells only). Scaled intensities (y-axis) are shown as box and whisker plots. (n=5)
(**A,C-E**) Data shown are mean±SEM. Statistical significance assessed by paired t-test (**A-D**) or one-way anova (**E**) respectively. *$p < 0.05$, **$p < 0.01$

4.3.2. Mitochondrial respiration is rapidly enhanced in activated EM cells

The findings above demonstrated that glycolysis and TCA cycle function is elevated in recently activated EM $CD8^+$ T cells but not in naïve counterparts. To further elaborate how glucose is metabolized in $CD8^+$ T cells immediately after activation, NV and EM T cells were incubated in uniformly labeled $^{13}C_6$-glucose and the isotopologue distribution of glucose-derived metabolites were assessed under non-activating and activating conditions by LC-MS. Consistent with the above results glucose derived lactate (*M+3*) was only found in activated EM cells (**Fig. 2A**). Intriguingly, glucose derived isotopologues of citrate (*M+2*) and malate (*M+2*) were increased in both activated NV and EM cells (**Fig. 2A**). This indicates that TCA cycle activity in both $CD8^+$ T cell subpopulations is rapidly enhanced following activation, albeit, glucose utilization in the TCA cycle was still greater in EM cells at this phase of the response. Lastly, glucose derived aspartate (*M+2*) was also detected in both cell populations (**Fig. 2A**). *M+2* labeled aspartate is likely generated from the malate–aspartate shuttle, which is important for the transport of NADH reducing equivalents from the cytoplasm to the mitochondrial matrix. A summary of glucose metabolism in NV and EM cells is shown in **Fig. 2B**.

Since TCA cycle metabolites were elevated upon T cell activation, we assessed the impact of activating signals on mitochondrial respiration. We last reported that unlike glycolysis, mitochondrial respiration is not rapidly altered following activation (85). Therefore, NV and EM cells were stimulated for 12h and mitochondrial respiration was then examined by metabolic flux analysis. There were no discernible differences in basal respiration, maximal respiration and spare respiratory capacity between non-activated and activated NV $CD8^+$ T cells (**Fig. 2C,D**). On the other hand, all three respiratory parameters were higher in activated EM counterparts (**Fig. 2C,D**). Since inhibition of mTORC2 blocked glycolytic switch in EM T cells, we then evaluated the impact of mTORC2 inhibitors OSI–027 and KU0063794 on activated EM T cell respiration (**Fig. 2E,F**). Both inhibitors significantly reduced the activation-induced increase in basal respiration of EM cells. However, there was no statistically significant decrease in maximal respiration and spare respiratory capacity. Since mTORC2 plays an important role in Akt activation and in the regulation of glycolytic switch, these findings suggest that the observed increase in mitochondrial respiration in EM cells is potentially due to increased glucose oxidation in the TCA cycle.

Pyruvate is primarily metabolized in two diverging pathways – conversion into acetyl CoA for use in the TCA cycle or conversion into lactate by lactate dehydrogenase A (LDHA) for regeneration of NAD^+. Lactate dehydrogenase inhibitors had minimal effects on IFN-γ production (data not shown), therefore we proceeded to interrogate whether pyruvate is sufficient in rescuing IFN-γ production in EM

cells exposed to glycolytic inhibitors. As expected, EM CD8$^+$ T cells activated in the presence of 2-DG exhibited reduced IFN-γ secretion (**Fig. 2G**). However, activation in the presence of both 2-DG and methyl pyruvate (2 or 10 mM), the cell membrane permeable analog of pyruvate, rescued IFN-γ production by EM CD8$^+$ T cells (**Fig. 2G**). Pyruvate oxidation in the TCA cycle results in increased oxygen consumption. The observed increase in mitochondrial respiratory parameters in activated EM cells suggests that complete glucose oxidation in the TCA cycle likely mediates this rise in respiration. Moreover, these findings indicate that glucose utilization in the TCA cycle is a key component of EM CD8$^+$ T cell recall response.

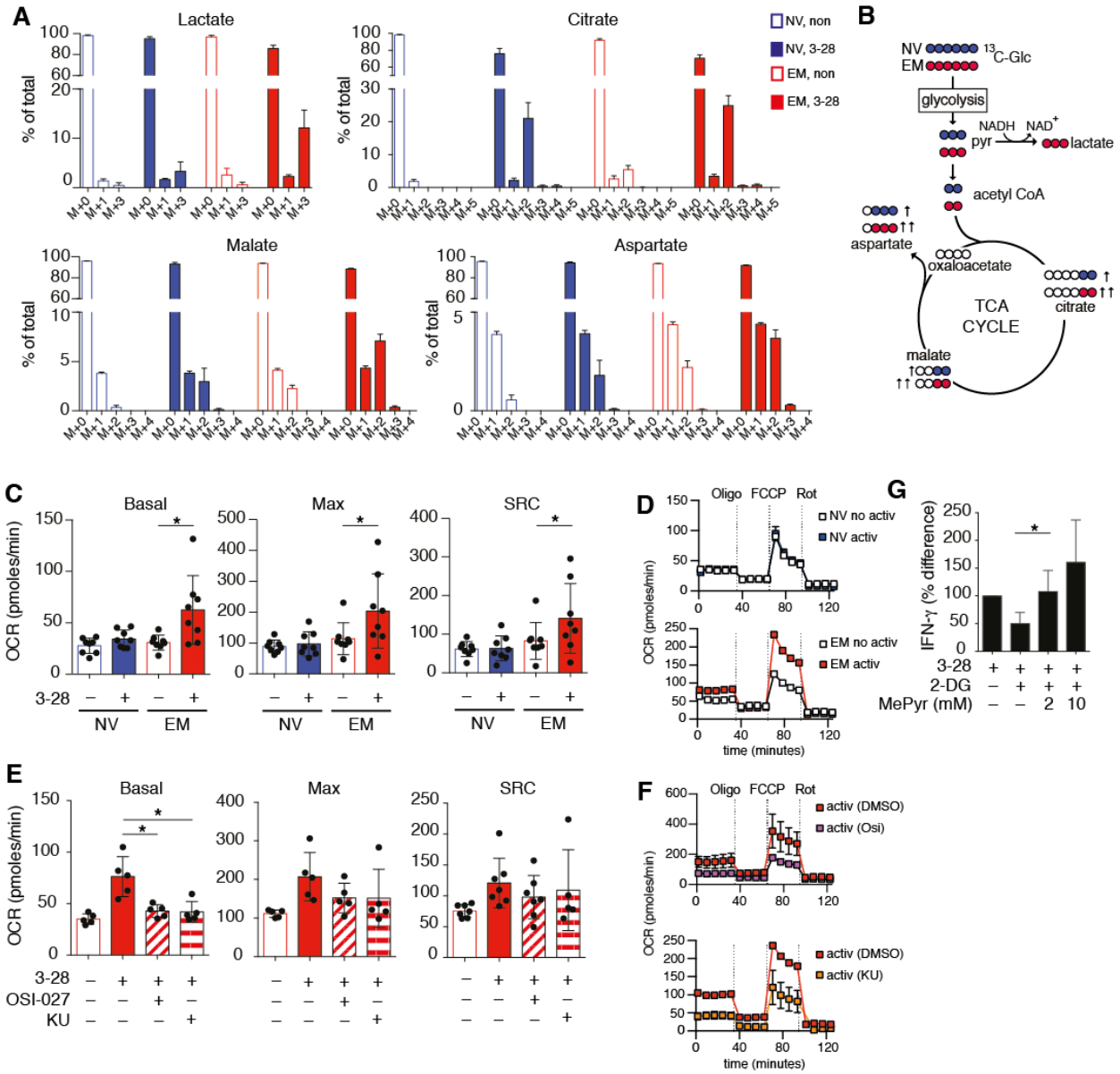

Figure 2. Mitochondrial respiration is enhanced in EM CD8+ T cells

(**A**) Fractional changes in 13C mass isotopologues of NV and EM cultured in the presence of uniformly labeled 13C-glucose under non-activating and activating conditions for 2h. Metabolites were extracted and analyzed by mass spectrometry. (n=5)

(**B**) Summary of glucose flux in NV (blue) and EM (red) following activation.

(**C**) Bar graphs of respiratory parameters (basal, maximal respiratory capacity and spare respiratory capacity) from NV and EM CD8+ T cells cultured for 12h under non-activating and activating conditions. (n=8)

(**D**) Representative mitochondrial perturbation profile of NV (top) and EM (bottom) CD8+ T cells ± 12h activation. (n=8)

(**E**) Bar graphs of respiratory parameters (basal, maximal respiratory capacity and spare respiratory capacity) from EM CD8+ T cells cultured for 12 h under non-activating and activating conditions ± OSI-027 (10 μM) or KU0063794 (10 μM). (n=5-7)

(**F**) Representative mitochondrial perturbation profile of EM CD8+ T cells ± activation in the presence of OSI-027 (top) or KU0063794 (bottom). (n=5-7)

(**G**) IFN-γ cytometric bead array analysis of EM CD8+ T cells cultured for 12h under non-activating or activating conditions in the presence of 2-DG (0.5 mM) and methyl pyruvate. (**C, E, G**) Data shown are mean±SD. Statistical significance assessed by paired t-test *$p < 0.05$

4.3.3. Mitochondrial respiration supports early IFN-γ production by EM CD8$^+$ T cells

Unpublished data from our group indicated that mitochondrial phenotype of naïve is distinct from EM CD8$^+$ T cells. Naïve CD8$^+$ T cells have shorter, fragmented mitochondria, whereas EM CD8$^+$ T cells appeared to be longer in shape and higher networked (95). Consistent with other cell types, hyperfused mitochondria in EM CD8+ T cells had increased mitochondrial membrane potential, indicating higher mitochondrial functionality (38,95). Moreover, mitochondrial functionality is an important component of T cell responses to cognate antigen (78). Contrary to traditional views on the function of mitochondria in cells, new studies have demonstrated that the role of mitochondria goes beyond ATP production. Mitochondria are also important for generation reactive oxygen species (ROS), calcium buffering, regulation of apoptosis, and for the synthesis of several biomolecules critical for cell function (33). To elucidate the role of mitochondria in EM CD8$^+$ T cell recall response, EM cells were activated in the presence of various mitochondrial respiration inhibitors, respiration uncouplers, and mitochondrial ROS inhibitors (**Fig. 3A**). We then probed for effects on proliferation (**Fig. 3B**), activation (by CD69 surface expression)(**Fig. 3C**), and IFN-γ production (**Fig. 3D**). All inhibitors that targeted mitochondrial electron transport chain (ETC) complexes I (rotenone), II (TTFA), III (antimycin-A), and V (oligomycin) blocked cell proliferation (**Fig. 3B**) but had little or no effect on CD69 surface expression (**Fig. 3C**), indicating that inhibition of mitochondrial respiration has a limited impact on early activation but it has a detrimental effect on cell proliferation potentially due to the reduction of ATP availability. Intriguingly, all ETC complex inhibitors reduced IFN-γ production by EM T cells indicating that maintenance of electron transport function and ATP production is an important aspect of the rapid recall response (**Fig. 3C**). Next, we assessed the impact of dissipating the mitochondrial proton gradient by using the mitochondrial uncoupler, FCCP. Chemical uncoupling of the proton gradient diminishes ATP production. If the deficit in ATP synthesis following inhibition of the ETC is important to the observed decrease in IFN-γ production then chemical uncoupling of the proton gradient should mimic this effect. Similar to the inhibition of ETC complexes, chemical uncoupling of mitochondrial respiration had little impact on CD69 expression and it also blocked EM CD8$^+$ T cell proliferation (data not shown). However, disruption of the electrochemical gradient did not inhibit IFN-γ production.

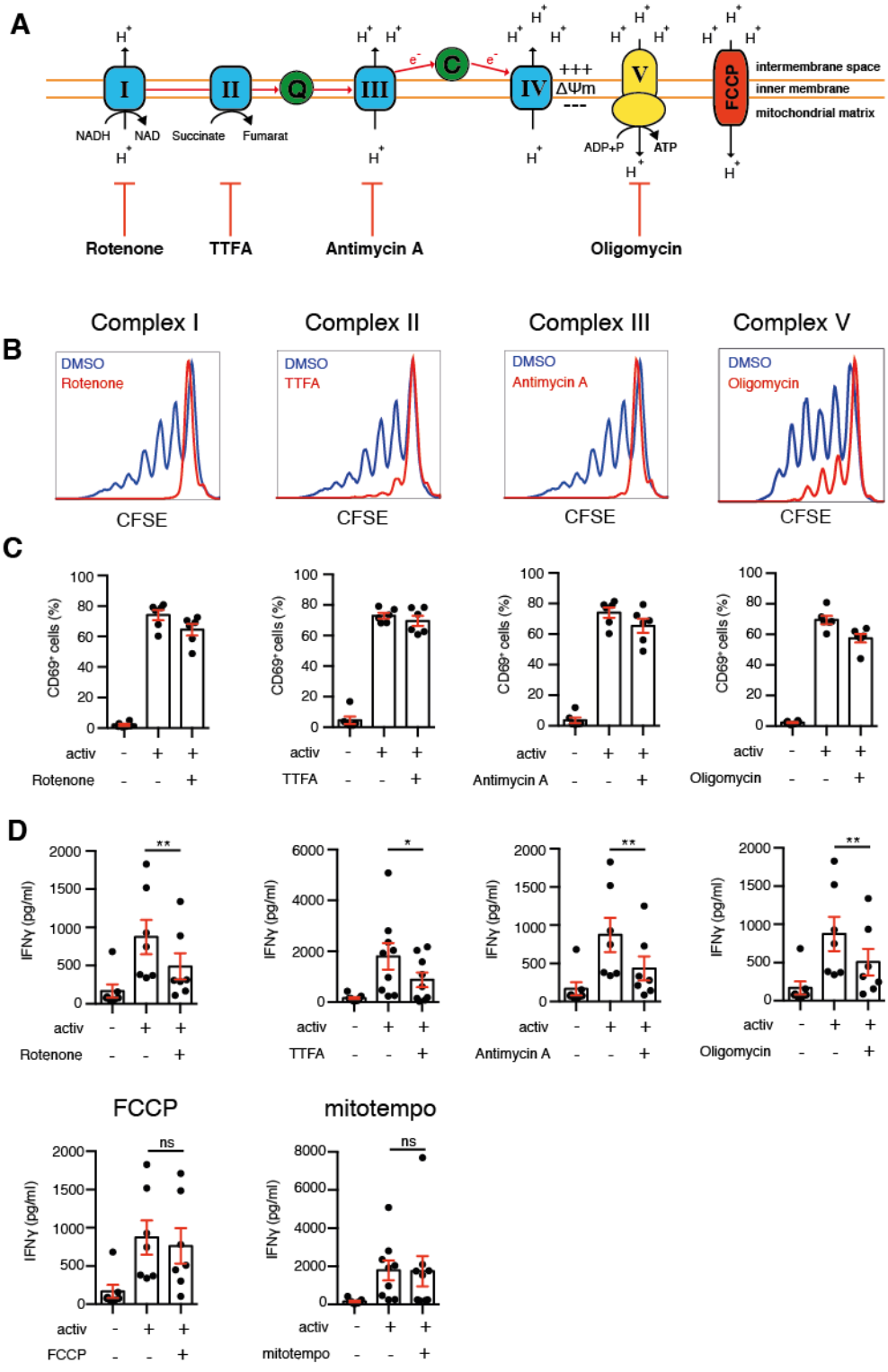

Figure 3. Mitochondrial respiration supports early IFN-γ production by EM CD8+ T cells.
(**A**) Schematic electron transfer chain, mitochondrial ATP generation and used inhibitors.
(**B**) Representative CFSE profile of non-activated or 3D activated effector memory CD8+ T cells in the presence or absence of Rotenone (1 µM), TTFA (200 µM), Antimycin A (2 µM) or Oligomycin (0.1 µM), respectively. Data shown is a representative histogram of n=3 independent donors.
(**C**) Summary bar graph of non-activated or 5h activated CD8+ T cells in the presence or absence of mitochondrial ETC inhibitors as in B, gated on effector memory CD8+ T cells and stained with anti-CD69. (n=6)
(**D**) ELISA of IFN-γ produced by effector memory CD8+ T cells left non-activated or activated for 12h in the presence or absence of mitochondrial ETC inhibitors as in B, FCCP (5 µM) or mitotempo (1 µM), respectively. (n=7-9)
(**B, C**) Data shown are mean±SEM. Statistical significance assessed by paired t-test. *$p < 0.05$, **$p < 0.01$

This indicates that decreased ATP production in the mitochondria is not essential for IFN-γ production. Mitochondrial ROS (mROS) has been shown to regulate IL-2 production in T cells (78). Increased electron flow in the ETC could also increase the generation of mitochondrial ROS (mROS). We examined the impact of mitochondrial ROS on IFN-γ production by treating activated EM $CD8^+$ T cells with a mitochondria targeted anti-oxidant (mitotempo). Targeting mitochondrial ROS did not have an effect on IFN-γ production (**Fig. 3D**). In all these findings suggest that mitochondrial respiration is important for the recall response but this independent of ATP synthesis and mitochondrial ROS signaling.

4.3.4. mTORC2-Akt components are localized in the MAM

The mTORC2–Akt axis is a key regulator of glucose metabolism. Although we previously established that this axis is important for the recall response of EM $CD8^+$ T cells, the molecular mechanism utilized by mTORC2–Akt to enhance glycolytic metabolism and IFN-γ production is still unclear. To determine if mTORC2 components are preferentially expressed in EM T cells, we probed for the expression of mTOR, rictor, raptor, and Sin1. There was no detectable difference in mTOR, rictor, and Sin1 expression in NV and EM cells (**Fig. 4A,B**). Interestingly, raptor expression was lower in EM T cells. These findings suggest that mTORC2 (mTOR and rictor) formation is potentially favored in EM cells, moreover, this further validates our previous finding that mTORC1 signaling does not impact early glycolytic reprogramming in EM T cells. Since Akt was differentially activated in naïve and EM cells, we then asked whether Akt targets are differentially phosphorylated in $CD8^+$ T cell subpopulations. We probed for phosphorylation of Akt targets in NV and EM $CD8^+$ T cells activated for 1 h by immunoblot analysis, using a monoclonal antibody targeted against the phosphorylated Akt substrate motif (RXRXXS*/T*) (**Fig. 4C**). Interestingly, a band in the 40-50 kD region was noticeably increased in activated EM cells. Akt has many known targets that modulate glycolytic metabolism. Once such target is GSK-3β, a 45 kD kinase that was previously demonstrated to negatively impact glycolysis by inhibition of glucokinase activity and inhibition of hexokinase recruitment to the outer mitochondrial membrane (120). Akt phosphorylation of Ser9 inhibits the kinase activity of Gsk-3β. To verify whether Gsk-3β is differentially phosphorylated by Akt in EM T cells, we probed for Gsk-3β phosphorylation at Ser9 in naïve and EM cells by immunoblot analysis (**Fig. 4D,E**). In agreement with our findings above, Gsk-3β was phosphorylated at Ser9 in EM but not in naïve cells indicating that Gsk-3β activity is potentially downmodulated in newly activated EM T cells.

Hexokinase attachment to the mitochondria protects against apoptosis and promotes glycolysis (121). Hexokinase association to the mitochondria is dependent on binding to the voltage dependent anion channel (VDAC). HK and VDAC interaction is inhibited by Gsk-3β phosphorylation of VDAC. To verify if hexokinase binding to the mitochondria is required for the rapid recall response in human $CD8^+$ T cells, we treated EM cells with clotrimazole, a drug that dissociates hexokinase binding to the mitochondria. IFN-γ production was decreased in activated EM cells treated with the drug (**Fig. 4F**). Interestingly, clotrimazole did not have an impact on the immediate-early glycolytic switch (data not shown), indicating that hexokinase association to the mitochondria is requisite for the rapid recall response of memory $CD8^+$ T cells.

The mitochondria associated membrane (MAM) of the endoplasmic reticulum (ER) is a specialized area in the cell that is important for intra-organelle communication between the ER and mitochondria (122). It was previously reported that components of the mTORC2–Akt axis are recruited to the MAM in insulin-stimulated fibroblasts (55). Moreover, both Gsk-3β and hexokinase were reported to be localized in the MAM in various cell types. Therefore, we proceeded to determine whether ER-mitochondria contacts in naïve and EM $CD8^+$ T cells by electron microscopy. Interestingly, ER-mitochondria contacts were increased in EM cells (**Fig. 4G**) signifying that MAM regions are enriched in EM cells. To further elaborate on this finding, we also examined the localization of mTORC2–Akt axis components by immunoblot analysis of crude mitochondrial fractions that are enriched for MAM and mitochondria. This approach was validated by probing for the MAM marker, Grp75, in crude MAM/mitochondrial fractions and in pure mitochondrial preparations from Jurkat T cells. We detected Grp75 in crude MAM/mitochondrial fractions but not in pure mitochondrial preparations (**Fig. 4H**). Moreover, actin was not present in pure mitochondrial preparations, and VDAC1, an outer mitochondrial membrane protein, was detected in both preparations (**Fig. 4H**). Lastly, ACC1, a cytoplasmic protein, was not present in crude MAM fractions but it was only detected in cell homogenate supernatant fractions (**Fig. 4H**). We then examined for the presence of mTORC2–Akt axis components and Grp75 in crude MAM fractions from NV and EM cells by probing for mTOR, rictor, and total Akt. All four proteins were detected in unstimulated NV and EM $CD8^+$ T cell subpopulations (**Fig. 4I**). Next, we assayed for hexokinase I recruitment to the MAM in stimulated $CD8^+$ T cells. At 6 h post stimulation, HK-I was enriched in crude MAM/mitochondria fractions (**Fig. 4J**). These findings suggest that mTORC2–Akt signaling through the MAM is an important component $CD8^+$ T cell signaling following activation. Moreover, increased mitochondria:ER contacts in EM $CD8^+$ T cells could help drive mTORC2–Akt signaling during the memory recall response.

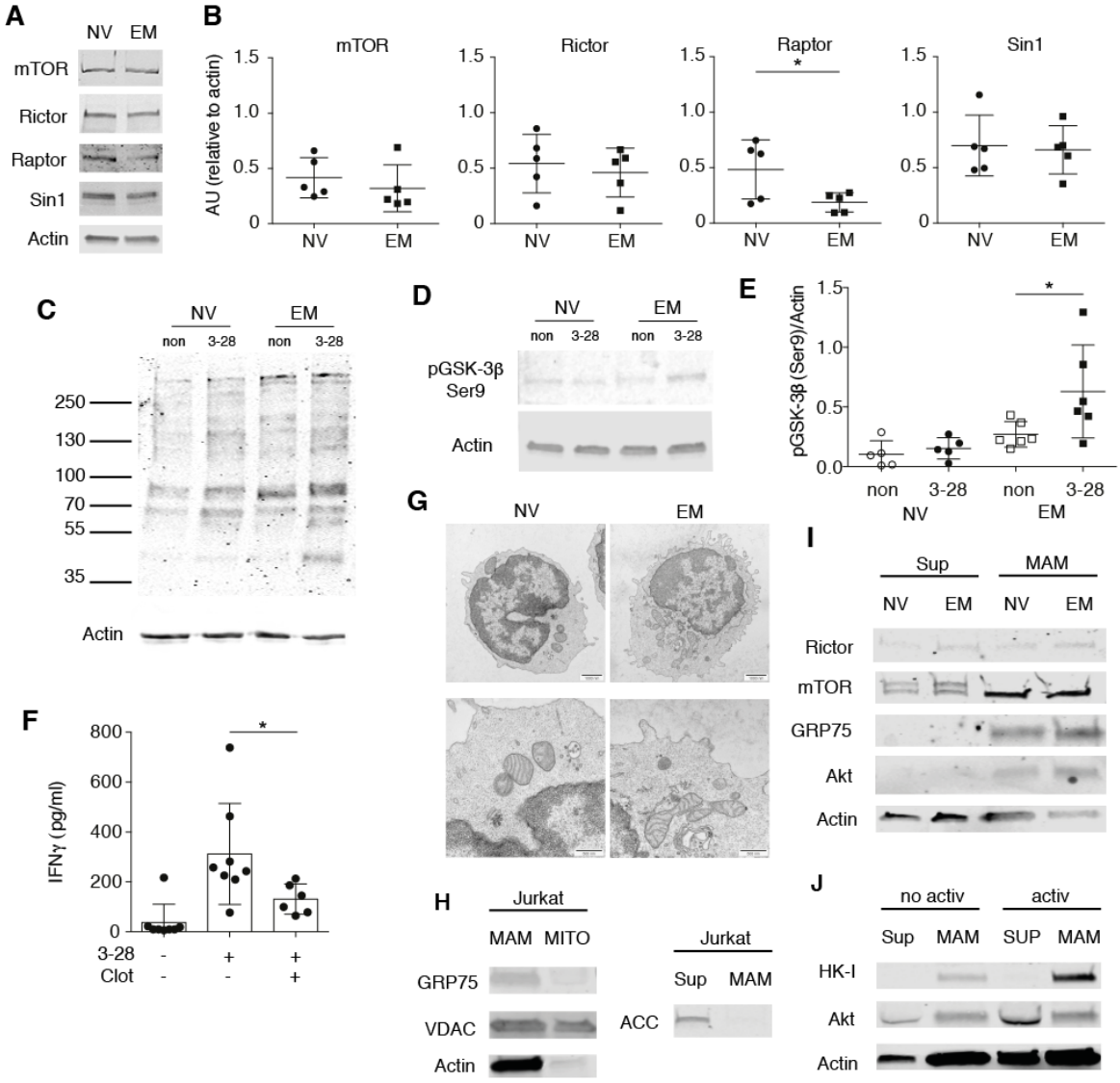

Figure 4. mTORC2-Akt signaling components are present in the mitochondria associated membrane
(**A**) Immunoblot analysis of total cell lysates from fresh sorted NV and EM CD8+ T cells. Blots were probed for mTOR, rictor, raptor, Sin1 and actin antibodies.
(**B**) Summary graphs of immunoblot analysis in (A) normalized to actin. (n=5)
(**C**) Immunoblot analysis of total cell lysates from NV and EM CD8+ T cells. Cells were either left non-activated or activated for 1h and lysates were probed with anti-phosphorylated Akt substrate motif (RXRXXS*/T*) monoclonal antibody to identify phosphorylated Akt substrates. Representative 1 of 4 donors.
(**D**) Immunoblot analysis of total cell lysates from NV and EM CD8+ T cells cultured under non-activating and activating conditions for 1h. Blots were probed for pGSK-3β Ser9 expression.
(**E**) Summary graph of pGSK-3β Ser9 immunoblot analysis. Normalized to actin. (n=5-6)
(**F**) IFN-γ CBA analysis of EM CD8+ T cells cultured for 12 h under non-activating and activating conditions and in the presence of 25 µM clotrimazole. (n=6-8)
(**G**) Transmission electron micrographs (magnification = x28'000) of NV and EM CD8+ T-cells. Scale bars = 1000 nm (top), 500 nm (bottom).
(**H**) Immunoblot analysis of crude MAM/mitochondria (MAM), pure mitochondrial (MITO), and mitochondria free cytoplasmic (SUP) fractions from Jurkat cells. Fractions were probed for Grp75, VDAC, ACC and actin.
(**I**) Immunoblot analysis of Sup and MAM fractions from 1h activated NV and EM CD8+ T cells (combined from 4 donors). Fractions were probed for Rictor, mTOR, Grp75, Akt and actin.
(**J**) Immunoblot analysis of Sup and MAM fractions from bulk CD8+ T cells cultured for 6 h under non-activating and activating conditions. Blots were probed for HK-I, Akt, and actin. (fractions were combined from n=4 donors).
(**B, E, F**) Data shown are mean±SEM. Statistical significance assessed by paired t-test. *$p < 0.05$

4.4. Discussion

Akt is an important regulator of immediate-early glycolytic switch in EM $CD8^+$ T cells. We previously demonstrated that the rapid induction of glycolysis is important for the recall response of memory T cells. However, glucose metabolism along the glycolytic pathway also involves oxidation in the mitochondria via the TCA cycle. Here, we show that mitochondrial function is also rapidly in increased in EM $CD8^+$ T cells compared to naïve counterparts. Blockade of mitochondrial function resulted in diminished memory T cell recall response. Ligation of CD3 and CD28 selectively induced the upregulation of glycolytic and TCA cycle metabolites in EM $CD8^+$ T cells. Intriguingly, citrate and malate were the predominant metabolites increased in EM T cells. Akt inhibition decreased citrate and malate abundance in activated EM cells. Further supporting our central premise that Akt modulation of glucose metabolism is crucial for the regulation of *IFNG* gene expression in EM $CD8^+$ T cells.

Citrate and malate play very important roles in the maintenance of two metabolic processes in the cytosol. Citrate is transported from the mitochondrial matrix to the cytosol by SLC25A1 where citrate is then cleaved into acetyl CoA and oxaloacetate by the enzyme ATP-citrate lyase (123). Acetyl CoA derived from citrate is the primary source of acetyl groups used for the acetylation of various proteins including histones (54). In our last report, we demonstrated that histone H3 acetylation at lysine 9 (H3K9ac) is rapidly enhance in activated EM T cells. This epigenetic mark is important for promoter remodeling and enhancing gene expression. Blockade of glycolysis reduced H3K9ac abundance in the *IFNG* promoter. Coupled with our new findings in this report, the reduction in H3K9ac could be due to decreased glycolytic flux and decreased citrate generation from glycolysis. Interestingly, ATP citrate lyase phosphorylation by Akt at Ser450 enhances the catalytic activity of the enzyme (124). Inhibition of Akt activity could impact acetyl CoA generation for use in protein acetylation.

Malate is an essential metabolite in the transfer of NADH equivalents from the cytosol to the mitochondria via the malate-aspartate shuttle. This pathway allows use of NADH generated in the cytosol by the mitochondrial electron transport chain. A byproduct of citrate breakdown to acetyl CoA is oxaloacetate, which can be converted to malate by cytosolic malate dehydrogenase and the oxidation of NADH to NAD+. The elevated malate levels could be due to increased citrate conversion to acetyl CoA and oxaloacetate. In our last report, we demonstrated that total NAD+ levels were increased in EM $CD8^+$ T cells within 6 h of activation, thus leading to an increase in the NAD^+/NADH ratio. Inhibition of the mitochondrial electron transport chain limits pyruvate entry into the TCA cycle due to the decrease in NAD^+/NADH ratio (125). Our observation that inhibition of ETC complexes also results in the reduction of IFN-γ production is potentially due to the alteration of this ratio. Blockade of ETC also lowers ATP

levels in cells. However, treatment of cells with FCCP, a mitochondrial uncoupler that decreases ATP synthesis, did not have an impact on IFN-γ production indicating that mitochondrial ATP production is not essential for the recall response.

Our results demonstrated that mTOR, rictor, and Akt were present in the MAM/crude mitochondria fraction in both NV and EM $CD8^+$ T cells. The MAM compartment plays an important role in the regulation of lipid synthesis, apoptosis and ER/mitochondrial calcium buffering (122). mTORC2-Akt accumulates in the MAM following insulin stimulation (122). mTORC2 deficient mouse embryonic fibroblasts have elevated cytosolic and mitochondrial calcium following stimulation with ATP (55). Moreover, Akt localization in the MAM was linked to the inhibition of IP3 receptor activity at the ER–mitochondrial interface. Pharmacologic inhibition of Akt or transfection with a dead kinase mutant resulted in a dysregulation of calcium flux from the IP3R (55). Release of intracellular calcium stores from the ER via the IP3R, uptake of extracellular calcium by the CRAC/ORAI channel, and buffering of high cytosolic calcium by the mitochondria are important molecular events that shape T cell effector maturation (126). Differences in calcium release and uptake has been observed in naïve and antigen experienced cells (127). However, the molecular cues that differentially regulate T cell calcium flux in both naïve and memory subpopulations are not well understood. Our finding that components of mTORC2–Akt axis are present in the MAM of $CD8^+$ T cells and that Akt is rapidly phosphorylated at Ser473 by mTORC2 in EM cells could point to differences in the regulation of calcium flux. In addition, the elevated mitochondrial mass of EM cells could enhance mitochondrial calcium buffering in these cells. Lastly, GSK-3β phosphorylation at Ser9, an Akt target, was also higher in EM cells following activation. Gsk-3β controls binding of hexokinase to VDAC at the MAM and phosphorylation at Ser9 decreases kinase activity (128). Hexokinase localized at the MAM supports the catabolic function of glycolysis (121). GSK-3β phosphorylation of VDAC destabilizes the VDAC–hexokinase interaction. Our finding that HK-I localization in the crude MAM/mitochondria fraction is enhanced following activation further suggests that Akt inhibition of GSK-3β is an important step in promoting rapid glycolytic switch in EM cells. How the mTORC2–Akt–GSK-3β axis enhances mitochondrial respiration is a focus for future studies.

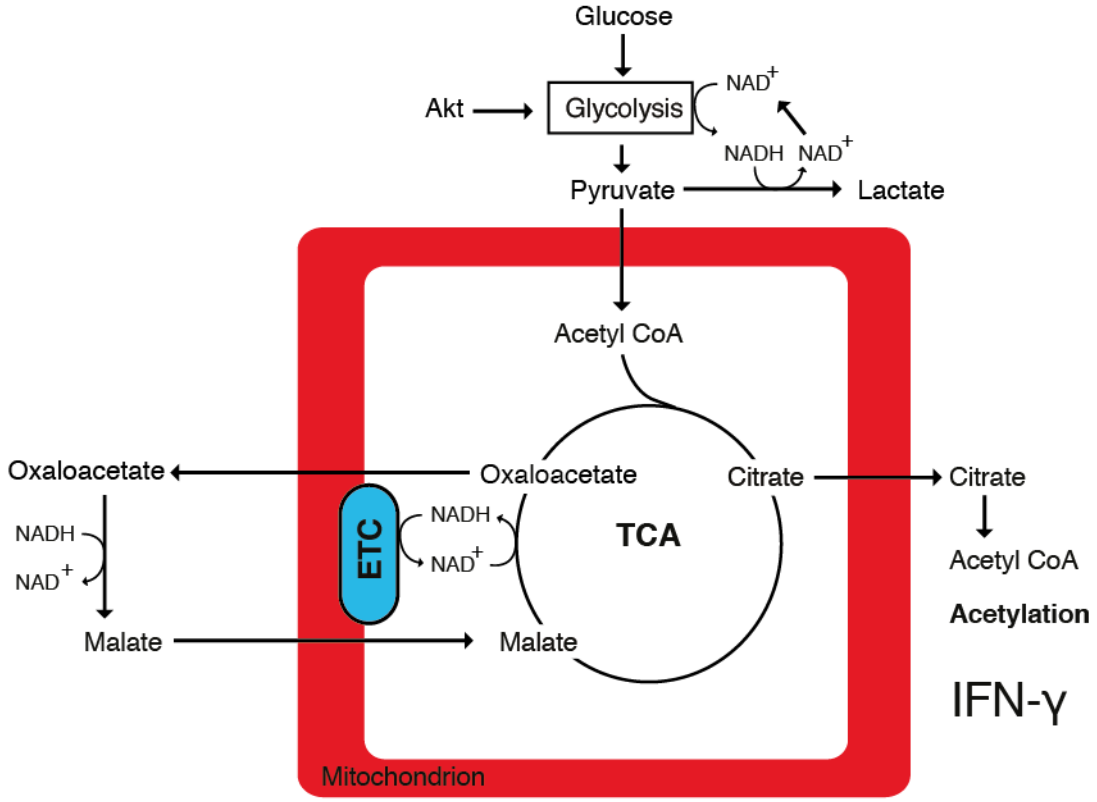

Graphical overview

5. Dual antibody bead coupling: a semi quantitative approach (Manuscript 3, Technical note)

5.1. Introduction

Classical T cell activation protocols mainly use soluble or plate-bound CD3 and CD28 monoclonal antibodies (mAb) with distinct antibody ratios (85,129). However *in vivo*, $CD8^+$ T cells and antigen-presenting cells (APC) form an immunological synapse leading to clustering of TCR/CD3 and CD28 molecules, which is important for activation induced downstream signaling (130). To form an immunological synapse *in vitro*, polarized activation is critical and can be induced by using antibody-coated micro-particles, mimicking an APC-T cell interaction. Coating a single effector protein (i.e. antibody) to a polymer-, silica- or magnetic microsphere is a straightforward approach. However, loading a distinct ratio of two antibodies is challenging and controlling the final ratio for each bead-batch is required to recognize and thus reduce variability.

Here we provide a protocol for dual antibody coupling on polystyrene beads. In addition, we propose an easy to implement semi-quantitative flow cytometric approach to assess antibody ratio bound to the beads, which can be used for optimizing antibody loading and quality control. Finally, we assessed the operational functionality of activation beads coated with different amount and ratio of antibodies for T cell activation in functional cellular *in vitro* assays.

5.2. Materials and Methods

5.2.1. Preparation of activation beads: coating of CD3 and CD28 mAb

To load antibodies on beads, 100µl containing $5x10^7$ beads suspension of Polybead Microspheres 4.5µm ∅ (#17135, Polyscience Washington, USA) and 900µl borate buffer (0.1 M boric acid pH 8.5) (#B6768, Sigma-Aldrich, Buchs, CH) were prepared using 1.5ml polypropylen microtubes (#72.692.405, Sarstedt, Germany). Beads were washed three times in 1000µl borate buffer and centrifuged at 1500xg for 5min each. Mouse anti-human CD28 IgG1 mAb (10-100µg, Clone 28.2, #302914, Biolegend, San Diego, USA) were diluted in total of 200µl borate buffer and gently mixed with the beads for 30min at room temperature, on a vertical shaker. Thereafter, mouse anti-human CD3

IgG2a mAb (1µg, Clone HIT3A, #300314, Biolegend, San Diego, USA) were diluted in 300µl borate buffer and added for another 30min incubation. Beads were blocked by washing three times with 1000µl borate buffer containing 10mg bovine serum albumin (Sigma-Aldrich) / ml and incubated for 15min each. Storage of antibody-loaded beads was performed according to the bead manufacturer's instruction.

5.2.2. Assessment of antibody-loading on activation-beads

To test antibody-loaded beads $1x10^5$ beads were stained using Allophycocyanin(APC)-conjugated goat anti-mouse IgG1 (#1070-11S, SouthernBiotech, Alabama, USA) for the detection of CD28 mAb or Phycoerythrin(PE)-conjugated goat anti-mouse IgG2a (#1080-09S, SouthernBiotech, Alabama, USA) for the detection of CD3 mAb, respectively.

Optimal staining concentration of both reporter antibodies (rep.-Ab) was determined using different amounts (0.04ng – 125ng) of rep.-Ab, separately added to $1x10^5$ beads, diluted in a total volume of 25µL staining buffer (PBS plus 1% bovine serum albumin) and were incubated for 30min at room-temperature. The same concentration of appropriate isotyp-controls PE labeled goat IgG (#0109-09, SouthernBiotech, Alabama, USA) and APC-labeled goat IgG (#0109-11, SouthernBiotech, Alabama, USA) was applied to determine unspecific binding. The concentration of 12ng for IgG1 APC or 50ng for IgG2a PE rep.-Ab in 25µL staining buffer revealed the highest signal (mean fluorescence intensity (MFI) of rep.-Ab) to noise (MFI of isotype-control) ratio and was therefore considered as optimal staining concentration and applied throughout all experiments (data not shown) (131). To indirectly determine the amount of coated activation antibody molecules per bead, we used Quantum™ MESF kits Quantum APC (#823, Bangslab, Fishers, USA) and Quantum PE (#827, Bangslab, Fishers, USA), consisting a series of fluorescent microsphere populations labeled with varying amounts of fluorochromes. These bead populations were acquired as a mixture in a separate tube using the same flow cytometer settings for each respective experiment. Data were acquired using a BD AccuriC6 flow cytometer (Becton Dickinson, Franklin Lake, USA) and analyzed with FlowJo 10.0.8 (Tree Star, Ashland, USA). The MFI signal of each MESF bead population was plotted against the respective MESF units (determined by the provider company) and all MFI signals of the rep.-Ab were converted into the respective MESF units according to manufacturer's instruction. KD values were determined using Prism 6.0h (GraphPad Software, USA), applying a non-linear binding regression / specific binding with hill slope on concentration (x-axis) versus %MESF (y-axis) data.

5.2.3. Cell Isolation

Blood samples were obtained from healthy blood donors as buffy coats after written informed consent (Blood donor centre, Basel). Peripheral blood mononuclear cells (PBMC) were isolated by standard density-gradient centrifugation protocols (#1114547, Lymphoprep Fresenius Kabi, Norway)(85). $CD8^+$ T cells were positively selected using magnetic $CD8^+$ beads ((#130-045-201, MiltenyiBiotec, Germany) or negative selected using EasySep Human $CD8^+$ T cell Isolation Kit (#19053, Stemcell Technology, Grenoble, France) following manufacturer's instruction. Cells were rested overnight in RPMI-1640 medium (#52400, Gibco, Waltham, USA) containing 10% FBS (#10270, Gibco, Waltham, USA), 50U penicillin/ml and 50ug streptomycin/ml (#15140-122, Gibco, Waltham, USA).

5.2.4. Flow-cytometric analysis of cell-bead mixtures and CD69 expression

$CD8^+$ T cells were plated into flat-bottom 96-well plates (5×10^5 cells per well) and activated using antibody-loaded beads for 5h at 37°C / 5%CO_2. Negatively selected and activated $CD8^+$ T cells were used to detect distinct populations of cell and bead populations in the forward and side scatter stained by fluorescein isothiocyanate (FITC)-conjugated anti-CD8 antibody (#555634, BD Bioscience, San Jose, USA) to detect $CD8^+$ T cells and previously described PE-conjugated anti-IgG2a to detect antibody-loaded beads. Positively selected and activated $CD8^+$ T cells were stained using APC-conjugated CD69 antibody (#21620696, ImmunoTools, Friesoythe, Germany). Data were acquired and analyzed as described above.

5.3. Results

5.3.1. Evaluation of activation beads

Each activation mAb was applied in a distinct IgG subclass (i.e. CD28 mAb: IgG1; CD3 mAb:IgG2a), in order to assure controlling antibody ratio on the beads with subclass specific rep.-Ab (**Fig. 1A**). These rep.-Ab were conjugated to a fluorochrome of high molecular size, ensuring a fluorochrome to protein (f:p) ratio of 1 (132). Rep.-Ab binding curves were used to determine the concentration of each rep.-Ab that reveals the highest signal to noise ratio to determine optimal staining concentrations. Our binding curves indicated the highest signal to noise ratio at 12ng anti-IgG1-APC and 50ng anti-IgG2a-PE applied in 25μL staining buffer (data not shown) and were therefore applied throughout all experiments.

Upon excitation, each fluorochrome – conjugated to the rep.-Ab – attains a different level of brightness, thus for quantitative calculations fluorescence intensities of two differently conjugated antibodies cannot be directly compared. To normalize for distinct fluorescence properties, we used the 'Molecules of Equivalent Soluble Fluorochrome' (MESF) approach. MESF units correspond to the fluorescence intensity of a given number of pure fluorochrome molecules in solution (133). Preliminary experiments measuring CD3 molecules on human PBMC using this approach, revealed comparable amount of molecules to previously published data (data not shown).

Parallel acquisition of MESF beads revealed the linear dependency of MFI signal and MESF units with PE displaying higher brightness per fluorochrome molecule compared to APC (**Fig. 1B**). Translation of fluorescence signal of each rep.-Ab into MESF units revealed the binding curves using single mAb coated, saturated beads displayed in **Fig. 1C+D** and were the basis for all subsequent calculations (**Fig. 1E**). The binding strength of each rep.-Ab may vary greatly from antibody to antibody and must be taken into account for quantitative comparison. An antibody binding curve allows indirect estimation of antibody-affinity and multiple binding motives via the calculation of the KD value. In order to compare (and subsequently correct for) the two antibody's affinities and multiple binding motives to their target, we normalized the two binding curves of each reporter antibody by setting saturation MESF units to 100% binding (**Fig. 1D**). Comparison of KD values of each rep.-Ab revealed a 1.07 higher affinity of anti-IgG1 rep.-Ab (recognizing the CD28 antibody coated to the bead) compared to the anti-IgG2a rep.-Ab (detecting the CD3 antibody coated on the bead), and was subsequently corrected (**Fig. 1E**).

The final workflow from initial MFI units to the final assessment of 'molecules of activating antibodies per bead' is visualized in **Fig. 1E** using a representative example.

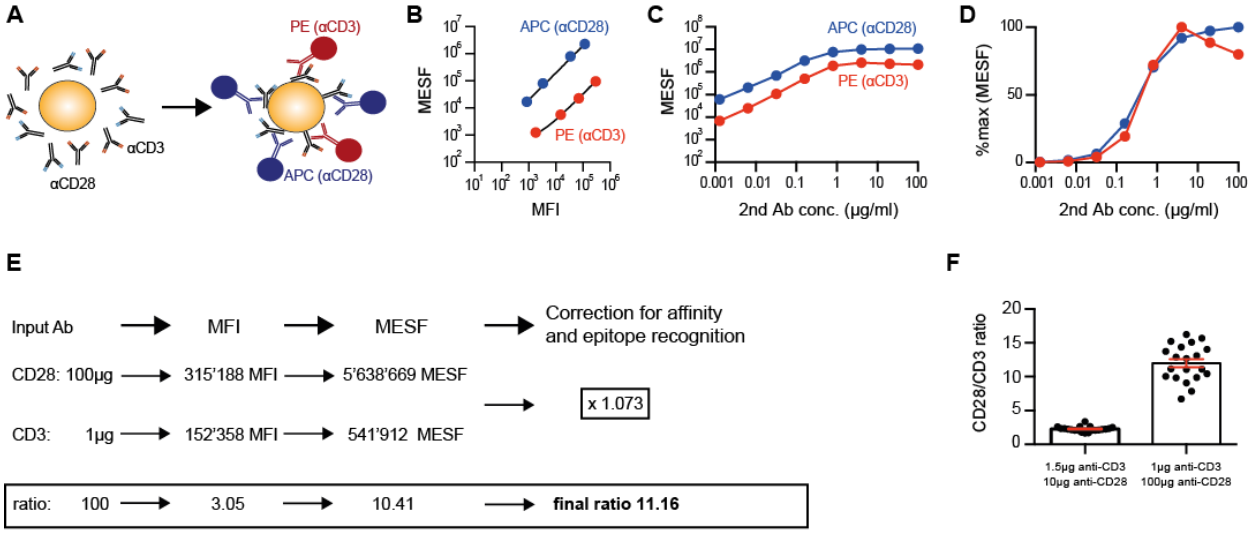

Figure 1. Principle of assessment of antibody-loaded beads using reporter antibodies
(**A**) Scheme of beads loaded with activation antibodies (CD3 and CD28) and loading control using reporter antibody.
(**B**) Representative MESF/MFI standard curve to calculate MESF values for CD3 mAb (red) and CD28 mAb (blue).
(**C**) Anti-IgG1 (blue) and anti-IgG2a (red) MESF % max dilution curve.
(**D**) Anti-IgG1 (blue) and anti-IgG2a (red) dilution curve and MESF values.
(**E**) Representative workflow to calculate CD3/CD28 ratio corrected for MESF, avidity and polyclonality.
(**F**) Assessment of lot to lot differences of beads coated with two different input CD28/3 ratio. n=20

5.3.2. Production of activation beads with distinct CD28/3 mAb ratio

Initial experiments assuming input ratio of antibodies correlates to similar passive binding on polystyrene beads were performed according to previous published methods (87). However, using our validation approach, and despite higher concentration of input CD28 mAb, we detected a higher proportion of CD3 mAb bound on the beads. Specifically, an input ratio of 10:1 CD28:CD3 mAb resulted in a final ratio of 0.319 (Standard deviation SD=0.009; n=3). This suggested distinct binding properties of the two coating mAb. Additional trial experiments identified that pre-incubation of one of the coating mAb, followed by adding the second coating mAb significantly changed the final binding ratio on the beads. Our final procedure comprised the pre-incubation of CD28 mAb, followed by admitting of CD3 mAb with an input ratio of 10:1.5 or 100:1 respectively. This final procedure obtained defined molecule-ratios of both antibodies on polystyrene beads (10:1.5; mean CD28:CD3 ratio of 2.276; SD= 0.3744) (100:1; mean CD28:CD3 ratio of 12.02; SD=2.703) (n=20) (**Fig. 1E**).

5.3.3. Flow-cytometric discrimination of T cells and activation beads

Beads, cells and bead-cell complexes were monitored in functional cellular *in vitro* experiments with T cells activated via the produced activation beads. Mixtures of $CD8^+$ T cells and activation beads formed three distinct subpopulations in the forward and side scatter (**Fig. S1**). Staining with FITC-conjugated anti-CD8 to detect $CD8^+$ T cells and PE-conjugated anti-IgG2a to detect the activation beads, revealed the following subsets: $CD8^{neg}$ $IgG2a^{pos}$, (**Fig. S1A**), representing unbound activation beads, $CD8^{pos}$ $IgG2a^{neg}$, (**Fig. S1B**), indicating exclusively T cells and $CD3^{pos}$ and $IgG2a^{pos}$, assigning beads conjugated to cells (**Fig. S1C**).

5.3.4. Functionality of antibody-loaded beads *in vitro*

We predicted a potential influence of different amounts of CD28 mAb coated on activation beads in human $CD8^+$ T cell activation. To confirm this hypothesis, we produced antibody-loaded beads using a fixed amount of CD3 mAb and different amounts of CD28 mAb to activate $CD8^+$ T cells. As expected, increased input CD28 mAb resulted in higher binding of CD28 mAb on the beads (**Fig. 2A**) and consequently higher CD28/3 ratios (**Fig. 2B**). To address the impact of an increased CD28 amount and CD28/3 ratio coated on activation beads, we assessed the expression of the early-activation marker CD69 on $CD8^+$ T cells activated using differently loaded activation beads. Indeed, $CD69^{pos}$ $CD8^+$ T cells were increased proportionally to increased ratio of CD28 and CD28/3 ratio (**Fig. 2C**). These results suggest a significant and relevant role of differently loaded beads on $CD8^+$ activation.

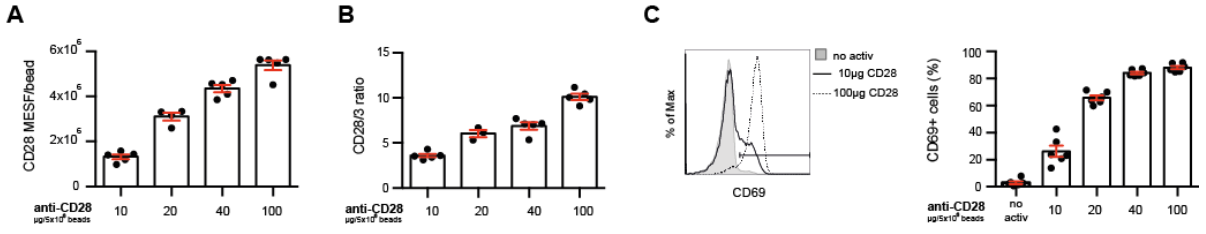

Figure 2. Increased amount of anti-CD28 mAb resulted in a higher CD28/3 ratio and increased CD69 frequency in CD8+ T cells
(A) Total anti-CD28 mAb molecules per bead loaded with different amount of anti-CD28 mAb (in µg) measured using reporter antibody. (n= 3-5)
(B) CD28/3 ratio per bead loaded with different amount of anti-CD28 mAb (in µg) measured using reporter antibody. (n=3-5)
(C) Representative CD69 profile CD8+ T cells stimulated using unloaded (grey), 10µg (continuous line) or 100µg (dashed line) anti-CD28 mAb for 5h; Summary bar graph of CD69+ CD8+ T cells stimulated using beads loaded with different amount of anti-CD28 mAb. (n=6)

5.4. Discussion

Synchronous stimulation of TCR and CD28 or alternative co-stimulatory molecules are increasingly used for *in vitro* stimulation of T cells and antibody coated microspheres have explicit advantages over soluble or plate coated antibodies (134). Here we propose a bead loading control method allowing the estimation of resulted ratio between two activation antibodies. Using this method, we were able to modify the bead coating process toward a reproducible final ratio. Our method demonstrated that input- and final-ratio of two coating antibodies on polystyrene beads is not comparable, although this is often assumed. Our controlling method is semi-quantitative, however it goes beyond MFI signal comparison, because MFI signals of two different reporter antibodies (i.e. conjugated to a different fluorochrome) are incomparable due to different excitation/emission properties of varied fluorochromes. Moreover, each antibody has different binding properties according to their distinct affinity and epitope(s) recognition. Estimation of accurate final binding proportions on the bead and subsequent calculation of the resulting ratio has to account for these differences and are therefore involved in our formula. In order to keep avoiding addition confounders, we resigned using reporter-antibodies conjugated to small fluorochromes (i.e. FITC) revealing a different fluorochrome:protein (f:p) ratio for each new lot. We rather used reporter-antibodies conjugated to fluorochrome of high molecular size (i.e. PE and APC), revealing a fluorochrome:protein ratio of 1.

Clearly, the here proposed controlling method has to be further applied to different sets of coating- and reporter-antibodies in order to confirm the universality of this method. Moreover, how other bead types beyond polystyrene beads interact with activation mAb requires investigation.

In this study, we have demonstrated that reproducible coating of two different antibodies on polystyrene beads is possible. Results of *in vitro* activated T cells between different publications using distinct coating protocols are often variable. Our data suggest that this variance might be partly due to differences in antibody loading on activation beads.

5.5. Supplemental Material

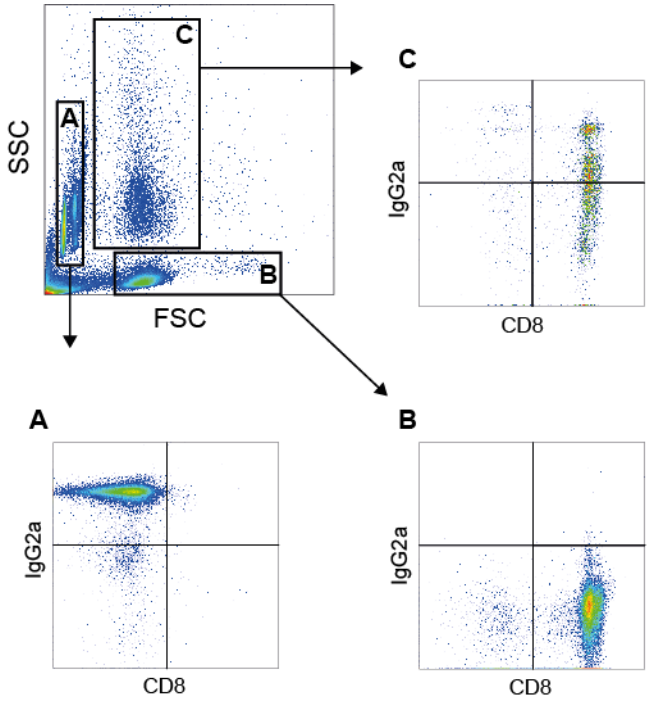

Supplementary Figure 1)
Forward (FSC) and side scatter (SSC) of untouched CD8+ T cells activated for 5h with activation beads. (A,B,C) Cells and beads were incubated with CD8 and IgG2a staining-antibody to discriminate cells and beads within the different populations in forward and side scatter.

6. Future perspective

T cell immune responses are tightly regulated to balance host defense and autoimmunity. However, there are several therapeutic applications where tipping the balance of T cell fate and function is clinically advantageous (**Fig. 10**) (30). A potential application is cancer immunotherapy, where increased protective T cell immunity through a robust induction of effector and memory responses has been demonstrated to increase patient survival. In contrast, suppression of dysfunctional T cell responses in autoimmune diseases has been shown to slow disease progression.

Cellular metabolism regulates T cell function, proliferation and migratory capacity (135). Therefore, targeting the metabolic reprogramming of activated T cells could provide a novel strategy to modulate T cell responses (136,137).

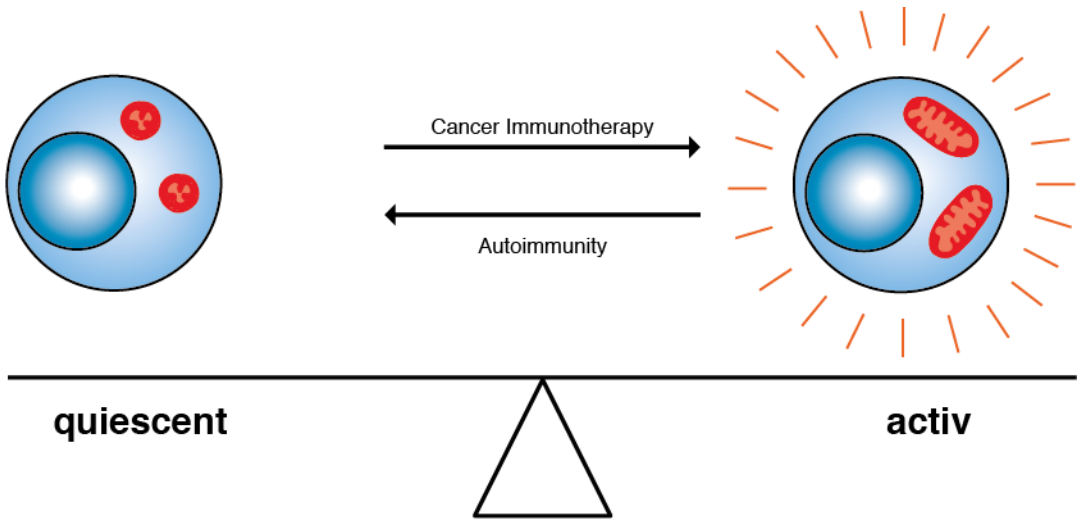

Figure 10) Conclusion

6.1. Modulation of cellular metabolism to increase immune responses

Tumor infiltrating lymphocytes (TIL) and specifically effector-memory $CD8^+$ T cells are important for controlling tumor growth, recurrence and consequently survival in various cancer types (138-140). However, there is a dynamic interaction between T cells and tumor cells promoting immune evasion by tumor cells. IFN-γ produced by T cells can induce PD-L1 expression on tumor cells, which inhibits T cells through PD-1/PD-L1 interaction (116,141). Recent developments in cancer therapy showed exciting improvements in clinical outcome by targeting pathways that regulate T cell activity (142). These immune checkpoint therapies (such as antibodies against CTLA-4, PD-1, PD-L1) block

inhibitory pathways of activated T cells and increasing effective antitumor responses against various tumor types (141). Unfortunately, only a fraction of patients can benefit from immune checkpoint therapy (142). Targeting cellular metabolism to potentiate T cell responses is an attractive approach to further improve T cell functions in tumors (143). Interestingly, pharmacologic blockade of glycolysis (i.e. 2-DG) or augmentation of catabolic pathways (i.e. metformin) during the priming phase of $CD8^+$ T cells results in increased memory formation and consequently in enhanced protective anti-tumor immunity, *in vivo* (30,93,144). Metformin treatment is associated with reduced cancer risk in type II diabetic patients (145). Although metformin has a direct anti-proliferative effect on tumor cells, modulation of metabolic reprogramming in $CD8^+$ T cells could contribute to the reduced cancer risk (146).

Tumor cells and T cells share similarities in their metabolic repertoire, such as the Warburg effect (147). Both cancer cells and activated $CD8^+$ T cells metabolize glucose by aerobic glycolysis to lactate (2,31). Tumor cells can create a microenvironment, which is nutrient restricted and T cells have to compete with tumor cells for substrates such as glucose and glutamine. Nutrient deprivation limits glycolysis and consequently the production of effector cytokines such as IFN-γ in T cells (79,85,116,117). Moreover, a recent publication showed that phosphoenol pyruvate (PEP) acts as a metabolic checkpoint for T cells indicating glucose availability and contribute to IFN-γ production in both $CD4^+$ and $CD8^+$ T cells. Interestingly, metabolic reprogramming towards a higher PEP accumulation in TIL increases anti-tumor response *in vivo* (117). Conversely, increased lactic acid concentration in the tumor microenvironment can downregulate glycolytic enzyme expression and consequently reduce glycolytic flux and cytolytic activity in $CD8^+$ T cells (135). Another recent publication suggest checkpoint blockade antibodies can restore effector function through decreased glycolysis in tumor cells and thereby increasing metabolic fitness of T cells to compete for nutrients (116).

These recent studies suggest metabolic reprogramming of both tumor and T cell metabolism is an attractive target for future therapeutic applications. However, additional studies are required to dissect metabolic differences between both cell types for a targeted, tumor-specific approach to inhibit tumor metabolism without negatively affecting T cell function (147). Alternatively, manipulation of T cell metabolism for *ex vivo* TIL expansion could potentially improve the efficiency of adoptive immunotherapy (30).

Metabolic differences between naïve and memory $CD8^+$ T cells provides memory T cells with increased metabolic plasticity to survive and perform effector functions in this competitive microenvironment (tumor microenvironment, inflammation). However, more studies are required to

dissect how cellular metabolism in different T cell subsets supports effector function in this hypoxic and nutrient restricted microenvironment.

6.2. Modulation of cellular metabolism to limit T cell responses

Pathologic T cells are a typical feature of autoimmunity (137). Interestingly, increased mitochondrial function is associated with certain autoimmune diseases (137). For example, PBMCs from rheumatic disease patients have increased mitochondrial respiration in comparison to non-active or healthy controls. Moreover, glucocorticoid treatment significantly reduce this increased basal respiration (148). This suggests that targeting cellular metabolism is a potential therapeutic strategy for immunosuppression.

In systemic lupus erythematosus (SLE), T cells contribute to aberrant B-cell autoantibody production (149). Interestingly, $CD4^+$ T cells from SLE patients and mouse models display enhanced catabolic activity with increased glycolysis and mitochondrial respiration (150). Combining both mitochondrial respiration and glycolysis inhibition normalized increased IFN-γ secretion in $CD4^+$ T cells *in vitro*. Moreover, *in vivo* application result in reduced SLE disease phenotype in mice (137,150).

Multiple sclerosis (MS) is an autoimmune disease characterized by the infiltration of activated T cells into the central nervous system. Experimental autoimmune encephalomyelitis (EAE) is a widely used animal model to study the disease (151). Mice treated with ETC or mROS inhibitors have lower inflammatory cytokine levels, delayed onset and decreased disease scores of EAE (151,152). Moreover, mice lacking the transcription factor ERRα, involved both in mitochondrial biogenesis and glycolysis had lower IL-17 and IFN-γ producing $CD4^+$ T cells and decreased susceptibility to EAE. Therefore, targeting metabolic regulation can impact T cell differentiation and function modulating disease progression (90).

All together, targeting glycolysis and mitochondrial respiration is a potential new therapeutic approach to control pathologic T cell response in autoimmunity. However, despite the increased body of literature in the field of immunometabolism, a better understanding on how T cell metabolism supports immune function is required. These findings, combined with the metabolic phenotyping of various autoimmune diseases, could provide new insights on the treatment of autoimmune diseases.

7. References

1. Mackay CR, Marston WL, Dudler L. Naive and memory T cells show distinct pathways of lymphocyte recirculation. J Exp Med. The Rockefeller University Press; 1990 Mar 1;171(3):801–17.

2. MacIver NJ, Michalek RD, Rathmell JC. Metabolic Regulation of T Lymphocytes. Annu Rev Immunol. 2013 Mar 21;31(1):259–83.

3. Nolz JC. Molecular mechanisms of CD8+ T cell trafficking and localization. Cellular and Molecular Life Sciences. Springer Basel; 2015 Apr 16;72(13):1–13.

4. Remakus S, Sigal LJ. Memory CD8$^+$ T cell protection. Adv Exp Med Biol. New York, NY: Springer New York; 2013;785(Chapter 9):77–86.

5. Banchereau J, Steinman RM. Dendritic cells and the control of immunity. Nature. 1998 Mar 19;392(6673):245–52.

6. Haring JS, Badovinac VP, Harty JT. Inflaming the CD8+ T Cell Response. Immunity. 2006 Jul;25(1):19–29.

7. Ahmed R, Bevan MJ, Reiner SL, Fearon DT. The precursors of memory: models and controversies. Nat Rev Immunol. 2009 Sep;9(9):662–8.

8. Murali-Krishna K, Altman JD, Suresh M, Sourdive DJ, Zajac AJ, Miller JD, et al. Counting antigen-specific CD8 T cells: a reevaluation of bystander activation during viral infection. Immunity. 1998 Feb;8(2):177–87.

9. Butz EA, Bevan MJ. Massive expansion of antigen-specific CD8+ T cells during an acute virus infection. Immunity. 1998 Feb;8(2):167–75.

10. Cui W, Kaech SM. Generation of effector CD8+ T cells and their conversion to memory T cells. Immunol Rev. 2010 Jul;236(1):151–66.

11. Yap M, Brouard S, Pecqueur C, Degauque N. Targeting CD8 T-Cell Metabolism in Transplantation. Front Immunol. 2015;6:547.

12. la Calle-Martin de O, Hernandez M, Ordi J, Casamitjana N, Arostegui JI, Caragol I, et al. Familial CD8 deficiency due to a mutation in the CD8 alpha gene. J Clin Invest. 2001 Jul;108(1):117–23.

13. Berke G. The CTL's kiss of death. Cell. 1995 Apr 7;81(1):9–12.

14. Harty JT, Tvinnereim AR, White DW. CD8+ T cell effector mechanisms in resistance to infection. Annu Rev Immunol. 2000;18(1):275–308.

15. Joshi NS, Cui W, Chandele A, Lee HK, Urso DR, Hagman J, et al. Inflammation directs memory precursor and short-lived effector CD8(+) T cell fates via the graded expression of T-bet transcription factor. Immunity. 2007 Aug;27(2):281–95.

16. Kaech SM, Cui W. Transcriptional control of effector and memory CD8+ T cell differentiation. Nature Publishing Group. 2012 Nov;12(11):749–61.

17. Miller JD, van der Most RG, Akondy RS, Glidewell JT, Albott S, Masopust D, et al. Human effector and memory CD8+ T cell responses to smallpox and yellow fever vaccines. Immunity. 2008 May;28(5):710–22.

18. Ahmed R, Gray D. Immunological memory and protective immunity: understanding their relation. Science. 1996 Apr 5;272(5258):54–60.

19. Kaech SM, Wherry EJ. Heterogeneity and Cell-Fate Decisions in Effector and Memory CD8+ T Cell Differentiation during Viral Infection. Immunity. 2007 Sep 21;27(3):393–405.

20. Mahnke YD, Brodie TM, Sallusto F, Roederer M, Lugli E. The who's who of T-cell differentiation: human memory T-cell subsets. Eur J Immunol. 2013 Nov;43(11):2797–809.

21. Farber DL, Yudanin NA, Restifo NP. Human memory T cells: generation, compartmentalization and homeostasis. Nat Rev Immunol. 2014 Jan;14(1):24–35.

22. Sallusto F, Lenig D, Förster R, Lipp M, Lanzavecchia A. Two subsets of memory T lymphocytes with distinct homing potentials and effector functions. Nature. 1999 Oct 14;401(6754):708–12.

23. Masopust D, Vezys V, Marzo AL, Lefrançois L. Preferential localization of effector memory cells in nonlymphoid tissue. Science. 2001 Mar 23;291(5512):2413–7.

24. Sallusto F, Geginat J, Lanzavecchia A. Central memory and effector memory T cell subsets: function, generation, and maintenance. Annu Rev Immunol. 2004;22(1):745–63.

25. Wang A, Chandran S, Shah SA, Chiu Y, Paria BC, Aghamolla T, et al. The stoichiometric production of IL-2 and IFN-γ mRNA defines memory T cells that can self-renew after adoptive transfer in humans. Sci Transl Med. 2012 Aug 29;4(149):149ra120–0.

26. Gattinoni L, Lugli E, Ji Y, Pos Z, Paulos CM, Quigley MF, et al. A human memory T cell subset with stem cell-like properties. Nat Med. 2011 Oct;17(10):1290–7.

27. Carbone FR, Mackay LK, Heath WR, Gebhardt T. Distinct resident and recirculating memory T cell subsets in non-lymphoid tissues. Current Opinion in Immunology. Elsevier Ltd; 2013 Jun 1;25(3):329–33.

28. Gebhardt T, Wakim LM, Eidsmo L, Reading PC, Heath WR, Carbone FR. Memory T cells in nonlymphoid tissue that provide enhanced local immunity during infection with herpes simplex virus. Nat Immunol. 2009 May;10(5):524–30.

29. Sathaliyawala T, Kubota M, Yudanin N, Turner D, Camp P, Thome JJC, et al. Distribution and compartmentalization of human circulating and tissue-resident memory T cell subsets. Immunity. 2013 Jan 24;38(1):187–97.

30. O'Sullivan D, Pearce EL. Targeting T cell metabolism for therapy. Trends Immunol. 2015 Feb;36(2):71–80.

31. Vander Heiden MG, Cantley LC, Thompson CB. Understanding the Warburg Effect: The Metabolic Requirements of Cell Proliferation. Science. 2009 May 21;324(5930):1029–33.

32. Weinberg SE, Chandel NS. Targeting mitochondria metabolism for cancer therapy. Nature Publishing Group. 2015 Jan;11(1):9–15.

33. Smith RAJ, Hartley RC, Cochemé HM, Murphy MP. Mitochondrial pharmacology. Trends in Pharmacological Sciences. Elsevier Ltd; 2012 Jun 1;33(6):341–52.

34. Soubannier V, McBride HM. Positioning mitochondrial plasticity within cellular signaling cascades. Biochim Biophys Acta. 2009 Jan;1793(1):154–70.

35. Palade GE. An electron microscope study of the mitochondrial structure. J Histochem Cytochem. 1953 Jul;1(4):188–211.

36. Koopman WJH, Willems PHGM, Smeitink JAM. Monogenic mitochondrial disorders. N Engl J Med. 2012 Mar 22;366(12):1132–41.

37. Benard G, Rossignol R. Ultrastructure of the Mitochondrion and Its Bearing on Function and Bioenergetics. Antioxidants & Redox Signaling. 2008 Aug;10(8):1313–42.

38. Westermann B. Bioenergetic role of mitochondrial fusion and fission. Biochim Biophys Acta. 2012 Oct;1817(10):1833–8.

39. Baixauli F, Acín-Pérez R, Villarroya-Beltrí C, Mazzeo C, Nuñez-Andrade N, Gabandé-Rodriguez E, et al. Mitochondrial Respiration Controls Lysosomal Function during Inflammatory T Cell Responses. Cell Metab. 2015 Sep 1;22(3):485–98.

40. van der Windt GJW, Pearce EL. Metabolic switching and fuel choice during T-cell differentiation and memory development. Immunol Rev. 2012 Sep;249(1):27–42.

41. Archer SL. Mitochondrial dynamics--mitochondrial fission and fusion in human diseases. N Engl J Med. 2013 Dec 5;369(23):2236–51.

42. Weinberg SE, Sena LA, Chandel NS. Mitochondria in the regulation of innate and adaptive immunity. Immunity. 2015 Mar 17;42(3):406–17.

43. Chang JT, Wherry EJ, Goldrath AW. Molecular regulation of effector and memory T cell differentiation. Nat Immunol. 2014 Dec;15(12):1104–15.

44. Sullivan LB, Gui DY, Hosios AM, Bush LN, Freinkman E, Vander Heiden MG. Supporting Aspartate Biosynthesis Is an Essential Function of Respiration in Proliferating Cells. Cell. Elsevier Inc; 2015 Jul 30;162(3):552–63.

45. Birsoy K, Wang T, Chen WW, Freinkman E, Abu-Remaileh M, Sabatini DM. An Essential Role of the Mitochondrial Electron Transport Chain in Cell Proliferation Is to Enable Aspartate Synthesis. Cell. Elsevier Inc; 2015 Jul 30;162(3):540–51.

46. Chandel NS. Evolution of Mitochondria as Signaling Organelles. Cell Metab. Elsevier Inc; 2015 Aug 4;22(2):204–6.

47. Yun J, Finkel T. Mitohormesis. Cell Metab. 2014 May 6;19(5):757–66.

48. Hawley SA, Ross FA, Chevtzoff C, Green KA, Evans A, Fogarty S, et al. Use of cells expressing gamma subunit variants to identify diverse mechanisms of AMPK activation. Cell Metab. 2010 Jun 9;11(6):554–65.

49. Hardie DG. AMPK: positive and negative regulation, and its role in whole-body energy homeostasis. Curr Opin Cell Biol. 2015 Apr;33:1–7.

50. Hardie DG, Ross FA, Hawley SA. AMPK: a nutrient and energy sensor that maintains energy homeostasis. Nat Rev Mol Cell Biol. Nature Publishing Group; 2012 Apr 1;13(4):251–62.

51. Murphy MP. How mitochondria produce reactive oxygen species. Biochem J. 2009 Jan 1;417(1):1–13.

52. Finkel T. Signal transduction by mitochondrial oxidants. J Biol Chem. 2012 Feb 10;287(7):4434–40.

53. McCormack JG, Halestrap AP, Denton RM. Role of calcium ions in regulation of mammalian intramitochondrial metabolism. Physiological Reviews. 1990 Apr;70(2):391–425.

54. Wellen KE, Hatzivassiliou G, Sachdeva UM, Bui TV, Cross JR, Thompson CB. ATP-citrate lyase links cellular metabolism to histone acetylation. Science. 2009 May 22;324(5930):1076–80.

55. Betz C, Stracka D, Prescianotto-Baschong C, Frieden M, Demaurex N, Hall MN. Feature Article: mTOR complex 2-Akt signaling at mitochondria-associated endoplasmic reticulum membranes (MAM) regulates mitochondrial physiology. Proc Natl Acad Sci U S A. National Acad Sciences; 2013 Jul 30;110(31):12526–34.

56. Arruda AP, Pers BM, Parlakgül G, Güney E, Inouye K, Hotamisligil GS. Chronic enrichment of hepatic endoplasmic reticulum-mitochondria contact leads to mitochondrial dysfunction in obesity. Nat Med. 2014 Dec;20(12):1427–35.

57. Picca A, Lezza AMS. Regulation of mitochondrial biogenesis through TFAM-mitochondrial DNA interactions: Useful insights from aging and calorie restriction studies. Mitochondrion. 2015 Oct 3;25:67–75.

58. Wenz T. Regulation of mitochondrial biogenesis and PGC-1α under cellular stress. Mitochondrion. 2013 Mar;13(2):134–42.

59. Saraste M. Oxidative phosphorylation at the fin de siècle. Science. 1999 Mar 5;283(5407):1488–93.

60. Dillon LM, Rebelo AP, Moraes CT. The role of PGC-1 coactivators in aging skeletal muscle and heart. IUBMB Life. 2012 Mar;64(3):231–41.

61. Gray MW. Mitochondrial evolution. 2012 Sep;4(9):a011403.

62. Hock MB, Kralli A. Transcriptional Control of Mitochondrial Biogenesis and Function. Annu Rev Physiol. 2009 Mar;71(1):177–203.

63. Villena JA. New insights into PGC-1 coactivators: redefining their role in the regulation of mitochondrial function and beyond. FEBS J. 2015 Feb;282(4):647–72.

64. Puigserver P, Wu Z, Park CW, Graves R, Wright M, Spiegelman BM. A cold-inducible coactivator of nuclear receptors linked to adaptive thermogenesis. Cell. 1998 Mar 20;92(6):829–39.

65. Andersson U, Scarpulla RC. Pgc-1-related coactivator, a novel, serum-inducible coactivator of nuclear respiratory factor 1-dependent transcription in mammalian cells. Molecular and Cellular Biology. American Society for Microbiology; 2001 Jun;21(11):3738–49.

66. Lin J, Handschin C, Spiegelman BM. Metabolic control through the PGC-1 family of transcription coactivators. Cell Metab. 2005 Jun;1(6):361–70.

67. Wu Z, Puigserver P, Andersson U, Zhang C, Adelmant G, Mootha V, et al. Mechanisms controlling mitochondrial biogenesis and respiration through the thermogenic coactivator PGC-1. Cell. 1999 Jul 9;98(1):115–24.

68. Mootha VK, Bunkenborg J, Olsen JV, Hjerrild M, Wisniewski JR, Stahl E, et al. Integrated analysis of protein composition, tissue diversity, and gene regulation in mouse mitochondria. Cell. 2003 Nov 26;115(5):629–40.

69. Fox CJ, Hammerman PS, Thompson CB. Fuel feeds function: energy metabolism and the T-cell response. Nat Rev Immunol. 2005 Oct 20;5(11):844–52.

70. Rathmell JC, Vander Heiden MG, Harris MH, Frauwirth KA, Thompson CB. In the absence of extrinsic signals, nutrient utilization by lymphocytes is insufficient to maintain either cell size or viability. Mol Cell. 2000 Sep;6(3):683–92.

71. Finlay DK, Rosenzweig E, Sinclair LV, Feijoo-Carnero C, Hukelmann JL, Rolf J, et al. PDK1 regulation of mTOR and hypoxia-inducible factor 1 integrate metabolism and migration of CD8+ T cells. Journal of Experimental Medicine. 2012 Dec 17;209(13):2441–53.

72. Buck MD, O'Sullivan D, Pearce EL. T cell metabolism drives immunity. Journal of Experimental Medicine. 2015 Aug 24;212(9):1345–60.

73. Pearce EL, Poffenberger MC, Chang C-H, Jones RG. Fueling Immunity: Insights into Metabolism and Lymphocyte Function. Science. 2013 Oct 11;342(6155):1242454–4.

74. Cham CM, Driessens G, O'Keefe JP, Gajewski TF. Glucose deprivation inhibits multiple key gene expression events and effector functions in CD8+ T cells. Eur J Immunol. 2008 Sep;38(9):2438–50.

75. Frauwirth KA, Riley JL, Harris MH, Parry RV, Rathmell JC, Plas DR, et al. The CD28 signaling pathway regulates glucose metabolism. Immunity. 2002 Jun;16(6):769–77.

76. Carr EL, Kelman A, Wu GS, Gopaul R, Senkevitch E, Aghvanyan A, et al. Glutamine uptake and metabolism are coordinately regulated by ERK/MAPK during T lymphocyte activation. The Journal of Immunology. 2010 Jul 15;185(2):1037–44.

77. Wang R, Dillon CP, Shi LZ, Milasta S, Carter R, Finkelstein D, et al. The transcription factor Myc controls metabolic reprogramming upon T lymphocyte activation. Immunity. 2011 Dec 23;35(6):871–82.

78. Sena LA, Li S, Jairaman A, Prakriya M, Ezponda T, Hildeman DA, et al. Mitochondria are required for antigen-specific T cell activation through reactive oxygen species signaling. Immunity. 2013 Feb 21;38(2):225–36.

79. Chang C-H, Curtis JD, Maggi LB, Faubert B, Villarino AV, O'Sullivan D, et al. Posttranscriptional control of T cell effector function by aerobic glycolysis. Cell. 2013 Jun 6;153(6):1239–51.

80. Renner K, Geiselhöringer A-L, Fante M, Bruss C, Färber S, Schönhammer G, et al. Metabolic plasticity of human T cells: Preserved cytokine production under glucose deprivation or mitochondrial restriction, but 2-deoxy-glucose affects effector functions. Eur J Immunol. 2015 Sep;45(9):2504–16.

81. van der Windt GJW, O'Sullivan D, Everts B, Huang SC-C, Buck MD, Curtis JD, et al. CD8 memory T cells have a bioenergetic advantage that underlies their rapid recall ability. Proc Natl Acad Sci U S A. 2013 Aug 27;110(35):14336–41.

82. Grayson JM, Laniewski NG, Lanier JG, Ahmed R. Mitochondrial potential and reactive oxygen intermediates in antigen-specific CD8+ T cells during viral infection. J Immunol. 2003 May 1;170(9):4745–51.

83. Kamiński MM, Sauer SW, Klemke C-D, Süss D, Okun JG, Krammer PH, et al. Mitochondrial reactive oxygen species control T cell activation by regulating IL-2 and IL-4 expression: mechanism of ciprofloxacin-mediated immunosuppression. The Journal of Immunology. American Association of Immunologists; 2010 May 1;184(9):4827–41.

84. van der Windt GJW, Everts B, Chang C-H, Curtis JD, Freitas TC, Amiel E, et al. Mitochondrial respiratory capacity is a critical regulator of CD8(+) T cell memory development. Immunity. 2012 Jan 27;36(1):68–78.

85. Gubser PM, Bantug GR, Razik L, Fischer M, Dimeloe S, Hoenger G, et al. Rapid effector function of memory CD8+ T cells requires an immediate-early glycolytic switch. Nat Immunol. 2013 Oct;14(10):1064–72.

86. Quintana A, Hoth M. Cell Calcium. Cell Calcium. Elsevier Ltd; 2012 Jul 1;52(1):57–63.

87. Quintana A, Schwindling C, Wenning AS, Becherer U, Rettig J, Schwarz EC, et al. T cell activation requires mitochondrial translocation to the immunological synapse. Proc Natl Acad Sci U S A. 2007 Sep 4;104(36):14418–23.

88. O'Sullivan D, van der Windt GJW, Huang SC-C, Curtis JD, Chang C-H, Buck MD, et al. Memory CD8(+) T cells use cell-intrinsic lipolysis to support the metabolic programming necessary for development. Immunity. 2014 Jul 17;41(1):75–88.

89. D'Souza AD, Parikh N, Kaech SM, Shadel GS. Convergence of multiple signaling pathways is required to coordinately up-regulate mtDNA and mitochondrial biogenesis during T cell activation. Mitochondrion. 2007 Dec;7(6):374–85.

90. Michalek RD, Gerriets VA, Nichols AG, Inoue M, Kazmin D, Chang C-Y, et al. Estrogen-related receptor-α is a metabolic regulator of effector T-cell activation and differentiation. Proc Natl Acad Sci U S A. 2011 Nov 8;108(45):18348–53.

91. MacIver NJ, Jacobs SR, Wieman HL, Wofford JA, Coloff JL, Rathmell JC. Glucose metabolism in lymphocytes is a regulated process with significant effects on immune cell function and survival. Journal of Leukocyte Biology. 2008 Jun 17;84(4):949–57.

92. Buttgereit F, Brand MD. A hierarchy of ATP-consuming processes in mammalian cells. Biochem J. 1995 Nov 15;312 (Pt 1):163–7.

93. Sukumar M, Liu J, Ji Y, Subramanian M, Crompton JG, Yu Z, et al. Inhibiting glycolytic metabolism enhances CD8+ T cell memory and antitumor function. J Clin Invest. 2013 Oct;123(10):4479–88.

94. Dimeloe S, Frick C, Fischer M, Gubser PM, Razik L, Bantug GR, et al. Human regulatory T cells lack the cyclophosphamide-extruding transporter ABCB1 and are more susceptible to cyclophosphamide-induced apoptosis. Eur J Immunol. 2014 Dec;44(12):3614–20.

95. Gubser P. Human memory CD8+ T-cells exhibit an intrinsic metabolic advantage as reflected by increased mitochondrialfunctionality and high glycolytic potential (unpublished doctoral thesis). 2013.

96. Schaller A, Hahn D, Jackson CB, Kern I, Chardot C, Belli DC, et al. Molecular and biochemical characterisation of a novel mutation in POLG associated with Alpers syndrome. BMC Neurology. BioMed Central Ltd; 2011 Jan 14;11(1):4.

97. Martinez-Outschoorn UE, Pavlides S, Sotgia F, Lisanti MP. Mitochondrial biogenesis drives tumor cell proliferation. Am J Pathol. Elsevier; 2011 May;178(5):1949–52.

98. Wu M, Neilson A, Swift AL, Moran R, Tamagnine J, Parslow D, et al. Multiparameter metabolic analysis reveals a close link between attenuated mitochondrial bioenergetic function and enhanced glycolysis dependency in human tumor cells. AJP: Cell Physiology. 2006 Sep 13;292(1):C125–36.

99. Obar JJ, Jellison ER, Sheridan BS, Blair DA, Pham Q-M, Zickovich JM, et al. Pathogen-induced inflammatory environment controls effector and memory CD8+ T cell differentiation. The Journal of Immunology. American Association of Immunologists; 2011 Nov 15;187(10):4967–78.

100. McKee EE, Ferguson M, Bentley AT, Marks TA. Inhibition of mammalian mitochondrial protein synthesis by oxazolidinones. Antimicrob Agents Chemother. 2006 Jun;50(6):2042–9.

101. Lamb R, Ozsvari B, Lisanti CL, Tanowitz HB, Howell A, Martinez-Outschoorn UE, et al. Antibiotics that target mitochondria effectively eradicate cancer stem cells, across multiple tumor types: treating cancer like an infectious disease. Oncotarget. 2015 Mar 10;6(7):4569–84.

102. Feau S, Arens R, Togher S, Schoenberger SP. Autocrine IL-2 is required for secondary population expansion of CD8(+) memory T cells. Nat Immunol. 2011 Sep;12(9):908–13.

103. Nashan B, Moore R, Amlot P, Schmidt AG, Abeywickrama K, Soulillou JP. Randomised trial of basiliximab versus placebo for control of acute cellular rejection in renal allograft recipients. CHIB 201 International Study Group. Lancet. 1997 Oct 25;350(9086):1193–8.

104. Parnham MJ, Erakovic Haber V, Giamarellos-Bourboulis EJ, Perletti G, Verleden GM, Vos R. Azithromycin: mechanisms of action and their relevance for clinical applications. Pharmacol Ther. 2014 Aug;143(2):225–45.

105. Bartold PM, Bois du AH, Gannon S, Haynes DR, Hirsch RS. Antibacterial and immunomodulatory properties of azithromycin treatment implications for periodontitis. Inflammopharmacology. 2013 Aug;21(4):321–38.

106. Kawakami K, Kadota J, Iida K, Fujii T, Shirai R, Matsubara Y, et al. Phenotypic characterization of T cells in bronchoalveolar lavage fluid (BALF) and peripheral blood of patients with diffuse panbronchiolitis; the importance of cytotoxic T cells. Clin Exp Immunol. Wiley-Blackwell; 1997 Feb;107(2):410–6.

107. Yi JS, Holbrook BC, Michalek RD, Laniewski NG, Grayson JM. Electron transport complex I is required for CD8+ T cell function. J Immunol. 2006 Jul 15;177(2):852–62.

108. Zenhaeusern G, Gubser P, Eisele P, Gasser O, Steinhuber A, Trampuz A, et al. A high-mobility, low-cost phenotype defines human effector-memory CD8+ T cells. Blood. 2009 Jan 2;113(1):95–9.

109. Morita M, Gravel S-P, Chénard V, Sikström K, Zheng L, Alain T, et al. mTORC1 controls mitochondrial activity and biogenesis through 4E-BP-dependent translational regulation. Cell Metab. 2013 Nov 5;18(5):698–711.

110. Vercauteren K, Gleyzer N, Scarpulla RC. PGC-1-related coactivator complexes with HCF-1 and NRF-2beta in mediating NRF-2(GABP)-dependent respiratory gene expression. Journal of Biological Chemistry. 2008 May 2;283(18):12102–11.

111. Caradec J, Sirab N, Keumeugni C, Moutereau S, Chimingqi M, Matar C, et al. “Desperate house genes”: the dramatic example of hypoxia. Br J Cancer. 2010 Mar 16;102(6):1037–43.

112. Zhang N, Bevan MJ. CD8(+) T cells: foot soldiers of the immune system. Immunity. 2011 Aug 26;35(2):161–8.

113. Harty JT, Badovinac VP. Shaping and reshaping CD8+ T-cell memory. Nature Publishing Group. 2008 Feb;8(2):107–19.

114. Fraser KA, Schenkel JM, Jameson SC, Vezys V, Masopust D. Preexisting high frequencies of memory CD8$^+$ T cells favor rapid memory differentiation and preservation of proliferative potential upon boosting. Immunity. 2013 Jul 25;39(1):171–83.

115. Cui G, Staron MM, Gray SM, Ho P-C, Amezquita RA, Wu J, et al. IL-7-Induced Glycerol Transport and TAG Synthesis Promotes Memory CD8+ T Cell Longevity. Cell. 2015 May 7;161(4):750–61.

116. Chang C-H, Qiu J, O’Sullivan D, Buck MD, Noguchi T, Curtis JD, et al. Metabolic Competition in the Tumor Microenvironment Is a Driver of Cancer Progression. Cell. Elsevier; 2015 Sep 10;162(6):1229–41.

117. Ho P-C, Bihuniak JD, Macintyre AN, Staron M, Liu X, Amezquita R, et al. Phosphoenolpyruvate Is a Metabolic Checkpoint of Anti-tumor T Cell Responses. Cell. 2015 Sep 10;162(6):1217–28.

118. Wieckowski MR, Giorgi C, Lebiedzinska M, Duszynski J, Pinton P. Isolation of mitochondria-associated membranes and mitochondria from animal tissues and cells. Nat Protoc. 2009;4(11):1582–90.

119. Krippner A, Matsuno-Yagi A, Gottlieb RA, Babior BM. Loss of function of cytochrome c in Jurkat cells undergoing fas-mediated apoptosis. Journal of Biological Chemistry. 1996 Aug 30;271(35):21629–36.

120. Pastorino JG, Hoek JB, Shulga N. Activation of glycogen synthase kinase 3beta disrupts the binding of hexokinase II to mitochondria by phosphorylating voltage-dependent anion channel and potentiates chemotherapy-induced cytotoxicity. Cancer Research. 2005 Nov 15;65(22):10545–54.

121. John S, Weiss JN, Ribalet B. Subcellular localization of hexokinases I and II directs the metabolic fate of glucose. PLoS ONE. 2011;6(3):e17674.

122. Raturi A, Simmen T. Where the endoplasmic reticulum and the mitochondrion tie the knot: the mitochondria-associated membrane (MAM). Biochim Biophys Acta. 2013 Jan;1833(1):213–24.

123. Catalina-Rodriguez O, Kolukula VK, Tomita Y, Preet A, Palmieri F, Wellstein A, et al. The mitochondrial citrate transporter, CIC, is essential for mitochondrial homeostasis. Oncotarget. 2012 Oct;3(10):1220–35.

124. Berwick DC, Hers I, Heesom KJ, Moule SK, Tavare JM. The identification of ATP-citrate lyase as a protein kinase B (Akt) substrate in primary adipocytes. Journal of Biological Chemistry. 2002 Sep 13;277(37):33895–900.

125. Adam-Vizi V, Chinopoulos C. Bioenergetics and the formation of mitochondrial reactive oxygen species. Trends in Pharmacological Sciences. 2006 Dec;27(12):639–45.

126. Feske S. Calcium signalling in lymphocyte activation and disease. Nat Rev Immunol. 2007 Sep;7(9):690–702.

127. Miller RA, Flurkey K, Molloy M, Luby T, Stadecker MJ. Differential sensitivity of virgin and memory T lymphocytes to calcium ionophores suggests a buoyant density separation method and a model for memory cell hyporesponsiveness to Con A. J Immunol. 1991 Nov 1;147(9):3080–6.

128. Loberg RD, Vesely E, Brosius FC. Enhanced glycogen synthase kinase-3beta activity mediates hypoxia-induced apoptosis of vascular smooth muscle cells and is prevented by glucose transport and metabolism. Journal of Biological Chemistry. 2002 Nov 1;277(44):41667–73.

129. Kolev M, Dimeloe S, Le Friec G, Navarini A, Arbore G, Povoleri GA, et al. Complement Regulates Nutrient Influx and Metabolic Reprogramming during Th1 Cell Responses. Immunity. Elsevier; 2015 Jun 16;42(6):1033–47.

130. Martín-Cófreces NB, Baixauli F, Sánchez-Madrid F. Immune synapse: conductor of orchestrated organelle movement. Trends Cell Biol. 2014 Jan;24(1):61–72.

131. Macey MG. Flow Cytometry. Springer Science & Business Media; 2007.

132. Gratama JW, D'hautcourt JL, Mandy F, Rothe G, Barnett D, Janossy G, et al. Flow cytometric quantitation of immunofluorescence intensity: problems and perspectives. European Working Group on Clinical Cell Analysis. Cytometry. 1998 Oct 1;33(2):166–78.

133. Schwartz A, Gaigalas AK, Wang L, Marti GE, Vogt RF, Fernandez-Repollet E. Formalization of the MESF unit of fluorescence intensity. Cytometry B Clin Cytom. 2004 Jan;57(1):1–6.

134. Arndt B, Poltorak M, Kowtharapu BS, Reichardt P, Philipsen L, Lindquist JA, et al. Analysis of TCR activation kinetics in primary human T cells upon focal or soluble stimulation. Journal of Immunological Methods. 2013 Jan 31;387(1-2):276–83.

135. Haas R, Smith J, Rocher-Ros V, Nadkarni S, Montero-Melendez T, D'Acquisto F, et al. Lactate Regulates Metabolic and Pro-inflammatory Circuits in Control of T Cell Migration and Effector Functions. PLoS Biol. 2015 Jul;13(7):e1002202.

136. Gattinoni L, Klebanoff CA, Restifo NP. Pharmacologic induction of CD8+ T cell memory: better living through chemistry. Sci Transl Med. American Association for the Advancement of Science; 2009 Dec 16;1(11):11ps12–2.

137. Norata GD, Caligiuri G, Chavakis T, Matarese G, Netea MG, Nicoletti A, et al. The Cellular and Molecular Basis of Translational Immunometabolism. Immunity. Elsevier Inc; 2015 Sep 15;43(3):421–34.

138. Pagès F, Berger A, Camus M, Sanchez-Cabo F, Costes A, Molidor R, et al. Effector memory T cells, early metastasis, and survival in colorectal cancer. N Engl J Med. 2005 Dec 22;353(25):2654–66.

139. Galon J, Costes A, Sanchez-Cabo F, Kirilovsky A, Mlecnik B, Lagorce-Pagès C, et al. Type, density, and location of immune cells within human colorectal tumors predict clinical outcome. Science. 2006 Sep 29;313(5795):1960–4.

140. Butterfield LH. Cancer vaccines. BMJ. 2015 Apr 22;350(apr22 14):h988–8.

141. Sharma P, Allison JP. The future of immune checkpoint therapy. Science. American Association for the Advancement of Science; 2015 Apr 3;348(6230):56–61.

142. Tang H, Qiao J, Fu Y-X. Immunotherapy and tumor microenvironment. Cancer Lett. 2015 Oct 19;370(1):85–90.

143. Siska PJ, Rathmell JC. T cell metabolic fitness in antitumor immunity. Trends Immunol. Elsevier; 2015 Apr;36(4):257–64.

144. Pearce EL, Walsh MC, Cejas PJ, Harms GM, Shen H, Wang L-S, et al. Enhancing CD8 T-cell memory by modulating fatty acid metabolism. Nature. Nature Publishing Group; 2009 Feb 7;460(7251):103–7.

145. Evans JMM, Donnelly LA, Emslie-Smith AM, Alessi DR, Morris AD. Metformin and reduced risk of cancer in diabetic patients. BMJ. 2005 Jun 4;330(7503):1304–5.

146. Viollet B, Guigas B, Sanz Garcia N, Leclerc J, Foretz M, Andreelli F. Cellular and molecular mechanisms of metformin: an overview. Clin Sci. 2012 Mar;122(6):253–70.

147. Altman BJ, Dang CV. Normal and cancer cell metabolism: lymphocytes and lymphoma. FEBS J. 2012 Aug;279(15):2598–609.

148. Kuhnke A, Burmester G-R, Krauss S, Buttgereit F. Bioenergetics of immune cells to assess rheumatic disease activity and efficacy of glucocorticoid treatment. Annals of the Rheumatic Diseases. BMJ Group; 2003 Feb;62(2):133–9.

149. Yang Z, Matteson EL, Goronzy JJ, Weyand CM. T-cell metabolism in autoimmune disease. Arthritis Res Ther. BioMed Central Ltd; 2015;17(1):29.

150. Yin Y, Choi S-C, Xu Z, Perry DJ, Seay H, Croker BP, et al. Normalization of CD4+ T cell metabolism reverses lupus. Sci Transl Med. American Association for the Advancement of Science; 2015 Feb 11;7(274):274ra18–8.

151. Nath N, Khan M, Paintlia MK, Singh I, Hoda MN, Giri S. Metformin attenuated the autoimmune disease of the central nervous system in animal models of multiple sclerosis. The Journal of Immunology. 2009 Jun 15;182(12):8005–14.

152. Mao P, Manczak M, Shirendeb UP, Reddy PH. MitoQ, a mitochondria-targeted antioxidant, delays disease progression and alleviates pathogenesis in an experimental autoimmune encephalomyelitis mouse model of multiple sclerosis. Biochim Biophys Acta. 2013 Dec;1832(12):2322–31.

8. Acknowledgments

First and foremost, I would like to thank Christoph Hess for giving me the opportunity to perform my MD PhD in his group. His great support and optimism kept me going during times when I lost mine. Special thanks goes to Glenn Bantug for his support and contributions to all projects and manuscripts. Good research is always a team effort, therefor I would like to thank all past and present members of the Immunobiology group: Sarah Dimeloe, Patrick Gubser, Leyla Develioglu, Gideon Hönger, Jasmin Grählert, Anne-Valerie Burgener, Maria Balmer and Réka Belle. All group members of the Immunobiology group contributed to this work.

I would also like to thank the Immunodeficiency group of Mike Recher, the Translational Immunology group of Christoph Berger and the Translational Neuroimmunology group of Matthias Mehling for their constructive feedbacks during our shared labmeetings.

I would like to thank all members of the blood donor centre Basel and the whole flow team (Danny Labes, Toni Krebs and Emmanuel Traunecker) who supplied us constantly with buffy coats and sorted cells to perform our experiments. I also thank Ursula Sauder for the beautiful electron microscopy pictures. I would like to acknowledge all members of my thesis committee, Prof. Christoph Handschin, Prof. Daniela Finke and Prof. Antonius Rolink for their support, willingness to review this thesis or for chairing the thesis exam.

I am deeply grateful to all my friends, my family and colleagues who accompanied me on this journey. Finally, my special thanks goes to Sheela for her support and patience, especially during long evenings, nights and weekends while I was working in the lab or writing this thesis.

9. Curriculum vitae